New Journal of Physics
The open access journal at the forefront of physics

Deutsche Physikalische Gesellschaft DPG IOP Institute of Physics International Year of Quantum Science and Technology

TOPICAL REVIEW • OPEN ACCESS

Conceptual and practical approaches for investigating irreversible processes

IOP Publishing New J. Phys. 27 (2025) 041201 https://doi.org/10.1088/1367-2630/adc6ab

New Journal of Physics
The open access journal at the forefront of physics

Deutsche Physikalische Gesellschaft DPG
IOP Institute of Physics

Published in partnership with: Deutsche Physikalische Gesellschaft and the Institute of Physics

OPEN ACCESS

RECEIVED
28 October 2024

REVISED
3 March 2025

ACCEPTED FOR PUBLICATION
28 March 2025

PUBLISHED
14 April 2025

TOPICAL REVIEW

Conceptual and practical approaches for investigating irreversible processes

Dario Lucente[1], Marco Baldovin[2,*], Fabio Cecconi[2,3], Massimo Cencini[2,5], Niccolò Cocciaglia[4,5], Andrea Puglisi[2,5], Massimiliano Viale[2,3] and Angelo Vulpiani[2,4]

[1] Department of Mathematics & Physics, University of Campania "Luigi Vanvitelli", Viale Lincoln 5, 81100 Caserta, Italy
[2] Institute for Complex Systems CNR, P.le Aldo Moro 2, 00185 Rome, Italy
[3] INFN, Sezione Roma1, P.le Aldo Moro 2, 00185 Rome, Italy
[4] Department of Physics, University of Rome "La Sapienza", P.le Aldo Moro 5, 00185 Rome, Italy
[5] INFN, Sezione Roma2, Via della Ricerca Scientifica 1, 00133 Rome, Italy
[*] Author to whom any correspondence should be addressed.

E-mail: marco.baldovin@cnr.it

Keywords: nonequilibrium systems, fluctuation theorems, statistical mechanics, stochastic thermodynamics, response theory

Abstract

Current research in statistical mechanics mostly concerns the investigation of out-of-equilibrium, irreversible processes, which are ubiquitous in nature and still far from being theoretically understood. Even the precise characterization of irreversibility is the object of an open debate: while in the context of Hamiltonian systems the one-century-old proposal by M. Smoluchowski looks still valid (*a process appears irreversible when the initial state has a recurrence time that is long compared to the time of observation* (Smoluchowski 1916 *Z. Phys.* **17** 557–85)), in dissipative systems, particularly in the case of stochastic processes, the problem is more involved, and quantifying the 'degree of irreversibility' is a pragmatic need. The most employed strategies rely on the estimation of entropy production: this quantity, although mathematically well-defined, is often difficult to compute, especially when analyzing experimental data. Moreover, being a global observable, entropy production fails to capture specific aspects of irreversibility in extended systems, such as the role of different currents and their spatial development. This review aims to address various conceptual and technical challenges encountered in the analysis of irreversibility, including the role of the coarse-graining procedure and the treatment of data in the absence of complete information. The discussion will be mostly based on simple models, analytically treatable, and supplemented by examples of complex, more realistic non-equilibrium systems.

At any time there is only a thin layer separating
what is trivial from what is impossibly difficult.
It is in that layer that discoveries are made...
(Andrei N. Kolmogorov)

1. Introduction

Understanding non-equilibrium phenomena (NEP) stands as a key frontier in modern statistical physics [1–6]. This field has emerged from two distinct objectives. Firstly, there is the extensive effort, rooted in Boltzmann's seminal contributions, to address the long-standing and challenging problem of linking the irreversible behavior of the macroscopic world with the reversible microscopic dynamics governed by Hamilton's equations [7]. In addition, there is a practical need to characterize the numerous non-equilibrium (irreversible) phenomena pervasive in science, particularly in physics and chemistry, as well as in various applications. Examples of such phenomena include transport, diffusion, and thermomechanical effects [8].

One of the most important characteristics of out-of-equilibrium systems is the presence of currents induced by external constraints or fields, which lead to the breaking of time-reversal symmetry and inhomogeneites between the system degrees of freedom (e.g. spatial inhomogeneities in extended systems).

Mathematically, we can say that a system is considered out of equilibrium if detailed balance does not hold, or equivalently, if the entropy production rate Σ is positive [9–12]. However, entropy production is difficult to measure in real systems, and can be explicitly calculated only for Markov processes, such as those described by Langevin and Master equations [12]. On the other hand, even when the entropy production is known, being a global quantity, it does not directly inform us about the physical currents between degrees of freedom [13]. For instance, even a system of linear Langevin equations can have a nonzero entropy production and be consistently classified as out of equilibrium; in such a case, due to the absence of a spatial structure, it is not trivial to individuate the currents [14, 15]. Furthermore, in general, quantifying entropy production requires detailed knowledge of the underlying system, including all its degrees of freedom and their interactions [15]. Conversely, in many practical situations, we only have access to a limited set of observables, representing a projection or coarse-graining of the system. Thus, it is natural to wonder in which cases and how we can infer non-equilibrium properties and characterize the breaking of time-reversal symmetry using such partial information.

In this review, we discuss various aspects of a broad class of non-equilibrium systems, from Markov chains to high-dimensional chaotic systems, analyzing both temporal and spatial aspects of non-equilibrium states. Our aim is not to provide an exhaustive compendium of the many facets of non-equilibrium statistical mechanics. Instead, we present a series of observations and ideas on specific aspects that need to be addressed in everyday research. We focus on the practical challenges and difficulties in characterizing the breaking of time-reversal symmetry, its connection with spatial structures, and the physical characteristics of the underlying system. We will discuss the use of several tools to this end, such as correlation functions, particularly those suited to detect asymmetries [16, 17], response theory and fluctuation-dissipation relations [18–20], recently introduced thermodynamic uncertainty relations (TURs) [21, 22], and causation analysis to characterize the irreversibility associated with non-reciprocal interactions between degrees of freedom [23, 24].

In the first part, we primarily focus on analytically treatable models (mostly in the context of Markov processes), which allow us to introduce the main tools of analysis and highlight key problems and subtleties arising from coarse-graining and the lack of complete information in data analysis. In particular, we will pay attention to the consequences of non-Gaussian perturbations, which can be relevant in small systems, and the necessity of a finite scale resolution. We will then progressively consider more complex systems, drawing examples from high-dimensional, spatially extended chaotic systems to realistic simulations of turbulent flows [25, 26] or models for turbulence, where non-equilibrium properties and irreversibility manifest over multiple spatio-temporal scales [27]. The motivation of comparing different tools is not to establish the one which performs the best but instead to investigate potentials and limits of each method that should be considered in real-world application.

The paper is organized as follows. Section 2, starting from the distinction between transient and persistent out-of-equilibrium states, summarizes some fundamental aspects of non-equilibrium statistical mechanics. In particular, we discuss the conceptual ingredients that are needed to a suitable thermodynamic description of the system, such as the presence of many degrees of freedom, typicality and coarse-graining. Some difficulties encountered in the understanding of experimental data and/or numerical calculations are also outlined. Finally, we introduce the indicators that are most commonly used to quantify time-reversal symmetry breaking, namely time-asymmetric correlation functions and entropy production rate. Section 3 is devoted to Markov processes, with a focus on linear stochastic systems and jump processes. Through a systematic use of the theory of stochastic processes, a general and well-defined mathematical formulation of systems in and out of equilibrium is provided. Fluctuation–dissipation theorems and their relations with equilibrium properties are extensively covered. Then, the problem of inferring the thermodynamic properties of a system from partial information is discussed in analytically treatable models. On the one hand, a no-go theorem stating the impossibility of inferring the equilibrium properties of a system by measuring a single stationary degree of freedom, valid for Gaussian processes, is discussed. On the other hand, it is shown that a generalized response allowing the understanding of the thermodynamic nature of the underlying model can be computed by comparing experiments performed under different conditions. Section 4 focuses on general strategies for the estimation of entropy production from data. More specifically, we discuss the TURs, which are lower bounds on entropy production obtained by analyzing the signal to noise ratio of a generic current, as well as some numerical brute-force techniques. Conceptual subtleties such as the dependence on coarse-graining levels, or on the observed currents of these empirical proxies, are carefully scrutinized in simple models: this study shows that useful information can be usually obtained only in cases where a good understanding of the system is available *ab origine*. Finally, other approaches based on the exit-time statistics or hidden Markov modeling are briefly discussed. Section 5 goes beyond entropy production rate examining the potential implications of causation indicators in the analysis of non-equilibrium systems. The two causal indicators taken into account are transfer entropy, which is an

information-theoretic measure of information fluxes between variables, and response function. As discussed there, the advantage of considering these indicators is that they not only discriminate between equilibrium and out-of-equilibrium systems, but also provide information on how the time-reversal symmetry is broken. Section 6 discusses non-equilibrium in turbulence: it is a remarkable case study where all the previous theoretical considerations naturally apply. In particular, it is shown that both correlations and responses of suitably defined observables not only are able to highlight the non-equilibrium nature of particles advected by turbulent velocity field, but also reveal other interesting aspects such as energy and/or enstrophy cascades. Finally, some conclusions are drawn in section 7.

2. Irreversibility in transient and persistent NEP

When discussing NEP, a first distinction can be identified between *transient* and *persistent* non-equilibrium. The former displays a non-equilibrium behavior for a limited amount of time only, before reaching their final equilibrium state, where the dynamics is reversible. Conversely, in persistent NEP time reversal symmetry is continuously broken[6]. They are kept out of equilibrium indefinitely (at least, with respect to the experimentally accessible times) by external drivings, or by intrinsically time-irreversible internal mechanisms.

A prototypical example of transient NEP is gas diffusion. Consider a large number $N \gg 1$ of particles, initially localized in a small region of the available volume $V \sim L^d$ of a d-dimensional box of side length L. The particles of the gas will uniformly distribute over V, in a characteristic time of $O(L^2)$. The reverse process will never be observed within astronomical time scales, as a consequence of Kac's lemma [28] (see discussion below): diffusion is therefore an irreversible process. Once the gas has occupied the whole available volume, the system undergoes an equilibrium dynamics, meaning that the NEP is transient. For an example of persistent NEP, one can think instead of the electric current j in a conductor, produced by an externally imposed electric field E. The well-known Ohm's law, $j = \sigma E$, defines the linear dependence of the two physical quantities, where the constant σ is the electric conductivity [29]. The presence of a preferential direction determined by the electric field, and of a persistent current of charge carriers j, clearly indicates the irreversible nature of the process. Remarkably, Ohm's law straightforwardly arises from linear response theory, specifically the Green–Kubo relation: σ, a non-equilibrium quantity, can be computed in terms of equilibrium properties, i.e. time correlations [2, 20].

This review will mostly focus on persistent NEP. However, in the following we also briefly revisit some general aspects of transient NEP, which played a crucial role in understanding the second law of thermodynamics. These concepts clarify how irreversibility arises in macroscopic systems from their microscopically reversible Hamiltonian dynamics, and will also be useful for the discussion of persistent NEP.

2.1. Transient NEP

2.1.1. The role of the number of degrees of freedom

Poincaré recurrence theorem states that a Hamiltonian system with N degrees of freedom in a confined domain will reach again a state arbitrarily close to its initial condition, after a very long time. Therefore, strictly speaking, transient NEP can be classified as non-equilibrium only when observed over a 'short' time, i.e. much shorter than Poincaré recurrence one. It is known from Kac's lemma that this time is of order e^{aN}: a here is a strictly positive constant, whose precise value depends on how close to the initial condition the system needs to be found at recurrence, and is not really important for the following considerations. The exponential dependence on N implies that, for a system made of a small number of particles, also the recurrence time is relatively small, and irreversibility is not *typical*. Roughly speaking, this means that the irreversible nature of the dynamics cannot be detected by just looking at a single trajectory, i.e. an averaging procedure over many realizations is needed. We will come back to this point in the following.

To explain the relevance of the number of degrees of freedom for the occurrence of irreversibility, we discuss the spreading of an ink drop [30], represented as a system of N_t tagged particles in a fluid, initially uniformly distributed in a small region V_0. We can study this phenomenon by considering a system of N_t particles interacting among themselves, as well as with the N_s solvent particles ($N_s \gg N_t$). In mathematical terms, the ink drop and the solvent correspond to phase-space points evolving through a symplectic dynamics that mimics the Hamilton equation (see [30] for details). A simple way to monitor the mixing process of the ink amounts to counting the number of ink particles $n(t)$ in a region V at time t (see figures 1(a)–(d)). In figures 1(e) and (f), we show the evolution of $n(t)$ in a single realization and its average over many realizations in two different cases: (e) for a small number of tagged particles, where in a single realization $n(t)$ does not display any irreversible tendency to a final state, and only the average $\langle n(t) \rangle$ shows

[6] We prefer to use the term 'persistent' instead of 'stationary', which is not completely general. For instance, an electric noisy circuit with a periodic forcing is in a persistent, but clearly not stationary, non-equilibrium state.

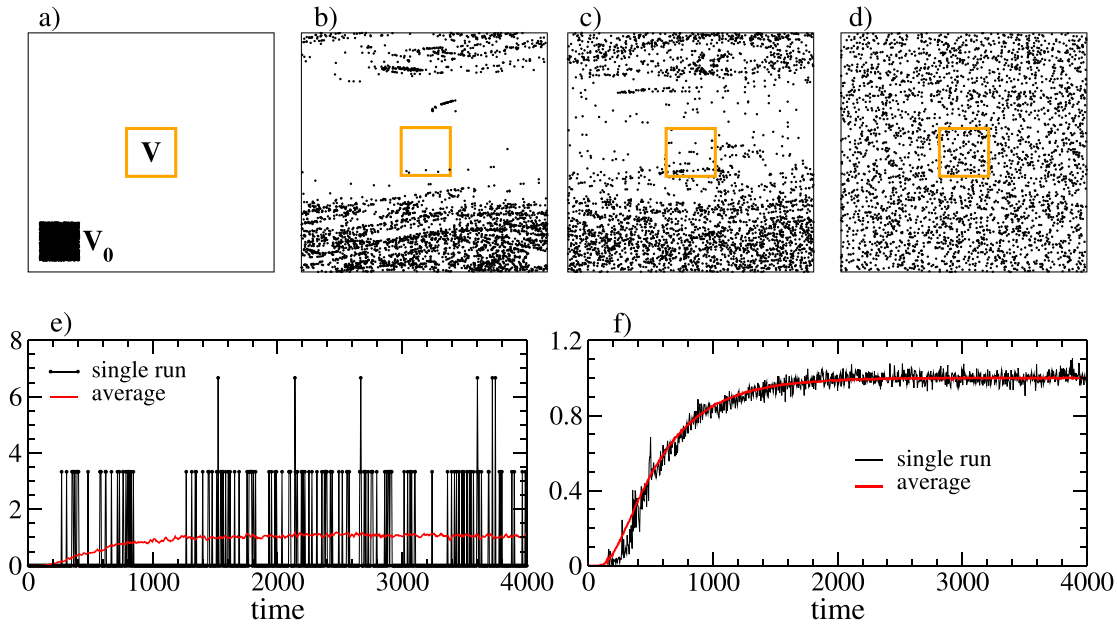

Figure 1. Irreversible spreading of an ink drop. Panels (a)–(d): time evolution of the ink particles. Ink particles start (a) uniformly distributed in V_0 and the instantaneous occupation $n(t)$ is monitored in the (orange) box V, panels (b)–(d) show the evolution till the ink particles are uniformly distributed in the whole contained. Panels (e) and (f) show the instantaneous occupation $n(t)/n_{\rm eq}$ (black curve) and its average $\langle n(t)\rangle/n_{\rm eq}$ (red curve) in the case of few $N_{\rm t}=8$ and many $N_{\rm t}=2.5\,10^4\gg 1$ ink particles, respectively. In (e) the average is over 500 independent initial conditions starting from V_0. When the number of particles is large (f), the irreversible behavior is well evident even looking at a single realization of $n(t)$, this is not the case when their number is small (e). See [30] for further details. Adapted from [30], Copyright (2016), with permission from Elsevier.

clear irreversibility; (f) for a large number of tagged particles ($N_{\rm t}\gg 1$), where the irreversible behavior is well evident even looking at a single realization of $n(t)$. In everyday experience, we have usually access to a single realization of a certain phenomenon. In order to decide whether it is reversible or not, we need the trajectory to be typical [31]. Given a system with many degrees of freedom, we say that its state is typical if its macroscopic observables (e.g. kinetic energy, density in a given region) are close to their averages. If this is the case, the (ir)reversible nature of the phenomenon is clear from a single realization. This is true only for macroscopic bodies, made of many interacting degrees of freedom.

The example above also exemplifies the conceptual difference between the physical irreversibility in a single (macroscopic) system $\mathbf{X}$, and the relaxation of a phase-space probability distribution $\rho(\mathbf{X},t)$ towards an invariant distribution. The latter is a property of an ensemble of initial conditions, which is verified whenever for large t one has $\rho(\mathbf{X},t)\to\rho_{\rm inv}(\mathbf{X})$, independently of the initial density distribution $\rho(\mathbf{X},0)$. Although this property is quite important from a mathematical point of view, it is not the mark of a genuinely irreversible behavior, as demonstrated by the above example.

The difference between relaxation of the probability distribution to an invariant one and the irreversibility in a unique system can be understood considering a low-dimensional symplectic chaotic system, e.g. the Arnold cat map [32]:

$$x_{t+1}=x_t+y_t \bmod 1 \tag{1a}$$

$$y_{t+1}=x_{t+1}+y_t \bmod 1\,. \tag{1b}$$

This map is chaotic and mixing, i.e. $\rho(\boldsymbol{X},t)\to\rho_{\rm inv}(\boldsymbol{X})$ (with $\boldsymbol{X}=(x,y)$), but at variance with the behavior of a macroscopic system, it is impossible to observe any qualitative difference between a single direct trajectory $\boldsymbol{X}_0,\boldsymbol{X}_1,\ldots,\boldsymbol{X}_{t-1},\boldsymbol{X}_t$ and its time reversed $\boldsymbol{X}_t,\boldsymbol{X}_{t-1},\ldots,\boldsymbol{X}_1,\boldsymbol{X}_0$. Even considering an ensemble of initial conditions, each of them evolving independently of the others, their behavior cannot represent the dynamics of a macroscopic body. Having a large number of interacting degrees of freedom is therefore a necessary condition for observing transient irreversibility of macroscopic systems[7].

[7] We remark that it is possible to have interesting results in agreement with statistical mechanics even in non interacting system [33]. Nonetheless, some (even weak) interaction among the particles is usually required to observe a genuine thermodynamic behavior, and thus irreversibility. For instance, consider $N\gg 1$ particles in a box, whose velocities at the initial time are extracted from the Maxwell–Boltzmann distribution at temperature T_1 for half of them and $T_2\neq T_1$ for the other half. In the absence of interaction, the momentum of each particle is conserved and, consequently, the time evolution of some macroscopic observables (e.g. the fourth moment of the particle momenta) will not attain the microcanonical equilibrium value.

2.1.2. Irreversibility and typicality

Consider a system with $N \gg 1$ degrees of freedom, interacting in some way, and an observable $\mathcal{O}$ depending on all (or at least many) of them. It is generally expected that, if the initial condition is far enough from equilibrium, i.e.

$$\mathcal{O}(0) = \langle \mathcal{O} \rangle_{\rm eq} + \delta\mathcal{O}(0)\,, \quad \text{with } |\delta\mathcal{O}(0)| \gg \sigma_{\mathcal{O}}\,, \tag{2}$$

where $\sigma_{\mathcal{O}}$ denotes the magnitude of the equilibrium fluctuations of the observable $\mathcal{O}$, then almost all trajectories $\mathcal{O}(t)$ will be close to the average $\langle \mathcal{O}(t) \rangle$, excluding very unlikely cases. In other words, the behavior of $\mathcal{O}(t)$ is expected to show an irreversible behavior (close to $\langle \theta(t) \rangle$), and in addition to be typical.

A general mathematical proof of the above statement is still missing. However, the result can be proved rigorously in certain stochastic processes (e.g. the celebrated Ehrenfest model [34]) and for dilute gases [35], in the so-called Grad–Boltzmann limit[8]. To exemplify this result, without entering into mathematical detail, we discuss here some numerical simulations supporting the scenario that for a generic macroscopic observable $\mathcal{O}$ satisfying (2), one has

$$\text{Prob}\left\{\mathcal{O}(t) \simeq \langle \mathcal{O}(t) \rangle\right\} \simeq 1\,. \tag{3}$$

The system we consider can be viewed as a simplified model of a piston [30], i.e. a channel containing N particles of mass m, closed by a fixed vertical wall on one end, and by a frictionless moving wall of mass M (the piston itself) on the other. We denote with $x_n(t)$ the coordinate of the nth particle parallel to the channel, in the framework of the fixed wall, and with $X(t)$ the position of the piston, so that $0 \leqslant x_n \leqslant X\ \forall n$. If we assume a constant force F to act on the piston, and we take into account the interactions between the particles inside the channel, the Hamiltonian of the total system reads:

$$H = \frac{P^2}{2M} + \sum_i \frac{|\boldsymbol{p}_i|^2}{2m} + \sum_{i<j} U\left(|\boldsymbol{q}_i - \boldsymbol{q}_j|\right) + U_w(\boldsymbol{q}_1, \ldots, \boldsymbol{q}_N, X) + FX\,,$$

where U is the interacting potential between the particles, and U_w denotes the interaction of the particles with the piston. In the case of non-interacting particles[9], one has $U = 0$, and U_w is the hard-wall potential, yielding elastic collisions. The dynamics is not chaotic, and it is easy to find the 'equilibrium' position of the piston, $\langle X \rangle_{\rm eq}$, and its variance σ_X^2. In the presence of interactions such as, e.g. $U(r) = U_0/r^{12}$ and $U_w = U_0 \sum_n |x_n - X|^{-12}$, it is not possible to determine analytically the equilibrium statistical properties of the system, however the problem can be easily studied numerically (see [30] for details). The system starts at $t = 0$, with the piston at rest ($\dot{X}(0) = 0$) in $X(0) = X_0$, and the initial microscopic state is set as an equilibrium configuration of the gas in the volume imposed by the piston position at a given temperature T_0. When the initial state is far enough from equilibrium, i.e. $|X_0 - X_{\rm eq}| \gg \sigma_X$, the evolution of $X(t)$ is irreversible, as shown in figure 2: damped oscillations around the equilibrium position are clearly detectable. From a conceptual point of view the important result is that the single trajectories are typical, i.e. close to the average, both for the chaotic and the non-chaotic case (i.e. either with or without inter-particle interactions). We also stress that, as one can directly inspect from the figure, the qualitative features of the chaotic and non-chaotic system are essentially indistinguishable with respect to irreversibility: chaos plays little role in irreversible behaviors (as well as for other statistical properties [36]).

2.1.3. Coarse-grained description

An aspect that will become important in the remainder of the paper is the level of description adopted when studying a given phenomenon or system. For the sake of simplicity, let us reconsider again the problem of diffusion. Similarly to the example of the 'ink' drop of figure 1, one can start from the microscopic (deterministic, Hamiltonian) dynamics of the particles of interest and of the solvent (in real world, the tagged or colloidal particles and the molecules of the gas or liquid in which they are embedded). Or, one can change the level of description and mimic the microscopic reversible dynamics in term of a suitable

[8] Consider a system of hard spheres of radius σ, with N particles per unitary volume. The Grad-Boltzmann limit corresponds to increasing the number of particles while decreasing their size, in such a way that the collision rate approaches a constant value, i.e. $N \to \infty$, $\sigma \to 0$ and $N\sigma^2 \to$ constant. By doing so, the volume occupied by the particles scales as $N\sigma^3 \to 0$, consistently with the physical interpretation of dilute-gas limit.

[9] Notice that even if the particles do not interact among each-other, their interaction is mediated by the collisions with the moving wall (the piston). As a consequence energy is redistributed.

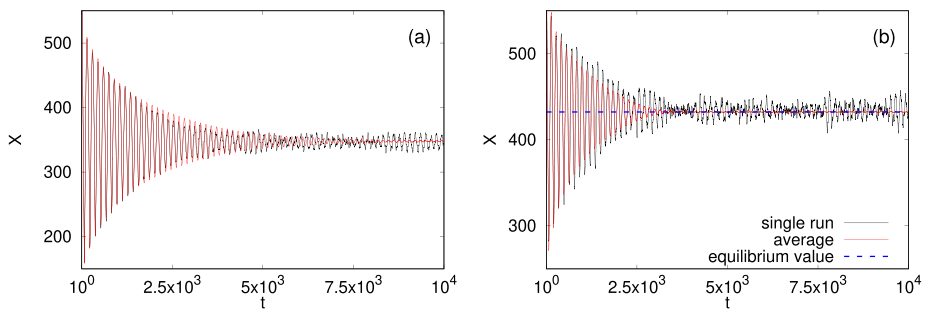

Figure 2. Evolution of the piston position $X(t)$: (a) for the interacting particle (chaotic) model, (b) for the non-interacting (non-chaotic) particle model. In both cases the number of 'gas' particles is $N = 1024$ with $m = 1$ while the piston has mass $M = 10$, the initial temperature is $T_0 = 10$, and the initial displacement of the piston position is $X(0) = X_{\rm eq} + 10\sigma_{\rm eq}$. Black curves denote $X(t)$ in a single realization; red curves refer to the ensemble average $\langle X(t)\rangle$, and in (b) the horizontal blue dashed line is the analytical equilibrium value. The results are taken from [30], where more details can be found. Adapted from [30], Copyright (2016), with permission from Elsevier.

stochastic process. For instance, the diffusion phenomena in a box can be described with a stochastic model, e.g. the overdamped Langevin equation [37]

$$\gamma\frac{\mathrm{d}\mathbf{x}}{\mathrm{d}t} = -\nabla U(\mathbf{x}) + \gamma\sqrt{2D}\boldsymbol{\eta}\,, \tag{4}$$

where η is a white noise (i.e. $\langle \eta_i(t)\eta_j(s)\rangle = \delta_{ij}\delta(t-s)$), and the potential $U(\mathbf{x})$ is zero inside the box and divergent on the boundary, so to confine the particles. Relaxing the overdamped approximation, one can use the (full) Langevin equation [37]

$$\begin{aligned}\frac{\mathrm{d}\mathbf{x}}{\mathrm{d}t} &= \mathbf{v}\,,\\ \frac{\mathrm{d}\mathbf{v}}{\mathrm{d}t} &= -\gamma\mathbf{v} - \nabla U(\mathbf{x}) + \gamma\sqrt{2D}\eta\,.\end{aligned} \tag{5}$$

Therefore, practically, there is the freedom to adopt different mathematical descriptions that are, under some aspects, equivalent up to a certain coarse-graining level. For the specific case of diffusion, the underlying idea is that the effect of fast collisions with the solvent molecules is modeled by the white noise term. As for the original, microscopic description, also in this case the irreversibility of the diffusion process can appear only if we look at a large number of particles, initially close, evolving with (4) or (5). Only in a few special cases, it is possible to perform experiments with good control following a system with many degrees of freedom and repeating many times the measurements with different initial conditions and then computing averages: therefore, usually the transient NEP can be described just at a qualitative level.

Let us notice that the overdamped description (4) can be seen as a coarse-graining in time of the underdamped one (5): the former dynamics is described by only d variables, $\mathbf{x} \in \mathbb{R}^d$, while the latter lives in $2d$ dimensions. Therefore, in general, the result of the computation of some quantities (e.g. entropy) depends on the used model, even if the physical phenomenon is the same. Such an unpleasant fact is an unavoidable aspect of the coarse-graining procedure. For a discussion of this problem under the point of view of entropy production see [38].

2.2. Persistent NEP: entropy production rate

Consider again the case of the conductor subject to an externally imposed electric field. If we can follow the position (or the velocity) of a charge carrier for a long time in a single experiment, we can realize that a current is present. Since there is a preferential direction of motion, and, hence, the time-reversal symmetry of the process is persistently broken, we can conclude that the system is in a (persistent) non-equilibrium state. The larger the current, the farther the system is from equilibrium.

The characterization of the non-equilibrium nature of a system in the general case is, of course, not as simple as this: in fact, in many cases the detection of the currents, which are responsible for the irreversible nature of the process, is a very challenging task. The problem needs, therefore, to be formalized in precise mathematical terms, e.g. by means of a systematic use of stochastic processes. The aim is to provide a general criterion valid independently of the details of the physical system.

A natural attempt in this direction could be to look at two observable functions of the state, $\mathbf{X}(t)$, of the system, $A(t) \equiv A(\mathbf{X}(t))$ and $B(t) \equiv B(\mathbf{X}(t))$, and to check whether their correlations show time-reversal

symmetry, i.e. if

$$\langle A(t)B(0)\rangle = \langle A(0)B(t)\rangle \,.$$

To identify a non-equilibrium system, it would then be sufficient to find two functions $A(t)$ and $B(t)$ for which the above relation does not hold. One might be tempted to define a 'degree of irreversibility' related to the quantity

$$\Delta C_{AB}(t) = \langle A(t)B(0)\rangle - \langle A(0)B(t)\rangle \,,$$

such as, e.g. $\int_0^\infty \mathrm{d}t|C_{AB}(t)|$, to quantify the time-reversal symmetry breaking. In [16, 17] it was proposed for instance to use a correlation function of the form

$$\Delta C_{xx^2}(t) = \langle x(t)x^2(0)\rangle - \langle x(0)x^2(t)\rangle \tag{6}$$

where x represents a generic observable of the system, but, of course, other choices are possible. Correlations functions of this kind can detect asymmetries (*viz.* irreversible behaviors) and thus inform us about the non-equilibrium character of the system from a single variable. However, the above approach has two main drawbacks.

First, ΔC_{AB} depends both on the choice of observable and the reference frame, meaning it is not an intrinsic quantity. Secondly, for processes characterized by Gaussian statistics, functions such as (6) may be trivially zero even if the system is out of equilibrium (see e.g. section 3).

Another way, which has a rather solid mathematical base, to decide whether a system is in a state of non-equilibrium (and to introduce an adequate characterization of the distance from equilibrium) is based on the comparison between the probability of forward (or direct) and inverse (or backward) trajectories. The idea is to recognize whether the direct trajectory is more typical than the inverse one.

The first step is to identify the direct and inverse trajectory. In a mechanical system, one has for the former

$$\mathbf{X}_{\rightarrow}^{(\mathcal{T})} = \{\mathbf{Q}(t), \mathbf{P}(t)\}_{0<t<\mathcal{T}}$$

where $\mathbf{Q}$ and $\mathbf{P}$ are the generalized coordinates and momenta. The inverse trajectory is then defined as

$$\mathbf{X}_{\leftarrow}^{(\mathcal{T})} = \{\mathbf{Q}(\mathcal{T}-t), -\mathbf{P}(\mathcal{T}-t)\}_{0<t<\mathcal{T}} \,,$$

taking into account the fact that, when the motion is reversed, the momenta $\mathbf{P}$ change sign because they are proportional to $\mathrm{d}\mathbf{Q}/\mathrm{d}t$. In the general case, the state of the system is described by a vector $\mathbf{x}(t) = (x_1(t), x_2(t), \ldots, x_D(t))$, and the direct trajectory reads

$$\mathbf{X}_{\rightarrow}^{(\mathcal{T})} = \{x_1(t), x_2(t), \ldots, x_D(t)\}_{0<t<\mathcal{T}}$$

while the inverse one is

$$\mathbf{X}_{\leftarrow}^{(\mathcal{T})} = \{\epsilon_1 x_1(\mathcal{T}-t), \epsilon_2 x_2(\mathcal{T}-t), \ldots, \epsilon_D x_D(\mathcal{T}-t)\}_{0<t<\mathcal{T}} \,,$$

where $\epsilon_i = \pm 1$ denotes the parity of the variable x_i: $+1$ (-1) for variables that are even (odd) with respect to time reversal. Notice that sometimes it can be not trivial to determine the parity [39]. The task is particularly challenging when the variables represent internal degrees of freedom and their parity is generally determined based on physical intuition. This clearly has an impact on the definition of entropy production, as demonstrated by the debate about the equilibrium nature of active Orstein-Uhlenbeck particles [40, 41].

Once $\mathbf{X}_{\rightarrow}^{(\mathcal{T})}$ and $\mathbf{X}_{\leftarrow}^{(\mathcal{T})}$ are identified, to evaluate the equilibrium properties of the system we need to compare the $\mathrm{Prob}(\mathbf{X}_{\rightarrow}^{(\mathcal{T})})$ with $\mathrm{Prob}(\mathbf{X}_{\leftarrow}^{(\mathcal{T})})$. To this aim it is convenient to define the entropy production rate [42]

$$\Sigma = \lim_{\mathcal{T}\to\infty} \left\langle \frac{1}{\mathcal{T}} \ln \frac{\mathrm{Prob}\left(\mathbf{X}_{\rightarrow}^{(\mathcal{T})}\right)}{\mathrm{Prob}\left(\mathbf{X}_{\leftarrow}^{(\mathcal{T})}\right)} \right\rangle = \lim_{\mathcal{T}\to\infty} \Sigma^{(\mathcal{T})} \tag{7}$$

where the average $\langle\cdot\rangle$ is made with respect to $\mathrm{Prob}(\mathbf{X}_{\rightarrow}^{(\mathcal{T})})$. The entropy production rate does not suffer from the same limitation of ΔC_{AB}: it is an intrinsic quantity, i.e it does not depend on the used variable $\mathbf{x}$ since it has the form of a Kullback–Leibler divergence. In addition, it is bounded from below by zero ($\Sigma \geqslant 0$) and it is equal to zero ($\Sigma = 0$) if and only if the forward and the backward path have the same probability, i.e. if

$\Delta C_{AB} = 0$ for every choice of the observables A, B. Another remarkable properties of Σ is that it cannot increase if some variables are integrated out [14, 43–45], that is $\Sigma \geqslant \Sigma_{cg}$ for

$$\Sigma_{cg} = \lim_{\mathcal{T}\to\infty} \left\langle \frac{1}{\mathcal{T}} \ln \left(\frac{\int \mathrm{d}X_1 \cdots \mathrm{d}X_k \mathrm{Prob}\left(\mathbf{X}_{\rightarrow}^{(\mathcal{T})}\right)}{\int \mathrm{d}X_1 \cdots \mathrm{d}X_k \mathrm{Prob}\left(\mathbf{X}_{\leftarrow}^{(\mathcal{T})}\right)} \right) \right\rangle . \tag{8}$$

This equation defines the coarse-grained entropy production as the marginalization of equation (7). However, alternative definition exist [46–48]: in this context it has been shown that, in particular cases (e.g. when starting from a reversible deterministic system), a coarse-graining protocol that does not commute with time-reversal operation can result in an increased entropy production rate [46, 49]. Note that equation (8) requires the use of the coarse-grained path, which is generally non-Markovian. If an approximation is used to compute the path probabilities, an increase in coarse-grained entropy production can be observed [50].

Although Σ is a well-defined quantity, it is often not sufficient to capture all the non-equilibrium characteristics, in particular temporal or spatial asymmetries. Furthermore, several practical difficulties have to be faced when calculating Σ: among the others, incomplete knowledge of the state and/or limited resolution of the measurement procedure. In such cases, one has to resort to alternative approaches, e.g. to study suitable (or generalized) response functions, or correlation functions able to detect the asymmetries. The identification of these indicators often relies on the knowledge of the physics of the system under investigation.

As stated in the Introduction our aim is to review such practical difficulties for the characterization of the irreversibility and to exemplify possible way out on the basis both of simplified systems and more complex examples taken from practical research. In particular, in the following section we provide a detailed discussion of the aforementioned problems in more specific situations, within the framework of linear stochastic processes, beginning with Markovian processes and then going beyond this class, e.g. considering Gaussian processes with colored noise or stochastic differential equations with Poisson noise.

3. About non-equilibrium in linear stochastic processes

In the case of Markov processes, it is possible to provide an expression for the entropy production rate Σ in terms of the transition probability $\mathcal{W}_t(\mathbf{x}|\mathbf{y})$, i.e. the conditional probability of having $\mathbf{x}$ at time t given $\mathbf{y}$ at time 0, and of the stationary probability density $\pi(\mathbf{x}) = \lim_{t\to\infty} \mathcal{W}_t(\mathbf{x}|\mathbf{y})$ which satisfy the chain rule $\pi(\mathbf{x}) = \int \mathrm{d}\mathbf{y}\, \pi(\mathbf{y}) \mathcal{W}_t(\mathbf{x}|\mathbf{y})$. The result is (see appendix A.2)

$$\begin{aligned} \Sigma &= \lim_{t\to 0} \frac{1}{t} \int \mathrm{d}\mathbf{x}\, \pi(\mathbf{x}) \int \mathrm{d}\mathbf{y}\, \mathcal{W}_t(\mathbf{y}|\mathbf{x}) \ln \frac{\mathcal{W}_t(\mathbf{y}|\mathbf{x})}{\mathcal{W}_t(\mathbf{x}|\mathbf{y})} = \\ &= \lim_{t\to 0} \frac{1}{t} \int \mathrm{d}\mathbf{x}\, \mathrm{d}\mathbf{y}\, P_t(\mathbf{x},\mathbf{y}) \ln \frac{P_t(\mathbf{x},\mathbf{y})}{P_t(\mathbf{y},\mathbf{x})} \end{aligned} \tag{9}$$

where $P_t(\mathbf{x},\mathbf{y}) = \pi(\mathbf{x})\, \mathcal{W}_t(\mathbf{y}|\mathbf{x})$ is the joint probability of having $\mathbf{x}$ at time 0 and $\mathbf{y}$ at time t. Equation (9) makes it explicit that, in the case of Markov processes, the equilibrium/non-equilibrium nature of the process can be decided by looking at the violation of the detailed balance condition [37], i.e

$$P_t(\mathbf{x},\mathbf{y}) = \pi(\mathbf{x})\, \mathcal{W}_t(\mathbf{y}|\mathbf{x}) = \pi(\mathbf{y})\, \mathcal{W}_t(\mathbf{x}|\mathbf{y}) = P_t(\mathbf{y},\mathbf{x}) , \tag{10}$$

which is indeed the condition that establishes the invariance under time reversal of the transition $\mathbf{x} \leftrightarrow \mathbf{y}\ \forall t > 0$. Note that equation (9) is formal and require explicit knowledge of both the stationary distribution $\pi(\mathbf{x})$ and the propagator $\mathcal{W}_t(\mathbf{y}|\mathbf{x})$. Thus, despite its good mathematical properties, entropy production is often hardly accessible, because the analytical computation of equation (9) is not always feasible, and moreover its measure in experiments is usually hard as it is based on estimation of probability distributions in possible high-dimensional spaces.

3.1. Equilibrium condition in Gaussian processes

Gaussian stochastic processes, particularly time-continuous ones, are commonly employed as useful effective models for describing, at least under some conditions, the dynamics of various physical and biological phenomena [51–56]. Given their amenability to analytical calculations, these processes are excellent cases for testing physical theories. In order to clarify some non-trivial peculiarities inherent to this class of processes, we summarize here some well-known aspects of their equilibrium properties and we discuss the problem of

unveiling temporal irreversibility from experimental signals. Let us consider the stochastic differential equation for the Ornstein-Uhlenbeck process in D dimensions:

$$\dot{\mathbf{x}} + \mathrm{A}\mathbf{x} = \boldsymbol{\xi} + \mathbf{h}(t) \qquad \left\langle \xi_i(t)\,\xi_j(t') \right\rangle = \mathrm{D}_{ij}\delta(t-t')\,, \tag{11}$$

where the real part of eigenvalues of A (a $D \times D$ real matrix) is positive (so that the system relaxes to a stationary probability density), D is the covariance matrix of the noise $\boldsymbol{\xi}$ and $\mathbf{h}$ is an external field introduced just to make the response function explicit. For simplicity, we are considering only even variables under time-reversal, although most considerations are true for odd variables as well. By direct integration of equation (11) we have

$$\mathbf{x}(t) = \mathrm{e}^{-(t-t')\mathrm{A}}\mathbf{x}(t') + \int_{t'}^{t} \mathrm{d}s\, \mathrm{e}^{-(t-s)\mathrm{A}}\left[\boldsymbol{\xi}(s) + \mathbf{h}(s)\right] \tag{12}$$

from which a simple computation [45] leads to explicit expressions for response and correlation functions:

$$\mathcal{R}_{ij}(t-t') = \left.\frac{\partial \langle x_i(t)\rangle}{\partial h_j(t')}\right|_{\mathbf{h}=0} \qquad \mathcal{R}(\tau) = \begin{cases} \mathrm{e}^{-\tau\mathrm{A}} & \tau \geqslant 0 \\ 0 & \tau < 0 \end{cases} \tag{13}$$

$$\mathcal{C}_{ij}(t-t') = \left\langle x_i(t)\,x_j(t')\right\rangle\big|_{\mathbf{h}=0} \qquad \mathcal{C}(\tau) = \begin{cases} \mathrm{e}^{-\tau\mathrm{A}}\mathrm{C} & \tau \geqslant 0 \\ \mathrm{C}\mathrm{e}^{-|\tau|\mathrm{A}^T} & \tau < 0 \end{cases} \tag{14}$$

$$\mathcal{C}(0) = \mathrm{C} = \int_0^\infty \mathrm{d}s\, \mathrm{e}^{-s\mathrm{A}}\mathrm{D}\mathrm{e}^{-s\mathrm{A}^T} \iff \qquad \mathrm{D} = \mathrm{C}\mathrm{A}^T + \mathrm{A}\mathrm{C}\,. \tag{15}$$

Note that the equations above, since they involve just average values, hold not only for Gaussian processes, but for any type of δ-correlated noise. However, in the case of Gaussian noise, we can add an explicit and compact expression for entropy production rate Σ too, which reads (see appendix A.2)

$$\Sigma = \mathrm{Tr}\left\{\left(\mathrm{C}\mathrm{A}^T - \mathrm{A}\mathrm{C}\right)\mathrm{D}^{-1}\mathrm{A}\right\} = \mathrm{Tr}\left\{\left(\mathrm{A}^T\mathrm{D}^{-1} - \mathrm{D}^{-1}\mathrm{A}\right)\mathrm{A}\mathrm{C}\right\}. \tag{16}$$

For equilibrium systems, i.e. $\Sigma = 0$, one recovers the celebrated Onsager reciprocal relations

$$\mathrm{A}\mathrm{C} = \mathrm{C}\mathrm{A}^T \iff \mathrm{A}^T\mathrm{D}^{-1} = \mathrm{D}^{-1}\mathrm{A} \iff \mathrm{D}\mathrm{A}^T = \mathrm{A}\mathrm{D}\,. \tag{17}$$

Note that, since the paths distribution is Gaussian, i.e.

$$\mathrm{Prob}\left(\mathbf{X}_{\rightarrow}^{(\mathcal{T})}\right) \sim \exp -\frac{1}{2}\sum_{ij}\int \mathrm{d}t \int \mathrm{d}t'\, x_i(t)\,\mathcal{D}_{ij}(t-t')\,x_j(t') \tag{18}$$

using the property

$$\left(\int \mathrm{d}s\,\mathcal{D}(t-s)\,\mathcal{C}(s-t')\right)_{ij} = \delta_{ij}\delta(t-t')\,, \tag{19}$$

it is possible to show that the condition

$$\mathrm{Prob}\left(\mathbf{X}_{\rightarrow}^{(\mathcal{T})}\right) = \mathrm{Prob}\left(\mathbf{X}_{\leftarrow}^{(\mathcal{T})}\right) \tag{20}$$

is equivalent to $\mathcal{C}(t) = \mathcal{C}(-t)$. Let us stress the fact that in order to understand if the system is in equilibrium it is necessary to have the knowledge of all dynamical variables in the system, a practical difficulty in real-world experiments. At equilibrium, a very important relation holds between correlation and response: since $\mathrm{C}\mathrm{A}^T = \mathrm{A}\mathrm{C}$ and $\mathrm{C}\mathrm{A}^T + \mathrm{A}\mathrm{C} = \mathrm{D}$, one has $2\mathrm{A}\mathrm{C} = \mathrm{D}$; therefore, the derivative of $\mathcal{C}(t)$ must satisfy, $\forall t > 0$,

$$\frac{\mathrm{d}\mathcal{C}(t)}{\mathrm{d}t} = -\frac{1}{2}\mathcal{R}(t)\,\mathrm{D}\,. \tag{21}$$

Such equation expresses the equilibrium condition for a linear Gaussian process in the familiar form of a fluctuation-dissipation theorem (FDT).

It is interesting to study the above relation in the reference frame that has the eigenstates of the symmetric matrix D as a basis, or, equivalently, when the covariance matrix of the noise is diagonal, i.e. $\mathrm{D}_{ij} = \left\langle \xi_i(t)\xi_j(t')\right\rangle = 2T_i\,\delta_{ij}\delta(t-t')$. In this case the contribution of the noise can be interpreted as the effect

of D thermal baths, with temperatures $\{T_i\}_{i=1,\dots,D}$. If we look at the i-th single dynamical variable only, we find

$$\frac{\mathrm{d}\mathcal{C}_{ii}(t)}{\mathrm{d}t} = -T_i\,\mathcal{R}_{ii}(t)\,. \tag{22}$$

Note that we obtained an equilibrium condition of the form (21) despite having D different temperatures. This is possible with a non-symmetric drift matrix A which satisfies the condition $\mathrm{A}_{ij}T_j = \mathrm{A}_{ji}T_i$, condition that implies a very special property for A, i.e. $\mathrm{A}_{ij}\mathrm{A}_{jk}\mathrm{A}_{ki} = \mathrm{A}_{ij}\mathrm{A}_{kj}\mathrm{A}_{ji}$, $\forall i<j<k$ [45]. In the same way then, the violation of equality equation (22) can be exploited as a measure of non-equilibrium of a system. In these cases typically the expression above is written in terms of their Fourier transforms $\widetilde{\mathcal{C}}(f)$ and $\widetilde{\mathcal{R}}(f)$ (see [45] for details about the derivation), i.e.

$$\widetilde{\mathcal{C}}(f) = 2\mathrm{Re}\left\{\widetilde{\mathcal{R}}(f)\right\}\mathrm{C} = -\frac{1}{2\pi f}\mathrm{Im}\left\{\widetilde{\mathcal{R}}(f)\right\}\mathrm{D}\,. \tag{23}$$

These equilibrium conditions turn out to be fundamental in some cases, for example when a Markovian process is projected onto a space of lower dimension, e.g. simply by considering only one or two variables. In this case, the projected dynamics is, in general, not Markovian anymore, and it contains memory terms. A precise definition of non-equilibrium is therefore more tricky. Indeed, as we will discuss in the next sections, it is possible to design non-Markovian out-of-equilibrium processes with time-reversal symmetry and vanishing entropy production by simply projecting a multidimensional Markov process onto a space of smaller dimension. In these situations, one possible mathematical formulation of non-Markovian equilibrium system relies on the generalized FDT which relates the response to external forcing $\mathcal{R}$ to the time-derivative of correlation functions ($\mathcal{R}\propto\dot{\mathcal{C}}$). Before entering this topic, however, we will briefly review some known results on the fluctuation-dissipation relations, and about the possibility to exploit them to infer the equilibrium properties of a system.

3.2. Fluctuation-dissipation relations

The first general fluctuation-dissipation relation has been derived by Kubo for Hamiltonian systems [39]. In a nutshell, the idea is to consider weak perturbations of an equilibrium system whose dynamics is encoded in the unperturbed Hamiltonian $\mathcal{H}_0(\mathbf{x})$. The perturbed Hamiltonian

$$\mathcal{H}(\mathbf{x},t) = \mathcal{H}_0(\mathbf{x}) - \mathcal{F}(t)\,A(\mathbf{x})$$

can be used to derive an expression for the average variation of a generic observable $B(\mathbf{x})$ due to the perturbation $A(\mathbf{x})$, modulated by the time-dependent function $\mathcal{F}(t)$. Without entering into the details of the derivation (which are discussed in [2, 19, 20, 39, 57]), we just recall the Kubo formula

$$\langle\Delta B(t)\rangle = \langle B(t)\rangle_{\mathcal{H}} - \langle B\rangle_{\mathcal{H}_0} = \int_{-\infty}^{t}\mathrm{d}\,t'\mathcal{R}_{BA}(t-t')\,\mathcal{F}(t')\,, \tag{24}$$

where $\mathcal{R}_{BA}(t)$ is defined as

$$\mathcal{R}_{BA}(t) = \beta\left\langle B(t)\frac{\mathrm{d}A(0)}{\mathrm{d}t}\right\rangle_{\mathcal{H}_0} = -\beta\left\langle\frac{\mathrm{d}B(t)}{\mathrm{d}t}A(0)\right\rangle_{\mathcal{H}_0} = -\beta\frac{\mathrm{d}\mathcal{C}_{BA}(t)}{\mathrm{d}t}\,, \tag{25}$$

and $\beta = 1/T$ is the inverse of temperature. Equation (25) describes the response of the system to an infinitesimal impulsive perturbation and can be reformulated as

$$\chi_{BA}(t) = \int_0^t\mathrm{d}\,t'\,\mathcal{R}_{BA} = -\beta\left\{\mathcal{C}_{BA}(t) - \mathcal{C}_{BA}(0)\right\}\,, \tag{26}$$

where $\chi_{BA}(t)$ is the susceptibility or admittance. This derivation is valid for systems close to equilibrium, since it relies on the assumption that the unperturbed stationary distribution is the canonical one ($\pi(\mathbf{x})\propto\mathrm{e}^{-\beta\mathcal{H}_0(\mathbf{x})}$). Several attempts to generalize the above formula to non-equilibrium systems have been made. For instance, in [58], it has been shown that a FDT in the form of equation (26) can be restored for the fluctuations of a non-equilibrium process in cases where the non equilibrium force does not change the property of the thermal bath. Later, it has been shown [59] that, in Markovian system, it is always possible to define suitable observables satisfying equation (26). Moreover, a generalized fluctuation relation for a large

class of systems admitting a non-singular invariant measure has been derived in [18, 20, 58]. This result relates the response to an initial perturbation $\delta x_j(0)$ with a properly defined correlation function, i.e.

$$\mathcal{R}_{ij}(t) = \lim_{\delta x_j(0)\to 0} \frac{\langle \delta x_i(t)\rangle}{\delta x_j(0)} = -\left\langle x_i(t)\frac{\partial \ln \pi(\mathbf{x})}{\partial x_j}\right\rangle , \tag{27}$$

where the average is performed on the unperturbed dynamics. The variation of a generic observable can be written as

$$\langle \Delta B(t)\rangle = -\sum_j \left\langle B(t)\frac{\partial \ln \pi(\mathbf{x})}{\partial x_j}\bigg|_{t=0}\delta x_j(0)\right\rangle . \tag{28}$$

Despite its generality, sometimes equation (27) is not very practical, because it requires the explicit knowledge of the stationary measure $\pi(\mathbf{x})$. For this reason, other forms of generalized fluctuation-dissipation relations involving derivatives of the propagator only have been derived for stochastic systems driven by white noise [60–62]. Interestingly, it has been also shown that under general hypothesis a generalized fluctuation theorem holds in the form of an equilibrium contribution plus a correction given by the correlation of the observable and the dynamical activity (frenesy) of the system [63]. It should be noted that equation (27) is a functional relation between correlations and responses that does not depend on the equilibrium nature of the system. This is particularly evident in linear systems where it takes the form $\mathcal{C}(t) = \mathcal{R}(t)C(0)\ \forall t > 0$ meaning that the temporal evolution of the correlation is ruled by the deterministic part of the dynamics.

Some authors, starting from the failure of equation (25) in non-equilibrium systems, introduced the concept of effective temperatures [64]. For a critical discussion of this topic see [65, 66]. While the violation of a generalization of equation (25) for stochastic processes effectively discriminates between equilibrium and non-equilibrium systems, the interpretation in terms of effective temperature is not always able to provide relevant indications regarding the system under investigation (see [14, 66] for details).

To understand the usefulness of fluctuation-dissipation relations in discriminating equilibrium and non-equilibrium, it is convenient to discuss the relation between response and correlation in the case of a Brownian particle evolving through a generalized Langevin equation for the velocity of the particle. Such relation is found by means of the Mori-Zwanzig formalism to derive effective stochastic equations, and its general form reads [67, 68]

$$\dot{v} + \int_0^t \mathrm{d}t'\,\gamma(t-t')\,v(t') = \xi(t) \quad t > 0, \tag{29}$$

where the memory kernel $\gamma(t-t')$ is a delayed friction force and the correlated noise verifies

$$\langle \xi(t)\xi(t')\rangle = \nu(t-t') .$$

We highlight that if

$$\gamma(t) = \gamma_0\delta(t) + \Theta(t)\sum_{i=1}^{D}\gamma_i \mathrm{e}^{-\lambda_i t},$$

where $\Theta(t)$ is the Heaviside step function, the equation can be regarded as a $D-$dimensional linear system projected onto a one-dimensional space (an example will be discuss in 3.3.1, see equation (41)). When γ is not a simple combination of exponential functions, equation (29) can still be interpreted as a projection of an infinite dimensional linear system.

Independently of the physical interpretation, equation (29) can be conveniently studied in Fourier space, i.e.

$$\widetilde{v}(f) = \frac{\widetilde{\xi}(f)}{i2\pi f + \widetilde{\gamma}(f)} = \widetilde{\mu}(f)\widetilde{\xi}(f) , \tag{30}$$

having defined the complex mobility as $\widetilde{\mu}(f) = (i2\pi f + \widetilde{\gamma}(f))^{-1}$. The relation between velocity correlation $\mathcal{C}(t)$, noise correlation ν and mobility μ takes now the form

$$\widetilde{\mathcal{C}}(f) = |\widetilde{\mu}(f)|^2\widetilde{\nu}(f) . \tag{31}$$

At the same time, if we multiply equation (29) by $v(0)$, performing an average over the noise we get [67, 68]

$$\widetilde{\mathcal{C}}(f) = 2\langle v^2\rangle |\widetilde{\mu}(f)|^2 \,\mathrm{Re}\{\widetilde{\gamma}(f)\} , \tag{32}$$

so that, by comparing equation (31) with equation (32), we obtain the relation to be satisfied by friction γ and noise ν in an equilibrium process [2, 19, 39], namely

$$\frac{\widetilde{\nu}(f)}{2\mathrm{Re}\left(\widetilde{\gamma}(f)\right)} = \left\langle v^2 \right\rangle = T, \tag{33}$$

or equivalently

$$\begin{aligned} \mathcal{C}(t) = \mathcal{C}(-t) = 2T\mu(t) \qquad t \geqslant 0 \\ \left\langle \xi(t)\xi(t') \right\rangle = \nu(t-t') = T\gamma\left(|t-t'|\right), \end{aligned} \tag{34}$$

where the equality $\left\langle v^2 \right\rangle = T$ follows from equipartition. Note that the first equation, which links correlation to response, is completely analogous to equation (21) and, by simple time-differentiation, to equation (25). The previous relation can also be inverted to obtain the so-called first- and second-kind fluctuation–dissipation relations [19]

$$\begin{aligned} \mathrm{Re}\left\{\widetilde{\mu}(f)\right\} = \frac{1}{2T}\int \mathrm{d}t \mathrm{e}^{-\mathrm{i}2\pi f t}\mathcal{C}(t), \\ \mathrm{Re}\left\{\widetilde{\gamma}(f)\right\} = \frac{1}{2T}\int \mathrm{d}t \mathrm{e}^{-\mathrm{i}2\pi f t}\nu(t), \end{aligned} \tag{35}$$

where the first can be regarded as an extension of the Einstein relation between mobility and diffusion coefficient, while the second one corresponds to a generalization of Nyquist results connecting dissipation and noise correlation [2]. We stress that while equation (27) has been derived under general hypotheses and holds also out of equilibrium, the relations (25) and (34) are instead only valid at equilibrium. For this reason, violations of equation (34) have been used by Harada and Sasa to quantify the average rate of energy dissipation in a class of Langevin equations [69, 70].

3.3. A no-go theorem for Gaussian processes

To highlight how information on all the variables which describe the system under investigation, as well as on the response, is essential to infer the equilibrium properties of a system, we now discuss a no-go theorem that holds for every Gaussian stochastic process. We set the discussion in the framework of time-continuous processes, but it can be easily generalized to any kind of process with Gaussian statistics for all relevant probabilities. First of all, the linearity of equation (11) allows us to integrate over some components to get an integro-differential stochastic equation for the remaining components of the process (see example in 3.3.1 equation (41)), i.e.

$$\mathcal{L}\mathbf{x} = \boldsymbol{\xi} \tag{36}$$

where $\mathcal{L} = \left\{\mathcal{L}_{ij}\right\}_{i,j=1,D}$ is a set of linear operators (e.g. differentiation or integration) acting on the subset of dynamical variables and the noise $\boldsymbol{\xi}(t)$ will be in general colored with zero mean $\langle \xi_i(t) \rangle = 0$ and covariance matrix $\left\langle \xi_i(t)\xi_j(t') \right\rangle = \nu_{ij}(t-t')$. The above formalism is a compact notation for discussing both under- and over-damped Markov linear systems as well as their projections onto low-dimensional sub-spaces which in general result in non-Markovian dynamics [45]: note however that equation (36) represents the most general class of stochastic linear processes. We recall the fundamental fact that, since the statistics of processes described by equation (36) is Gaussian (multivariate in both time and variables) only averages and correlations are needed to fully specify the process.

The explicit stationary properties of equation (36) can be obtained in Fourier space, where the operator $\widetilde{\mathcal{L}}(f)$ can be easily computed, and the correlation function $\widetilde{\mathcal{C}}(f)$ can be computed as $\left\langle \widetilde{\mathbf{x}}(f)\widetilde{\mathbf{x}}^{\dagger}(f) \right\rangle$. In this way response and correlations read [45]

$$\begin{aligned} \widetilde{\mathcal{C}}(f) = \widetilde{\mathcal{R}}(f)\widetilde{\nu}(f)\widetilde{\mathcal{R}}(f)^{\dagger}, \\ \widetilde{\mathcal{R}}(f) = \widetilde{\mathcal{L}}(f)^{-1} \end{aligned} \tag{37}$$

where $\mathrm{M}^{\dagger}$ denotes the conjugate transpose of matrix M. From the above formula, one immediately realizes that—apart from special cases—it is not possible to infer both the response $\widetilde{\mathcal{R}}(f)$ and the noise correlation $\widetilde{\nu}(f)$ from the knowledge of $\widetilde{\mathcal{C}}(f)$ only. As a consequence we have that, in the case of Gaussian noise, since the process is completely determined by its first two moments, one cannot discriminate between the infinitely

many models sharing the same correlation $\widetilde{\mathcal{C}}(f)$. For instance, it is immediately evident that it is not possible to find a unique model for the following correlation function:

$$\widetilde{\mathcal{C}}(f) = \frac{\nu}{\left((2\pi f)^2 + \lambda^2\right)\left((2\pi f)^2 + \mu^2\right)} \qquad \mu > \lambda \tag{38}$$

$$\mathcal{C}(t) = \frac{\nu}{2(\mu^2 - \lambda^2)}\left(\frac{\mathrm{e}^{-\lambda|t|}}{\lambda} - \frac{\mathrm{e}^{-\mu|t|}}{\mu}\right), \tag{39}$$

Simple computations show that the three following processes are all compatible with $\widetilde{\mathcal{C}}(f)$ in (39)

$$\mathrm{I}\begin{cases} \dot{x} + \lambda x = \xi \\ \langle \xi(t)\xi(t')\rangle = \nu \mathrm{e}^{-\mu|t-t'|}/2\mu \\ \mathcal{R}(t) = \Theta(t)\,\mathrm{e}^{-\lambda t} \end{cases} \quad \mathrm{II}\begin{cases} \dot{x} + \mu x = \xi \\ \langle \xi(t)\xi(t')\rangle = \nu \mathrm{e}^{-\lambda|t-t'|}/2\lambda \\ \mathcal{R}(t) = \Theta(t)\,\mathrm{e}^{-\mu t} \end{cases}$$

$$\mathrm{III}\begin{cases} \ddot{x} + (\lambda+\mu)\dot{x} + (\lambda\mu)x = \xi \\ \langle \xi(t)\xi(t')\rangle = \nu\delta(t-t') \\ \mathcal{R}(t) = \Theta(t)\left(\mathrm{e}^{-\lambda t} - \mathrm{e}^{-\mu t}\right)/(\mu - \lambda)\,. \end{cases}$$

Note that any two-dimensional matrix with trace equal to $\lambda + \mu$ and determinant equal to $\lambda\mu$ could be considered a drift compatible with the correlation function above by providing a suitable covariance for the noise. This would not be an issue if all compatible models had the same nature (i.e. if they were all equilibrium/non-equilibrium processes), but unfortunately this is not the case: by time-differentiating $\mathcal{C}(t)$

$$\frac{\mathrm{d}\mathcal{C}(t)}{\mathrm{d}t} = -\frac{\nu}{2(\lambda+\mu)}\left(\frac{\mathrm{e}^{-\lambda t} - \mathrm{e}^{-\mu t}}{\mu - \lambda}\right), \qquad t \geqslant 0$$

we can note that only the stochastic process III satisfies the fluctuation-dissipation relation equation (22), once the temperature T is fixed in such a way to satisfy the usual relation between friction and noise variance $2T(\lambda + \mu) = \nu$.

3.3.1. An example: the Brownian gyrator

In the following we discuss in some details a system described by equation (11) focusing on the situation where just one variable is experimentally accessible. It is natural to wonder whether such information is sufficient to decide about the equilibrium/non-equilibrium nature of the underlying model. As shown in the following this is impossible. Here we consider the case of the so-called Brownian gyrator [51, 71–73], consisting of the two-dimensional linear system

$$\begin{cases} \dot{x} + ax = by + \sqrt{2T_x}\xi_x \\ \dot{y} + dy = cx + \sqrt{2T_y}\xi_y \end{cases}. \tag{40}$$

Explicit computation shows that, whenever Onsager reciprocal relations are not satisfied, i.e.

$$\mathrm{C}\mathrm{A}^T - \mathrm{A}\mathrm{C} = \Delta \propto bT_y - cT_x \neq 0\,,$$

the system experiences a systematic torque: defining $\theta = \arctan(y/x)$, a rotational current

$$j_\theta = \left\langle \dot{\theta} \right\rangle \simeq \langle \dot{x}y - \dot{y}x\rangle / \left\langle x^2 + y^2 \right\rangle \propto \Delta$$

arises and the entropy production rate is proportional to the square of this current, $\Sigma \propto j_\theta^2$. The 'effective' dynamics of the accessible variable x is non-Markovian

$$\begin{cases} \dot{x} + ax - bc\int_{-\infty}^{t} \mathrm{e}^{-d(t-t')}x(t') = \eta(t) \\ \langle \eta(t)\eta(t')\rangle = 2\left(T_x\delta(t-t') + T_y\mathrm{e}^{-d(t-t')}/d\right) \end{cases} \tag{41}$$

and its correlation function $\mathcal{C}_x(t) = \langle x(0)x(t)\rangle$ in Fourier space reads

$$\widetilde{\mathcal{C}}_x(f) = \frac{c_0 + c_1(2\pi f)^2}{\left(\mathcal{D} - (2\pi f)^2\right)^2 + \mathcal{T}^2(2\pi f)^2} \quad \text{where} \quad \begin{cases} \mathcal{T} = a + d = \lambda_+ + \lambda_- \\ \mathcal{D} = ad - bc = \lambda_+\lambda_- \\ c_0 \propto T_x d^2 + T_y b^2 \\ c_1 \propto T_x \\ \Delta \propto bT_y - cT_x \end{cases}.$$

Thus, once we choose $\mathcal{C}_x(t)$ and Δ, we have only five equations to determine the parameters: two for the trace $\mathcal{T}$ and the determinant $\mathcal{D}$ of the drift matrix, two for the coefficients c_0 and c_1 of the correlation function, and one for the expression of Δ. Therefore, being the problem underdetermined, it seems possible to build models with different entropy production values while, since $\mathcal{C}_x(t) = \mathcal{C}_x(-t)$ for any 1-D Gaussian process, the time-series of x will appear always invariant under time-reversal. Actually, by solving the system of equations above with the conditions $T_x > 0$ and $T_y > 0$, we can prove that the system is surely out-of-equilibrium if the ratio c_0/c_1 falls outside of a certain interval (λ_-, λ_+) determined by the eigenvalues of the matrix A. Nevertheless, this result is based on the crucial assumption that both variables of the system are even under time reversal. In fact, if one of the two variables changes sign under time reversal (in this case $\Delta \propto abT_y + cdT_x$ [45]), the non-equilibrium condition related to the ratio c_0/c_1 becomes exactly the opposite. This then means that, if we have no information about some variables of the system or how these change under time reversal, we have no hope of deducing the equilibrium properties of a system and it is necessary to acquire more information, for example with perturbation-response experiments with which we are typically able to separate the contributions of the drift from that of the noise and infer the equilibrium properties of the system by looking at the violation of a generalized fluctuation theorem.

However, the above consideration does not exclude the possibility to obtain some guesses by running experiments where the measure of response is meant in a broader and more general way. In some cases, it is also possible to measure the entropy production rate of a system performing experiments under slightly different conditions. As an explicit example, we consider again the case of the Brownian Gyrator equation (40) and we assume to be able to manipulate the temperature T_x of one thermal bath. In this case, useful information are obtained by comparing the xx correlation function at temperatures $T_x^{(1)}$ to $T_x^{(2)}$ ($\mathcal{C}_x^{(1)}(t)$ and $\mathcal{C}_x^{(2)}(t)$ respectively). Indeed, from the correlation functions we can fit the relaxation times $1/\lambda$ and $1/\mu$ and the four coefficients $c_{\lambda,\mu}^{(1,2)}$ which are functions of the system parameters $a, b, c, d, T_x^{(1,2)}$ and T_y, i.e.

$$\begin{cases} \mathcal{C}_x^{(1,2)}(t) = c_\lambda^{(1,2)} \mathrm{e}^{-\lambda t} + c_\mu^{(1,2)} \mathrm{e}^{-\mu t} \\ r^{(1,2)} = \lambda\mu \left(\lambda c_\mu^{(1,2)} + \mu c_\lambda^{(1,2)} \right) \end{cases} \rightarrow \begin{cases} T_x^{(1,2)} = \lambda c_\lambda^{(1,2)} + \mu c_\mu^{(1,2)} \\ d = \sqrt{\left(r^{(2)} - r^{(1)}\right) / \left(T_x^{(2)} - T_x^{(1)}\right)} \\ b^2 T_y = r^{(1,2)} - T_x^{(1,2)} d^2 \\ a + d = \lambda + \mu \\ bc = (\lambda + \mu - d)\, d - \lambda\mu \end{cases} .$$

Although we cannot uniquely determine the model, we get a peculiar combination of parameters that enables us to compute the exact value for Σ in both cases:

$$\Sigma^{(1,2)} = \frac{\left(cT_x^{(1,2)} - bT_y\right)^2}{2(a+d)\, T_x^{(1,2)} T_y} = \frac{\left((bc)\, T_x^{(1,2)} - b^2 T_y\right)^2}{2(a+d)\, T_x^{(1,2)} \left(b^2 T_y\right)}$$

Figure 3 shows an application of the formula above on model (40) simulated for two different values of T_x.

3.4. Non-equilibrium induced by Poisson noise

Although the use of Gaussian noise has rather obvious motivations, in some contexts, e.g. in small systems, this assumption appears inadequate, and other kinds of noise must be considered. We now examine another wide class of stochastic process with independent and stationary increments, which naturally arises in certain physics experiments: the compound Poisson process [75–77]. This type of noise, common in granular systems [15, 78–81], has been considered to model active forces [82–84], neural systems [85] and anomalous diffusion [86]. In this dynamics jumps of random amplitude occur at random times, distributed according to a Poissonian statistics. We are interested in understanding how the equilibrium/non-equilibrium nature of the system changes, with respect to models characterized by Wiener noise only, when this additional noise is taken into account. Consider for instance the following linear equation

$$\begin{cases} \dot{\mathbf{x}} + \mathrm{A}\mathbf{x} = \boldsymbol{\xi}(t) + \boldsymbol{\zeta}(t) \\ \boldsymbol{\zeta}(t) = \sum_k \mathbf{u}^{(k)} \delta(t - t_k) \end{cases} \quad \begin{cases} \boldsymbol{\xi} \sim \mathcal{G}_{\mathrm{D}}(\boldsymbol{\xi}) \\ \mathbf{u}^{(k)} \sim \mathcal{P}\left(\mathbf{u}^{(k)}\right) \\ t_k - t_{k-1} \sim \mathcal{Q}_\lambda(t_k - t_{k-1}) = \lambda e^{-\lambda(t_k - t_{k-1})} \end{cases} \tag{42}$$

where $y \sim \mathcal{P}(y)$ means that $\mathcal{P}(y)$ is the probability density function (PDF) of the stochastic process y, and $\boldsymbol{\xi}(t)$ is the usual Wiener process with $\left\langle \xi_i(t)\xi_j(t') \right\rangle = \mathrm{D}_{ij}\delta(t - t')$. The amplitude of the jumps $\underline{\mathbf{u}} = \left\{\mathbf{u}^{(k)}\right\}_k$ are i.i.d. drawn from a generic distribution $\mathcal{P}(\mathbf{u})$ with covariance matrix $\left\langle u_i^{(k)} u_j^{(k')} \right\rangle = \Gamma_{ij}\delta_{kk'}$, while the intervals

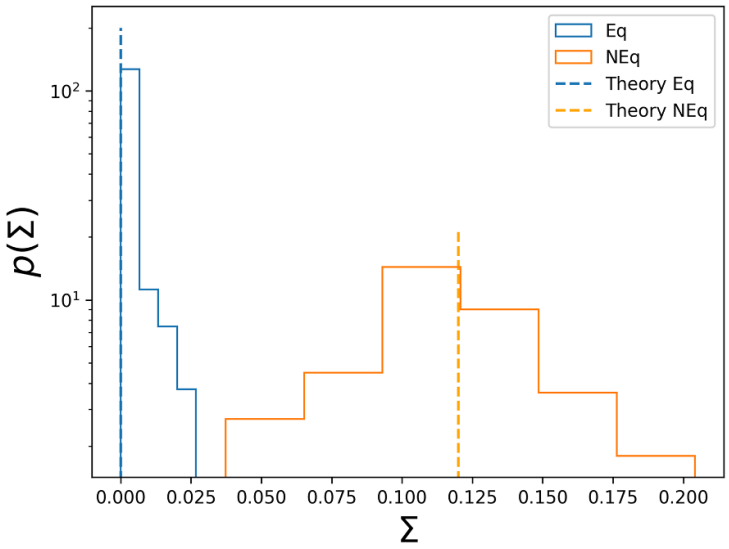

Figure 3. Histogram of entropy production rate estimated with our approach from 40 independent realizations of process equation (40) simulated at two different system parameters. The distributions of the outcomes are correctly centered around the theoretical values (dots line) both for equilibrium and out-of-equilibrium systems [74]. The parameters used for numerical simulations are $a = \frac{8}{3}$, $b = c = -d = -\frac{2}{3}$, $T_y = \frac{1}{2}$ and $T_x^{(1)} = \frac{1}{5}$ (orange) or $T_x^{(2)} = \frac{1}{2}$ (blue). Adapted from [74].

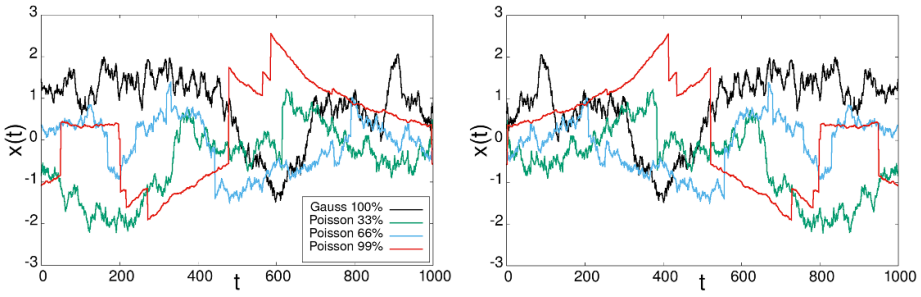

Figure 4. Examples of direct (left) and time-reversed (right) trajectories for processes driven by a Gaussian and Poisson noise, the amplitude of the jumps are sampled from Gaussian distribution with covariance matrix Γ. We keep the variance of the total noise $\nu' = \nu + \lambda\Gamma$ constant and we vary the fraction of Poissonian noise of the process. It is evident that, as the Poissonian contribution increases, the time-reversed trajectory becomes more and more incompatible with the direct one, i.e. it is difficult to find any piece of the latter in the former.

$\Delta t = t_k - t_{k-1}$ between two consecutive jumps are i.i.d. and extracted from an exponential distribution $\lambda e^{-\lambda \Delta t}$. It is easy to understand that a system driven only by $\boldsymbol{\zeta}(t)$ cannot be at equilibrium. Consider the time interval between two jumps: in the direct path, the system relaxes toward its mean value, while in the time-reversal one, the system moves away from its stationary state. The impossibility of observing the reverse paths is quite obvious and it is well illustrated in figure 4 showing direct (left) and inverse (right) trajectories of a one-dimensional Ornstein-Uhlenbeck process driven by Gaussian or Poissonian noise.

More formally, one can prove that such processes lack detailed balance. Indeed, this property must be satisfied separately by the jump process and by the continuous part. Regarding the discontinuous part, it takes the form

$$\pi(\mathbf{x})\,\mathcal{P}(\mathbf{y}-\mathbf{x}) = \pi(\mathbf{y})\,\mathcal{P}(\mathbf{x}-\mathbf{y})\,. \tag{43}$$

Thus, assuming a symmetric distribution of jump amplitudes $\mathcal{P}(\mathbf{u}) = \mathcal{P}(-\mathbf{u})$ and a generic spatially non-uniform stationary measure ($\pi(\mathbf{x}) \neq \pi(\mathbf{y})$ for $\mathbf{x} \neq \mathbf{y}$), the detailed balance condition cannot be satisfied. Interestingly, despite its non-equilibrium nature, the relationship between correlation $\mathcal{C}(t)$ and responses $\mathcal{R}(t)$ has the same structure of a Gaussian process (i.e. $\mathcal{C}(t) = \mathcal{R}(t)\mathrm{C} = e^{-t\mathrm{A}}\mathrm{C}$) but with different noise matrix $\mathrm{D}' = \mathrm{D} + \lambda\Gamma = \mathrm{C}\mathrm{A}^T + \mathrm{A}\mathrm{C}$. This implies that the usual equilibrium relations valid for Gaussian systems (Onsager $\mathrm{A}\mathrm{C} = \mathrm{C}\mathrm{A}^T$ and generalized fluctuation-dissipation relations $\dot{\mathcal{C}}(t) = -\mathcal{R}(t)\mathrm{D}'$) are not sufficient anymore to conclude that the system is in equilibrium. The above results are just a consequence of the linear structure of the system and the absence of moments of degree higher than the second in the

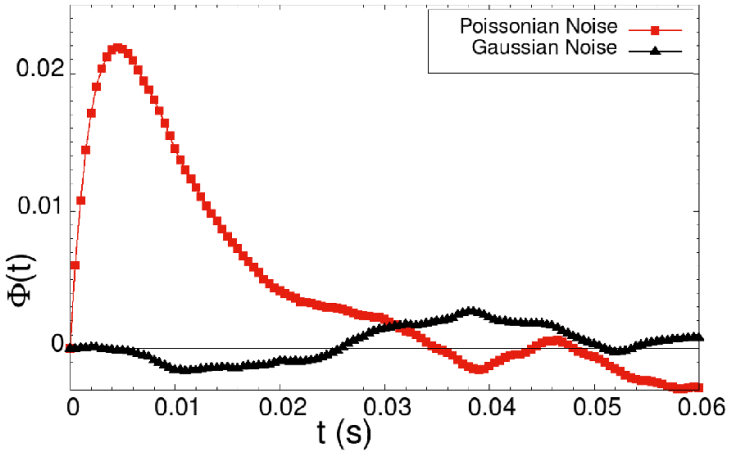

Figure 5. Degree of irreversibility $\Phi(t)$ for Gaussian (black) and Poissonian (red) process for a two-dimensional linear process. Using the same nomenclature of (40) for elements of the drift matrix A, the parameters used for numerical simulations are $a = 122.9$, $b = 1$, $c = 0$, $d = 26.1$. Regarding the noise, in the Poissonian case we consider $\lambda = 1261$, $\Gamma = \begin{pmatrix} 2.002\,225 & 0 \\ 0 & 0 \end{pmatrix}$ and $D = \begin{pmatrix} 0 & 0 \\ 0 & 1647 \end{pmatrix}$ while in the Gaussian regime $D = \begin{pmatrix} 2524.8 & 0 \\ 0 & 1647 \end{pmatrix}$. Note that parameters are chosen to make the two-point correlation function $\mathcal{C}(t)$ identical for both noises and their values have been obtained by fitting a real experimental signal of a granular system (see [15] for further details). Adapted (figure) with permission from [15], Copyright (2023) by the American Physical Society.

expressions of $\mathcal{C}(t)$ and $\mathcal{R}(t)$. When instead we take into consideration quantities that depend on such higher moments, we can better appreciate the differences with respect to a purely Gaussian process. For instance, the entropy production rate Σ, as proven in the appendix of [74], reads

$$\Sigma = \mathrm{Tr}\left[(\Delta + \lambda\Gamma)\,\mathrm{D}^{-1}\mathrm{A}\right] \qquad \Delta = \mathrm{C}\mathrm{A}^{T} - \mathrm{A}\mathrm{C}. \tag{44}$$

The expression is formally analogous to equation (16), but it should be noted that only the Gaussian 'temperatures', described by the matrix D, enter the expression of Σ, while the Poisson noise contributes through the stationary covariance $\lambda\Gamma$, see [74]. This observation clarifies why such processes are often called 'athermal'[78, 80, 81, 87]. A direct inspection shows that $\Sigma > 0$ and the minimum is attained for $\mathrm{AC} = \mathrm{CA}^{T}$, i.e. in correspondence of 'classical' equilibrium $\Delta = 0$ as defined by Onsager [74]. Finally, since the system is not Gaussian, its non-equilibrium nature can be inferred from higher-order correlation functions even from a single time-series. As mentioned in section 2.2, Pomeau suggests to compare $\langle x(0)x^3(t)\rangle$ and $\langle x^3(0)x(t)\rangle$ [16]: this choice allows us to estimate the degree of irreversibility of a process. For instance, figure 5 shows the differences between Gaussian and Poissonian noise for the quantity

$$\Phi(t) = \left\langle x(0)\,x^3(t) - x(0)^3\,x(t)\right\rangle / \left\langle x^4\right\rangle$$

in the case of a two-dimensional linear process.

4. Estimates of entropy production

4.1. Scale-dependent entropy production $\Sigma(\epsilon, \Delta t)$

Measuring entropy production represents a formidable challenge, both because it requires knowledge of all the variables of the system and because of the considerable amount of data to obtain reliable estimations. Here we discuss the role played by resolution, i.e. the relevance of time sampling and coarse graining, introducing the concepts of scale-dependent entropy production $\Sigma(\epsilon, \Delta t)$ (in analogy with the ϵ-entropy [88–90] used in dynamical system). In a nutshell, the idea is:

1. Introduce a partition $\left\{B_i^{(\epsilon)}\right\}_{1\leqslant i\leqslant K}$ of size ϵ of the phase space.
2. Define an empirical Markov chain

$$\pi_i = \overline{\mathbf{1}_{B_i^{(\epsilon)}}(x(t))}$$
$$\pi_i P_{ij} = \overline{\mathbf{1}_{B_j^{(\epsilon)}}(x(t+\Delta t))\cdot\mathbf{1}_{B_i^{(\epsilon)}}(x(t))}$$

where we have dropped from π_i and P_{ij} the ϵ and Δt dependence and $\mathbf{1}_A(x)$ is the characteristic function of set A. i.e.

$$\mathbf{1}_A(x) = \begin{cases} 1 & \text{if } x \in A \\ 0 & \text{otherwise} \end{cases}$$

and $\overline{f(x)}$ is the time average of $f(x)$, i.e

$$\overline{f(x)} = \frac{1}{n}\sum_{k=1}^{n} f(x(t_k))$$

where $t_k = t_0 + k\Delta t$ and $n \gg 1$.

3. Add a regularization for the missing reverse transitions. For example, if we have $P_{ij} > 0$ but $P_{ji} = 0$, we introduce an offset parameter δ, we impose $P_{ji} = \delta < 1/t_{\max}$ or $P_{ji} = \delta P_{ij}$ $(\delta \ll 1)$ and we rescale appropriately the empirical frequencies in order to have a well normalized probability (i.e. $\sum_j P_{ij} = 1$). In this way we avoid the divergence arising from $\log P_{ji}$[10].
4. Compute the entropy production rate of such Markov chain as

$$\Sigma(\epsilon, \Delta t) = \frac{1}{\Delta t}\sum_{ij} \pi_i P_{ij} \log\left(\frac{P_{ij}}{P_{ji}}\right).$$

5. Take the limit $\epsilon \to 0$ and $\Delta t \to 0$ of $\Sigma(\epsilon, \Delta t)$.

In the limit of infinite data and for $\epsilon \to 0$ and $\Delta t \to 0$ one has $\Sigma(\epsilon, \Delta t) \to \Sigma$ [74]. However, we stress that $\Sigma(\epsilon, \Delta t)$ in general is just a proxy, neither a lower nor an upper bound for the entropy production rate Σ. The reason is that the coarse-grained process is not Markovian, while the scale-dependent entropy estimation relies on a Markovian approximation and therefore can exceed the entropy production of the microscopic system [50]. Let us highlight the relevance of scale resolution for the behavior of $\Sigma(\epsilon, \Delta t)$ through an example. Consider the one-dimensional system

$$\dot{x} = -\nabla_x V(x) + f + \xi(t) + \zeta(t), \tag{45}$$

$$V(x) = \frac{LV_0}{2\pi}\left(1 - \cos\frac{2\pi x}{L}\right). \tag{46}$$

which describes a particle moving on a tilted periodic potential subject to Gaussian ($\langle \xi^2 \rangle = 2T$) and Poisson ($\langle \zeta^2 \rangle = 2\lambda\Gamma$) noises. Such a system is widely employed as a minimal model for transport phenomena [84, 87, 91–95], and several properties have been established. The pulling force f induces a stationary current j_s (even in the Gaussian case) and Σ is positive. In Gaussian systems, the relation between entropy production rate and current is [10, 11, 96]

$$\Sigma \propto \frac{j_s^2}{T}, \tag{47}$$

while for the system driven by Poisson noise it takes the form

$$\Sigma = \frac{j_s}{T} f + \Delta\Sigma_p \tag{48}$$

where

$$\Delta\Sigma_p = \frac{\lambda V_0 L}{2\pi T}\left\langle \cos\frac{2\pi x}{L}\right\rangle \left(1 - \mathrm{e}^{-2(\pi\Gamma/L)^2}\right) \tag{49}$$

and $\langle\cdot\rangle$ is the average over the stationary measure (see [74] for the derivation). In order to understand the effect of scale-resolution on the entropy production measurements, it is important to identify the characteristic scales of the system. The deterministic part of the dynamics has two relevant time-scales: the relaxation time τ_r inside each well and the average exit time τ_e. The other characteristic times come from

[10] One can always evaluate *a posteriori* the goodness of regularization by observing how the results depend on the offset δ. Typically, if the sample is large enough and the fraction of unobserved reverse transitions is small, the results depend very little on the type of regularization and do not undergo significant variations even if the offset decreases by a couple of orders of magnitude and this happens in the cases we show.

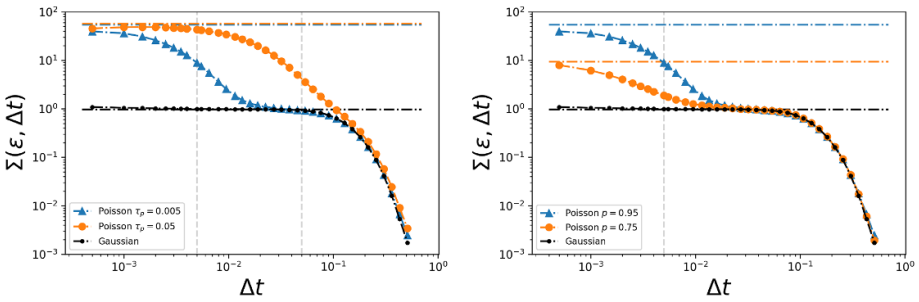

Figure 6. Empirical entropy production rate $\Sigma(\epsilon, \Delta t)$ as a function of Δt for a particle in a symmetric periodic potential $V(X)$ and pulled by a constant force f, $\epsilon \simeq 4 \cdot 10^{-3}$. Left panel show $\Sigma(\epsilon, \Delta t)$ for two different Poisson jump rates τ_p ($\tau_p = 0.05$ red, $\tau_p = 0.005$ blue). Right panel shows the convergence of $\Sigma(\epsilon, \Delta t)$ towards the theoretical values (horizontal lines) for different levels of Poisson noise (75%, 95%) for $\tau_p = 0.005$ (left).

Poisson noise, which has an intrinsic temporal scale $\tau_p = 1/\lambda$ (the average inter-events time) while the average amplitude size $\sigma_p \sim \sqrt{u^2}$ fixes the characteristic length scale. For coarse-graining resolutions ϵ greater than σ_p, the scale-dependent entropy production misses the contribution of Poisson noise since transitions to different cells due to jumps are unlikely. Therefore, if the temporal resolution Δt is much bigger than τ_p the contribution of Poisson noise to the scale-dependent entropy production $\Sigma(\epsilon, \Delta t)$ cannot be appreciated. However, regarding the temporal behavior of $\Sigma(\epsilon, \Delta t)$ one should discuss separately the two cases $\tau_r < \tau_p$ and $\tau_r > \tau_p$. In the former, the noisy part of the dynamics is dominated by Poisson noise and hence the dynamics never resembles its Gaussian counterparts. In the latter, instead, since in a time-interval of order τ_r a large number of jumps occur, central limit theorem applies and the statistic of ζ on this time-scale is well described by a Gaussian process. Thus, for $\tau_r \gg \Delta t \gg \tau_p$ the scale-dependent entropy production $\Sigma(\epsilon, \Delta t)$ takes values close to the ones computed for Gaussian system, i.e. $\Sigma(\epsilon, \Delta t) \sim j_s^2 / T_{\text{eff}}$ with $T_{\text{eff}} = T + \lambda\Gamma$, while for $\Delta t \ll \tau_p$ the contribution of Poisson noise is correctly taken into account.

The above considerations are supported by numerical simulations, as shown in figure 6. The left panel shows that the Gaussian plateau arises only for intermediate temporal resolution ($\tau_r \gg \Delta t \gg \tau_p$). From a close inspection of the right panel, it becomes evident that differences between Gaussian and non-Gaussian cases (as well as differences between different Poisson noises) only arise for $\Delta t < \tau_p$.

4.2. TURs

We have already seen that entropy production Σ in its most general definition is a powerful concept but it has several disadvantages, particularly when Σ has to be estimated from experimental/numerical data. In the cases where the full dynamical equations are known, Σ can take the form of a time-integrated functional of some complicated function of—in principle—*all the degrees of freedom* involved in such a dynamics. Therefore, a partial empirical observation cannot faithfully estimate the entropy production: in fact, not even its average rate. The estimation of Σ is even more challenging for those physical systems that do not benefit from an accurate theoretical modeling: as we have already seen in section 4.1, general recipes starting from experimental data of a few observables—possibly at a coarse resolution in time and space—are hardly useful for approximating the entropy production rate.

In recent years, several works have been devoted to understanding the relation between the average entropy production rate (or other quantities related to it) and the currents crossing non-equilibrium systems, especially in its steady state [97]. It is clear that one cannot hope to get—in general—information about the total entropy production rate starting from any average current. Indeed complex systems, typically involving many time-scales and several relevant variables, can be traversed by many physical currents and the total entropy production rate is somehow the result of the combination of all of them [98]. The clearest example of such a principle is found in irreversible thermodynamics [1], where

$$\Sigma = \sum_{\alpha=1}^{n} A_\alpha J_\alpha \tag{50}$$

where A_α is the α-th affinity or thermodynamic force, while J_α is the associated average current. A detailed treatment of this decomposition principle can be found in the Schnakenberg network theory [99], that decomposes a non-equilibrium Markov process (living in a discrete space of states) into fundamental cycles

(such as those in an electric circuit) each crossed by its own current:

$$\Sigma = \sum_{\alpha=1}^{n} A\left(\vec{C}_\alpha\right) J\left(\vec{C}_\alpha\right) \tag{51}$$

where $\vec{C}_\alpha$ are the n fundamental cycles of the graph associated to the process, $A(\vec{C}_\alpha)$ is the affinity or thermodynamic force that acts directly in cycle α (a kind of total asymmetry in the transition rates of the edges of that cycle), while $J(\vec{C}_\alpha)$ is the average net current in that cycle. Close to equilibrium the currents are linear combinations of the affinities with coefficients that compose the symmetric Onsager matrix. We do not intend to delve into the details of such a theory, but it is clear that equations (50) and (51) require lot of information to retrieve a valid estimate of Σ. An interesting alternative to this direct measurement is represented by the so-called TURs [100], which establish a link between the entropy production and the first two cumulants of the fluctuations of any kind of current measured in the system (instead of knowing the average of all of them and also the corresponding affinities).

The most common TUR discussed in the recent literature provides a lower bound for the integrated (in a time t) entropy production Σ_t in the form of a 'precision rate' for the fluctuations of *any* non-equilibrium current integrated for the same time t, J_t, in the system (in the following we take $k_B = 1$ for the Boltzmann constant):

$$\Sigma_t \geqslant 2\,\frac{\langle J_t\rangle^2}{\mathrm{Var}\,(J_t)}. \tag{52}$$

The relation (52) was first derived for all continuous-time Markov process with a discrete number of states in [21] and then generalized to Markov processes in steady states in [101]. We note that in a steady state for large t, one has $\Sigma_t = t\Sigma$, $\langle J_t\rangle = tJ$ and $\mathrm{Var}(J_t) \sim 2D_J t$, where D_J is the diffusivity associated to the current rate whose average we denote by J, leading to a rate version of equation (52):

$$\Sigma \geqslant \frac{J^2}{D_J}. \tag{53}$$

The power of this relation comes from its generality: it stands true for a very wide set of situations and physical systems, and it involves any observable current. Its downside, obviously, is in the fact that it only provides us with an inequality which cannot, in general, be proved to be tight.

In the few years after the TUR was first proved, several follow-up results have better enlightened the origins of the inequality and its applicability to non-equilibrium thermodynamics, see [100] for a first review with perspectives. To better understand the meaning of equation (52), it is interesting to discuss what happens in the close-to-equilibrium limit: in that case, as mentioned above, the linearity between currents and affinities makes the entropy production rate take a bilinear form $\Sigma = \sum_{\beta,\gamma} L_{\beta\gamma} A_\gamma A_\beta$.[11] The Einstein relation implies that the diffusion coefficient for the fluctuations of the time-integral of the current J_α is $D_\alpha = L_{\alpha\alpha}$, therefore the TUR relation for the α current reads [21]

$$\frac{\Sigma}{J_\alpha^2/D_\alpha} = \frac{L_{\alpha\alpha}\sum_{\beta,\gamma} L_{\beta\gamma}A_\beta A_\gamma}{\sum_{\beta,\gamma} L_{\alpha\beta}L_{\alpha\gamma}A_\beta A_\gamma} \geqslant \left(1 + \frac{\sum_{\beta,\gamma\neq\alpha} G_{\beta\gamma}A_\beta A_\gamma}{J_\alpha^2}\right) \geqslant 1, \tag{54}$$

where in the last passage we have used the fact that $G_{\beta\gamma} = (L_{\alpha\alpha}L_{\beta\gamma} - L_{\alpha\beta}L_{\alpha\gamma})$ can be proven to be a positive semi-definite matrix (this is a consequence of the fact that the Onsager matrix L is also positive semi-definite). From these few lines of calculations, one learns that, in the equilibrium limit, the equality is obtained if $A_\beta = 0$ for each $\beta \neq \alpha$.

Generalizations of the TUR and its applications to various inference problems, particularly for the maximum efficiency of molecular motors and for the minimal number of intermediate states in enzymatic networks, are discussed in [97]. Several techniques have been employed to derive TURs, including large deviation theory [101, 102], bounds to the scaled cumulant generating function (see for instance [103, 104] and [104, 105]), and other approaches. An interesting way to derive it, is the application of the generalized Cramér–Rao inequality [106], which includes quantifying the Fisher information of the Onsager–Machlup measure of the path and a virtual 'tilt' of the original dynamics. However, such a strategy cannot be directly applied to a system with underdamped dynamics, for which can be shown through explicit example that

[11] This form is much more general than the case discussed above of Markov processes on a network, it encompasses all cases where a discrete set of currents can be identified in a system close to equilibrium.

equation (52) does not hold [107]. Notwithstanding, generalization of such inequality can be derived pursuing alternative approaches (see [108, 109]). The Cramér–Rao approach has been used to derive generalized TURs that are optimized to give a lower bound for diffusivity of a tracer particle under the action of non-linear friction and non-equilibrium baths with multiple time-scales and multiple temperatures [110, 111]. A recent more direct derivation of TUR, with a discussion about how it can be saturated, has been proposed in [112].

As discussed in [102], the TUR bound is most useful if it is tight, but there are two main reasons why it might be loose: (1) the distribution of the current fluctuations is non-Gaussian and (2) the choice of the current can be sub-optimal, i.e. it does not contain enough information about the total entropy production. First applications to the problem of inferring Σ from the study of currents fluctuations were obtained in works [102, 113].

In order to give an idea of the limits of the TUR strategy in the entropy production inference, in the following we discuss some interesting attempts to evaluate it. In [102], a diffusion process in two dimensions is studied, with an external field driving the system across the four wells of a landscape. The transitions among the four quadrants, each containing one of the wells, are measured to play the role of J as mentioned earlier. This task requires measuring *all the degrees of freedom*, i.e. the process in its full dimensionality. The authors concluded that the TUR can underestimate the entropy production by a factor which is between 0.2 and 0.8 and, interestingly, the error on the estimate is not seriously affected by the strength of the external driving, but rather, it is affected by the depth of the wells. The estimated power of the TUR increases when the wells are deeper, likely because the coarse-graining into four quadrants is closer to the physics of the process. In [113], a two-dimensional 'bead-spring' model, in practice a Brownian Gyrator with conservative coupling and different temperatures, was studied and the authors compared two approaches to estimate Σ: (1) an empirical direct measurement of the entropy production from a *vectorial* time-series of the numerical solution of the model (an approach that not only requires knowledge of all relevant degrees of freedom, but even when all d.o.f. can be measured it is doomed to fail as the dimensionality of the problem increases); (2) a measure of the average and variance of a scalar current obtained from some projection of all the d.o.f.: these two cumulants are easy to obtain with a small amount of data and can be plugged into equation (53) in order to get an estimate of Σ; the authors first proved that an optimal choice (leading to estimates close to the real value of Σ in the same order of magnitude) of the measured current is $j_F = \int \mathrm{d}\mathbf{x}\,\mathbf{F}(\mathbf{x})\cdot\mathbf{j}(\mathbf{x})$ where $\mathbf{F}(\mathbf{x})$ is the thermodynamic force acting on the system at point $\mathbf{x}$ and $\mathbf{j}(\mathbf{x})$ is the local current, where both quantities are empirically determined (by averaging over a long trajectory) but, again, they require the knowledge of all the degrees of freedom of the system. Further investigation about the power of inference of the TUR was conducted in [114], where a deterministic method to estimate entropy production based on the TUR for classical Markovian dynamics was suggested, by computing an 'optimal' current that maximizes the lower bound. In this context, it was shown that the optimal current saturates the TUR for overdamped Langevin dynamics driven by Gaussian white noise, but, as it will become clear in the following, for general Markovian processes this is not always granted. Inference, however, relies on a wise choice of a basis for currents (in principle any functional basis) and again the measurement of all the relevant degrees of freedom. Thus, real applications in [114] are limited to simple systems such as a four states Markov jump process, a driven Brownian particle that circulates on a ring with a periodic potential, finally a multidimensional bead spring model (a Gaussian continuous process), where the knowledge of all the variables is needed. Notably, other strategies relying upon the measurement of an optimal current have been proposed [115, 116]. In [115], the authors build a large set of currents as random linear combinations of empirical microscopic currents and define the optimal choice as the one that maximizes the bound in the limit of infinitely short trajectories. It is shown that such a procedure provides estimates of the average entropy production rate arbitrarily close to the real value and, moreover, can also be used to obtain its probability distribution. In [116] instead, the authors consider the possibility of finding the best estimate (largest bound) by using machine learning procedures. All the methods discussed so far improve the bound through an optimization scheme for the observable to be measured. In [117], the authors adopt a completely different point of view. Introducing a continuous family of stochastic dynamics the authors derive a tighter version of the TUR connecting entropy production rate and currents between different members of the family. In addition, it is shown that this bound is saturated by an appropriate choice of the observable. A more practical approach consists in improving TURs by considering more information besides the fluctuations of a current: this obvious concept has been put in an interesting form in [118], where it has been shown that

$$\eta_J + \chi^2_{J_t,Z} \leqslant 1 \tag{55}$$

$$\eta_J = \frac{2\langle J_t\rangle^2}{\mathrm{Var}\,(J_t)\,\Sigma_t} \tag{56}$$

$$\chi_{J_t,Z} = \mathrm{Cov}\left(J_t, Z\right) / \sqrt{\mathrm{Var}\left(J_t\right)\mathrm{Var}\left(Z\right)} \tag{57}$$

where $\chi_{J_t,Z}$ is the Pearson correlation coefficient between J_t and any variable Z, while $\mathrm{Cov}(a,b)$ is the covariance between variables a and b. Note that the usual TUR states that $\eta_J \leqslant 1$ while the term $\chi_{J_t,Z}$ is bounded ($-1 \leqslant \chi_{J_t,Z} \leqslant 1$) and actually improves the estimate. It is also important to mention that, recently, another relation, named Variance Sum Rule, connecting the entropy production to force fluctuations has been derived [119]. The power of this relation is that it is an *equality*, rather than an inequality and it has been successfully applied to determine the entropy production in experiments with an optically trapped colloid and with in-vivo red blood cells. At first glance, the approach requires the explicit knowledge of the process in its full dimensionality and the forces acting on the system; however the novelty of this recipe makes it difficult to estimate its future applications.

Although in specific cases TURs have been proven to survive in the thermodynamic limits [120], from the previous discussion we understand that for systems with many degrees of freedom and several currents in general lead to loose bounds. There is an interesting case, however, where the TUR could be useful in a 're-normalised' form also in the case of several degrees of freedom. That is the case where a single macroscopic current is measured, of the form

$$J_t^{\mathrm{macro}} = \frac{1}{n}\sum_{\alpha=1}^{n} J_t^{\alpha}, \tag{58}$$

and the J_α are all related to *equivalent* degrees of freedom. A typical example of this condition is the case of flagella in microscopic living systems, for instance the tail of a sperm cell or the two flagella making a C. reinhardti algae swim (both examples belong to the same category of flagella that are constituted by a so-called 'axoneme' with a very conserved structure, occurring also in other cells or living beings) [121]. In these flagella, a travelling wave produces the noisy periodic beating—which is responsible for swimming under viscous conditions. The accumulation of periods (phase) of the travelling wave represents an integrated current J_{macro} whose fluctuations could be used in the TUR to estimate the entropy production of the flagellum. However such a wave is produced by the concurrence of n molecular motors ('dyneins') innervating the axoneme, with $n \sim 10^3$–10^5 (depending on the length of the flagellum, which on its turn depends upon the organism and/or its age) [122]. Each molecular motor performs its own periodic motion whose accumulated phase represents a microscopic current J_α: the dynein is known to be close to optimal in the TUR sense, as the bound is smaller than the real dissipation rate by a factor $\eta \approx 0.2$–0.5 (see [123]). If the organism dissipates energy almost only in the ATP consumption for feeding the molecular motors, as it happens for a sperm cell, then the total dissipation rate of the structure is of order n times the dissipation rate of a single molecular motor. While the average of J_t^{macro} is the same as the average of the molecular motor currents, i.e. $\langle J_t^{\mathrm{macro}}\rangle = tJ_{\mathrm{macro}} = tJ_\alpha$ for any α (all motors are equivalent), its diffusivity D_{macro} can take values between a minimum D_α/n in the case of totally asynchronous motors, and a maximum D_α in the extreme case of totally synchronized motors. Then, in the case of totally asynchronous motors, the TUR is close to be saturated (with similar efficiency η) because $J^2_{\mathrm{macro}}/D_{\mathrm{macro}} = nJ^2_\alpha/D_\alpha$ and the macroscopic dissipation rate is n times larger than the motor one. On the contrary, in the extreme case of totally synchronized motors, the real total entropy production rate is n times larger than the TUR bound which take a similar value to the bound for the single molecular motor $J^2_{\mathrm{macro}}/D_{\mathrm{macro}} = J^2_\alpha/D_\alpha$. Recent experiments with sperms flagella and a study of synchronization models with different kinds of noise suggest that the second situation is more likely to happen in real axonemes, corroborating a conjecture of strong coupling between adjacent molecular motors, see [124, 125].

As discussed before, when the statistics of the process under investigation is Gaussian and a limited set of variables can be measured (smaller than the complete set of relevant degrees of freedom) the discrimination of equilibrium from non-equilibrium is basically impossible on a general ground, since the same empirical time series is compatible with both equilibrium and non-equilibrium models. However, in particular cases, one may invoke additional hypothesis and assumptions that restrict the field of compatible models, making the discrimination possible. For instance in [110] it is seen that a TUR can be proven for the diffusion of the position $\theta(t)$ of a tracer particle under the influence of multiple baths, taking the form:

$$\langle \Delta\theta\left(t\right)^2\rangle \geqslant \frac{2\langle\Delta\theta\left(t\right)\rangle^2}{\Sigma_t^{\mathrm{ext}} + \mathcal{I}} \tag{59}$$

where Σ_t^{ext} is the part of the entropy production (integrated along the time t), which only originates from the presence of an external driving force (i.e. excluding the entropy produced because of heat flowing between different thermal baths), while $\mathcal{I}$ is related to the Fisher information for a linear perturbation of the

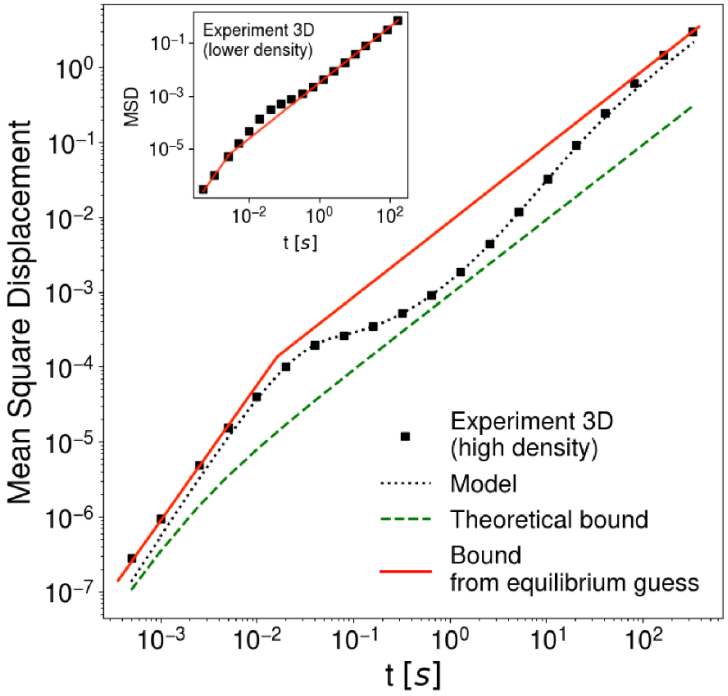

Figure 7. MSD of a large intruder immersed in a vibrated granular fluid at high density, see [110]. The equilibrium guess is constructed by connecting the two slopes of the ballistic and the diffusive regime following what we would expect at equilibrium from equation (60). The experimental data are below the equilibrium guess and therefore equation (60) is violated, i.e. the data are not compatible with equilibrium. The inset shows an MSD (in the dilute regime) whose form is compatible with thermodynamic equilibrium. Adapted (figure) with permission from [110], Copyright (2023) by the American Physical Society.

dynamics [43]. When the multiple baths are at thermal equilibrium, it appears that equation (59) reduces to a simpler expression

$$\langle \Delta\theta(t)^2 \rangle \geqslant \frac{t^2}{at+b} \tag{60}$$

where $a = 1/(2D)$ being D the diffusivity of the tracer particle, while $b = m/T$ being m and T the mass and temperature of the tracer particle: in this way the full bound can be deduced by observing the mean squared displacement in the long time limit ($\sim Dt$ with D the diffusivity) and in the short one ($\sim T/mt^2$) and therefore an immediate evaluation of the validity or violation of inequality (60) can be done, see an example with experimental data in figure 7. If the inequality is violated, then the equilibrium hypothesis can be immediately ruled out. If the inequality is not violated, however, nothing can be said about the equilibrium or non-equilibrium character of the system. A similar situation has been discussed in the recent [126], where constraints on the power spectrum of a continuous stochastic process can be used in the same way: it can exclude equilibrium in specific situations.

4.3. An application for TUR and $\Sigma(\epsilon, \Delta t)$: the Poissonian–Brownian gyrator

Let us now illustrate with a practical example some critical issues related to the techniques described above. Consider the case of Brownian gyrators defined in section 3.3.1 by equation (40) when the drift is isotropic ($d = a$ and $c = b$) and add a Poissonian jump process with rate λ just along the x component, i.e.

$$\begin{cases} \dot{x} + ax = by + \xi + \sum_k u_k \delta(t - t_k) & \langle \xi^2 \rangle = 2Tr(1-p) \\ \dot{y} + ay = bx + \xi' & \langle \xi'^2 \rangle = 2T(1-r) \\ \lambda\sigma^2 = 2Trp & \langle u_k^2 \rangle = \sigma^2 \ \forall k \end{cases} \tag{61}$$

We have seen that, for a purely Gaussian process, when the quantity $\Delta = b(T_y - T_x)$ is different from zero (in our model when $p = 0$ and $r \neq 1/2$), such system exhibits a non-zero probability current that makes it rotate around the origin. We can better appreciate this by noting that the average of the angular momentum $\langle l(t) \rangle = \langle x(t)\dot{y}(t) - y\dot{x}(t) \rangle \propto \Delta$ is different from zero. Therefore, it seems natural to consider the integral of the angular momentum $A(t) = \int_0^t \mathrm{d}t' l(t')$ to estimate the entropy production through the TUR shown in

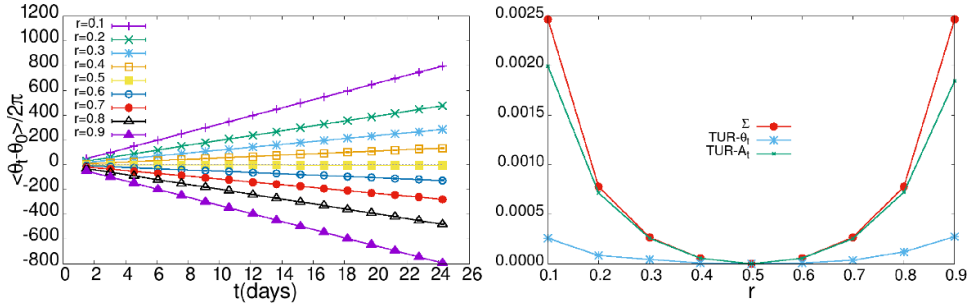

Figure 8. Currents in Brownian Gyrator. Left: the average rotation angle traveled by the system as a function of time, different plots represent different values of r. The angular velocity of the system can be obtained by looking at the slope of the lines. Right: lower bounds obtained by looking at the TUR computed with the 'integrate currents' $A(t)$ (green) and $\theta(t)$(blue) compared to the true value of entropy production (red). See footnote for details of the numerical simulations that produced the figures of this section.

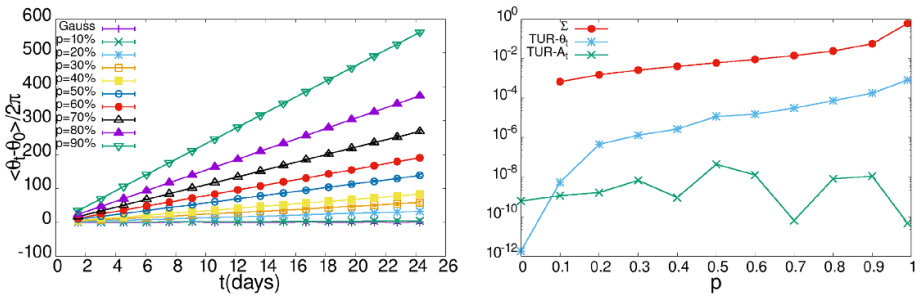

Figure 9. Currents in Poissonian Gyrator when Onsager equilibrium condition holds ($r = 0.5$). Left: average rotation angle for increasing Poisson noise contribution $p \in [0.1, 0.9]$. We can note that, although the average of angular momentum $\langle l(t) \rangle$ vanish, the system is clearly rotating around the origin faster and faster as p increases. Right: comparison between the TURs and the true value of entropy production. The TUR computed with $A(t)$ it is not significant, the one computed with $\theta(t)$ is better but, however, two orders of magnitude smaller than the true value.

section 4.2 equation (52). As figure 8 shows[12], this estimate (green line) is quite good. For comparison we show the TUR estimate obtained using a different current, i.e. the rotation angle $\theta(t) = \int_0^t \mathrm{d}t' \omega(t')$ where $\omega(t') = \frac{\mathrm{d}}{\mathrm{d}t'} \arctan[y(t')/x(t')]$ (blue line), which appears considerably worse. Note that, at equilibrium for $r = 0.5$, rotation is absent and $\Sigma = 0$. But, what does it happen when we add jumps to the equation? Once r and λ are fixed, we can study the contribution of Poissonian noise by varying parameter p in the interval $[0, 1]$. In this way the two-time correlations do not change as p varies and this means that, for example, the average of the angular momentum $\langle l(t) \rangle$ will not depend on the fraction p of Poissonian noise present in the system. We know from the previous section that the addition of a Poissonian noise, even in the case of Onsager equilibrium (for which $r = 0.5$ corresponds to $\mathbb{AC} - \mathbb{CA}^T = \Delta = 0$), brings the system out of equilibrium and with an entropy production rate which is strictly positive $\Sigma \propto p/(1-p)$. Because of the lack of sensitivity of $A(t)$ to the Poissonian noise, the TUR computed with the integrated angular momentum $A(t)$ will not be significant, although a rotation of the system is observed and increases as the Poissonian noise increases (figure 9). This is because the statistic of the rotation θ depends on all the moments of the path distribution, not only on the second one, making it well affected by the amount of Poissonian noise. As clear from figure 9, the estimate obtained with the TUR is now better if $\theta(t)$ is used instead of $A(t)$, however in both cases it is not particularly good. The worst results with TURs in the case of Poissonian noise is coherent with what discussed above, i.e. that optimal estimates can be reached only in the case of Gaussian fluctuations, provided that proper currents are measured.

One can also verify the possibility of stall points: with the addition of Poissonian noise, just as the system rotates even when $\Delta = 0$, in the same way the system may stop rotating even when $\Delta > 0$. As we show in the left panel of figure 10, although we weakly break the Onsager condition ($r = 0.6$), we can find a value of p (in our case $p = 0.5$) for which there is no rotation at all. The rotation current changes sign when going through

[12] All numerical simulations are based on the exact algorithm described in the appendix A.3 and the main parameters are $a = 6.25 \cdot 10^{-2}$, $b = 2.18 \cdot 10^{-2}$, $T = 10^{-2}$ and $\lambda = 1/960$. In this way the correlations are $\mathcal{O}(1)$ and the two typical time scales due to the drift are approximately $\tau_< = 120$ and $\tau_> = 240$ steps (our time step is fixed to 1), well below the average time between two jump $1/\lambda = 960$.

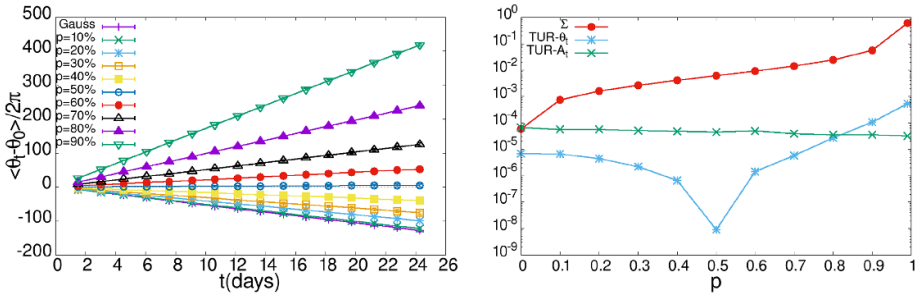

Figure 10. Currents in Poissonian Gyrator when Onsager equilibrium condition is broken ($r = 0.6$). Left: as the Poissonian contribution increases the angular current changes sign. Right: TUR estimates are quite bad for both $A(t)$ and $\theta(t)$. Note that, for each value of p, the one obtained with $A(t)$ is more or less the value that the entropy production rate would have in the case of pure Gaussian noise ($p = 0$).

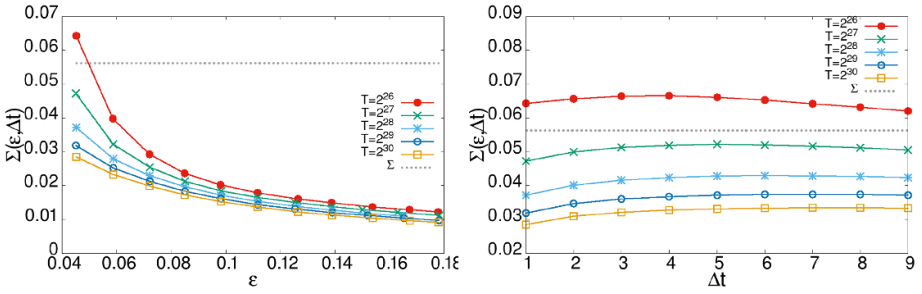

Figure 11. $\Sigma(\epsilon, \Delta t)$ for the Poissonian Gyrator (61). Left: we fix $\Delta t = 1$ and we look at the trends with $\epsilon \to 0$. Right: we fix $\epsilon = 4.5 \cdot 10^{-2}$ and we look at the trends with $\Delta t \to 0$. The simulations have $r = 0.5$ and $p = 0.9$. The typical displacement for $\Delta t = 1$ is order $\sqrt{\langle dx^2 + dy^2 \rangle} \simeq 0.1$.

this stall point. Obviously, as we show in the right panel of figure 10, these points have destructive consequences on the TUR estimates.

We conclude this section with a comparison of TUR-estimates with the numerical algorithm described in the section 4.1. Compared to the examples of figure 6, for which we had to partition a simple one-dimensional ring, in the case of gyrator we have to deal with an unbounded two dimensional phase space. This requires additional approximations (e.g. to partition the system only up to a certain distance from the origin and neglect the dynamics that occur outside) that could spoil the effectiveness of our method which, when informed with a finite statistics, tends to be too sensitive to several details, e.g. to the regularization necessary to manage the large number of the missing reverse transitions: it seems practically impossible to sample effectively the dynamics and extrapolate Σ from $\Sigma(\epsilon, \Delta t)$ for $\epsilon, \Delta t \to 0$. In figure 11 we show the dependence on ϵ and Δt of $\Sigma(\epsilon, \Delta t)$ for different lengths T of the samples used to estimate the transition probabilities, from some millions to a billion of steps. We can note that, although the order of magnitude seems reasonable, a precise value of Σ cannot be deduced from the trend we obtained even with very expensive numerical simulations.

Finally, in order to mitigate at least the problem of under-sampled dynamics, we can ask ourselves what we would have obtained by looking at a single variable of the system, one of the two components x or y, the distance from the origin $\rho = \sqrt{x^2 + y^2}$ or the angle $\theta = \arctan y/x$. The results are shown in figure 12 and they indicate once again how important it is the choice of the observable. Even ignoring the problem of the limit for $\epsilon \to 0$, see the right panel of figure 12, we see that the best entropy production estimate is obtained by considering the signal $x(t)$. This is due to the fact that variable feels directly the effect of the jumps. The estimates provided by the signals ρ and θ are in between those provided by x and y separately as ρ and θ are non-linear combination of these two signals.

The above analysis shows, in general, how difficult it is to have a correct estimate of the entropy production rate from experimental or numerical data, even in simple cases.

4.4. Exit times statistics and hidden Markov modeling

An alternative strategy that has been proposed in recent years consists in using other observables, rather than current fluctuations, in order to prove or disprove the hypothesis of an equilibrium model underlying the empirical data. Such a strategy is typically not aimed to retrieve an exact value for the entropy production

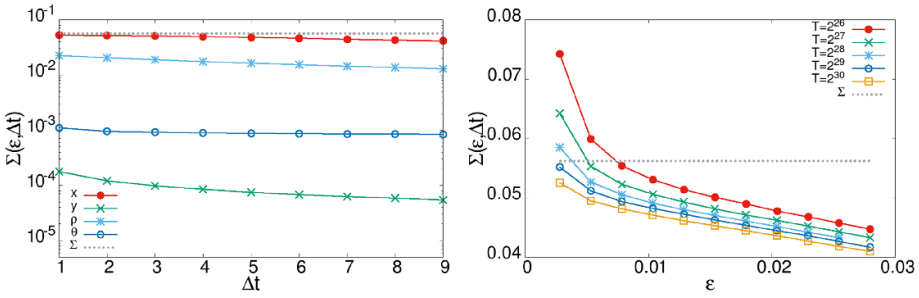

Figure 12. $\Sigma(\epsilon, \Delta t)$ computed with 1D signals. Left: dependence on Δt at fixed little ϵ of $\Sigma(\epsilon, \Delta t)$ for several observable. Right: dependence on ϵ at fixed $\Delta t = 1$ of $\Sigma(\epsilon, \Delta t)$ computed with the x-component only.

rate, but again some kind of lower bound which should be sufficient, when not zero, to put in evidence the non-equilibrium nature of the system. One of the underlying ideas, here, is to exploit the information-theoretic formulation of entropy production to decompose it into different contributions depending on the experimentally accessible information. These approaches are interesting because they have unveiled non-trivial aspects of the theory of stochastic processes, but at the same time they suffer from the same limitations encountered in the TURs, i.e. the general and obvious fact that partial information cannot account for the full information required to characterize the entropy production of a given dynamics.

To be more specific, let us consider a Markov process s taking values in finite (countable) space $\Omega = \{1 \cdots N\}$. According to equation (7), the entropy production of such process reads

$$\Sigma^{(\Omega)} = \lim_{t\to\infty} \frac{1}{t} \sum_{\mathbf{s}^{(t)}} P\left(\mathbf{s}^{(t)}\right) \log\left(\frac{P\left(\mathbf{s}^{(t)}\right)}{P\left(\mathbf{s}^{(t)}_{\leftarrow}\right)}\right). \tag{62}$$

Generally, in an experiment the micro-space Ω is not accessible and only some macroscopic quantities $a(s)$ can be measured. Denoting Γ the state-space corresponding to these macroscopic observables, a general result in information theory [14, 43] guarantees

$$\Sigma^{(\Omega)} \geqslant \Sigma^{(\Gamma)} = \lim_{t\to\infty} \frac{1}{t} \sum_{\mathbf{a}^{(t)}} P\left(\mathbf{a}^{(t)}\right) \log\left(\frac{P\left(\mathbf{a}^{(t)}\right)}{P\left(\mathbf{a}^{(t)}_{\leftarrow}\right)}\right). \tag{63}$$

Starting from the above formula, several bounds can be established depending on the assumptions on the dynamics in the state-spaces Ω and Γ.

For example, in [127] the authors provide a semi-analytical formula for an efficient estimation of the right-hand-side of equation (63) based on the theory of products of random matrices. Their results rely on the assumption that the set of 'macroscopic' variables a consists in a sub-set of the micro-state s, for instance $s = \{s_1, s_2\}$ and $a = s_1$. Moreover, their approximation requires the knowledge of the dynamics behind the observations and therefore is not practical for modeling real-world experiments. In [47], a new approach for estimating the entropy production from time-series measurements is proposed. The central result consists in an analytical expression for the entropy production of a semi-Markov process, i.e. a generalization of Markov processes where the waiting-time distributions can be non-Poissonian. It is shown that the entropy production rate has two different sources. One source accounts for the irreversibility generated by transitions between the states of the process regardless of the transition-times distribution, while the second contribution is due to the non-exponential distributions of the exit times. Treating molecular motors and partially hidden Markov networks, the authors provided evidence that their method is able to detect time irreversibility even in the absence of observable currents. This approach, however, is limited to scenarios where the coarse-graining operation commutes with time-reversal [48], as it fails to correctly identify broken detailed balance in other cases [49]. In [128, 129] the problem is approached from a different perspective. Motivated by models used in neuroscience, the authors consider the case of multipartite dynamics. In short, each micro-state $s = (s_1, \cdots, s_D)$ is a list of D degrees of freedom corresponding to separate units in the system, and for sufficiently short sampling times two successive micro-states $s = (s_1, \cdots, s_D)$ and $s' = (s'_1, \cdots, s'_D)$ differ by the value of one unit only ($s_i = s'_i$ for all $i \neq j$). For these systems, the authors show that the entropy production rate can be decomposed into two contributions $\Sigma = \Sigma_{\text{ind}} + \Sigma_{\text{int}}$. The term Σ_{ind}

is related to single unit time series $(\mathbf{s}_1, \cdots \mathbf{s}_D)$ considered independently one from each other taking the form

$$\Sigma_{\text{ind}} = \lim_{t\to\infty} \frac{1}{t} \sum_{i=1}^{D} \sum_{\mathbf{s}_i} P(\mathbf{s}_i) \log\left(\frac{P(\mathbf{s}_i)}{P(\mathbf{s}_{i,\leftarrow})}\right) \tag{64}$$

while the term $\Sigma_{\text{int}} = (\Sigma - \Sigma_{\text{ind}}) \geqslant 0$ accounts for the interaction between units. Moreover, exploiting a hierarchy of bounds on entropy production, obtained by including more and more macroscopic variables a in the coarse-grained description (see [130] for further details), it is also shown that the interaction term can be further decomposed in contributions which accounts separately for nth order interactions (interactions among $n \leqslant D$ units). Another particularly fascinating approach in this framework consists in studying the transition statistics of the system, i.e. for instance the distribution of the waiting times for the return or the passage of some observables through a given value. This approach has been studied for instance in [131, 132]. Differently from [47], the authors do not make additional assumption on the coarse-grained dynamics, and instead they look for the Markov model with hidden variables, compatible with the observed waiting times distribution, that minimizes the entropy production. If this minimum entropy production is non-zero, then the observed data must originate from a non-equilibrium system. In Skinner [132] this approach has been applied to experimental data for gene regulatory networks, mammalian behavioral dynamics, and numerous other biological processes such as the heartbeat regulation in humans, dogs, and mice. As for [47], the interest of this approach is that it can retrieve some non-zero lower bound for the entropy production even with data that are time-reversal symmetric, e.g. when there are no visible currents. The bound coming from jump rates, however, can be quite loose, especially in these last cases. An alternative approach is presented in [133], that uses all observable data (not only transition rates) to find an underlying hidden Markov model responsible for generating the observed non-Markovian dynamics. Recently, some authors realized that considering non-conventional coarse-graining procedures in which macroscopic variables a are identified with microscopic transitions (i.e. transitions between microstates s and s') leads to semi-Markovian dynamics for the coarse-grained processes [134]. Thus, in complete analogy with [47, 133], a lower bound for the entropy production rate is derived that equals the sum of two non-negative contributions, one due to the statistics of transitions (conditional probabilities of observed occurrence of the system in some state) and a second due to the statistics of intertransition times. The applications to experimentally validated biophysical models of kinesin and dynein molecular motors, and in a minimal model for template-directed polymerization reveals, again, that this strategy is suitable for detecting irreversibility even in the absence of net currents in the transition time series. A general theory encompassing all the above-mentioned cases was developed in [50, 135]. This theory does not make any kind of assumptions about the dynamics of coarse-grained variables, but instead considers the observables in a very general way as a joint collection of events and waiting times. By exploiting these generalized waiting times distribution, the authors formulate entropy estimators resembling the formulas appeared in [47, 133, 134] whose efficiency can be evaluated from the data themselves. Furthermore, in certain cases, these estimators allow one to retrieve information regarding the topology of the underlying network. As with other estimators based on waiting times, with this approach it is possible to obtain non-zero entropy production even if all macroscopic events are invariant under time-reversal. To do so, however, the joint distribution $\psi(t_1, \cdots, t_k)$ of the waiting times should not be invariant under time-reversal, i.e. $\psi(t_1, \cdots, t_k) \neq \psi(t_k, \cdots, t_1)$ for some $\{t_1, \cdots, t_k\}$, and, as clearly explained in [50], the difference $\psi(t_1, \cdots, t_k) - \psi(t_k, \cdots, t_1)$ play the role of a steady current. To conclude the section, we recall that in certain cases serious limitations appear for the above approaches. Imagine that the states-space Ω contain the states of a discrete-time Markov chain while the coarse-grained space Γ contains just two elements $\{a_0, a_1\}$ with $a_0 = \{1\}$ and $a_1 = \{2, \cdots, N\}$. As shown in [45], the resulting process is a 2-state semi-Markov process and the entropy production vanishes, regardless of whether the Markov chain defined on Ω satisfies or not detailed balance. For this class of processes it therefore seems impossible to determine the thermodynamic nature of the system without making further assumptions on the models that generate the observations.

5. Lack of equilibrium and causation indicators

As discussed in the previous sections, entropy production quantifies the degree of irreversibility in the dynamics of non-equilibrium systems. Due to its global nature, it lacks sensitivity to the structural details of a system, e.g., inhomogeneity in temperature and chemical gradients, or non-reciprocal interactions [136, 137], such as asymmetries in the couplings between different sites or degrees of freedom. Therefore, if one is interested in the specific description of the internal currents driving the system out of equilibrium, it is mandatory resorting to more microscopic or local observables. To this goal, promising candidates are the transfer entropy (TE) [138, 139] and Response functions [2, 140], which are usually employed to detect

causal relationships between system variables [13, 141]. In fact, it is intuitively expected that the presence of a physical current—usually a signature of time-irreversibility—determines an information flow and, therefore, causal relations among different parts of the system. In this section, we show by means of simple models that local causal indicators can provide insights into how spatial asymmetries and non-reciprocal interactions drive the system towards non-equilibrium states.

Before delving into the definitions of TE and response functions, it is essential to make a brief excursion through the notion of causation that stands as a cornerstone concept across various disciplines, including philosophy, natural and social sciences and engineering. Also, it helps the comprehension of our everyday experience, allowing us to make informed decisions. Cause-effect principles are implicitly or explicitly employed when quantitative theories are developed in terms of equations involving parameters and quantities. Nowadays, in the era of Big Data and Artificial Intelligence, the concept of causation is gaining even more importance.

The philosopher David Hume was among the pioneers in formalizing the concept of causation [142], by proposing the idea of simultaneous recurrence of events: a causal relationship between A and B (represented symbolically as $A \to B$) can be inferred when the consistent observation of B is always preceded by A. In more precise words, finding causation between a set $\{X_1, X_2, \ldots, X_M\}$ of events, variables, or observables etc means to construct a directed graph where each X_i represents a node and the causal connections are oriented links pointing from X_i (cause) $\to X_j$(effect). In this respect, causal indicators, algorithmic procedures and statistical tests become fundamental tools to establish quantitatively the connections among nodes [143].

Two different strategies can be followed in the definition of causal indicators. The first one, deriving directly from Hume's view, can be referred to as *observational*, because causality is detected only by observation of time series of events or data. In a nutshell, the goal is to understand from data whether, and to what extent, the knowledge of a certain variable is useful to the actual determination of present and future values of another one. In other words, if one observes that knowledge of the past states of variable $Y(t)$ improves the accuracy of forecasting future values of $X(t)$, it can be deduced that Y has a certain influence on X: in symbols, $Y \to X$. This is the spirit of Granger Causality [144] as well as of TE [138].

The other approach, termed *interventional*, assumes that two variables are in a cause-effect relationship if an external action on one of them changes the observed value of the other. J. Pearl formalized this idea through the notion of 'Do' operation [145], used to express interventions where a variable is set to a specific value to see the system's response. In this context, causality coincides with the possibility to predict the result of the intervention. The interventional definition is a more physics-inspired interpretation of cause-effect relationships that can be quantified by a well-known observable, the response function [28]. This approach to the study of causation has been recently analyzed and used in a series of works [23, 24, 141, 146–148].

In the following, we briefly provide a mathematical definition of these two causal indicators, also leading to their operational employment.

5.1. Transfer entropy

TE from process X_t to process Y_t is a concept borrowed from information theory introduced by Schreiber [138] in the context of stochastic processes and dynamical systems and then reformulated by Paluš *et al* [149] as conditional mutual information. Generally speaking, the entropy transfer from the evolution of the degree of freedom $x_j(t)$ to the evolution of the degree of freedom $x_i(t)$ is defined as the information (uncertainty) that we gain (lose) on the future states of x_i, if we not only consider the history of x_i, but we also include the past of x_j. It quantifies the causal influence of x_j on x_i, in formulae,

$$\mathrm{TE}_{j\to i}(\tau) = \left\langle \ln \frac{P\left[x_i(t) \,\middle|\, \mathbf{X}_i^{(\tau)}, \mathbf{X}_j^{(\tau)}\right]}{P\left[x_i(t) \,\middle|\, \mathbf{X}_i^{(\tau)}\right]} \right\rangle. \tag{65}$$

Here t is a time index, $\mathbf{X}_i^{(\ell)} = \{x_i(t-1), \ldots, x_i(t-\tau)\}$ and $\mathbf{X}_j^{(\tau)} = \{x_j(t-1), \ldots, x_j(t-\tau)\}$ are the past states of variables $x_i(t)$ and $x_j(t)$ respectively. The angular-brackets denote the average over the joint probability density $P\left[x_i(t), \mathbf{X}_i^{(\tau)}, \mathbf{X}_j^{(\tau)}\right]$, while $P\left[x_i(t) \,\middle|\, \mathbf{X}_i^{\tau}, \mathbf{X}_j^{(\tau)}\right]$ and $P\left[x_i(t) \,\middle|\, \mathbf{X}_i^{\tau}\right]$ are the probability densities of $x_i(t)$ conditioned to the past histories. Notice that TE identically vanishes for $i = j$ and is by definition asymmetric, $\mathrm{TE}_{j\to i} \neq \mathrm{TE}_{i\to j}$, thus naturally incorporating a direction of the entropy/information transfer from $x_j \to x_i$, that is generally different from $x_i \to x_j$. Note that the asymmetry is a natural consequence of the non-interchangeability between conditioning and conditioned events.

As clear from equation (65), TE measures how much information is gained on the future of x_i when taking into account the past history, $\mathbf{X}_j^{(\tau)}$,

$$\mathrm{TE}_{j\to i} = H\left[x_i(t) \,|\mathbf{X}_i^{(\tau)}\right] - H\left[x_i(t) \,|\mathbf{X}_i^{(\tau)}, \mathbf{X}_j^{(\tau)}\right], \tag{66}$$

where $H[A|B]$ indicates the conditional Entropy of the state A given the state B. Note that equation (66) implicitly assumes stationary processes.

The TE among degrees of freedom of a multivariate linear Gaussian Markov system (Ornstein-Uhlenbeck process often employed in this review),

$$\dot{\mathbf{x}} = -\mathrm{A}\mathbf{x} + \boldsymbol{\xi}\,,$$

can be easily expressed in terms of their time correlations $\mathcal{C}_{ij}(t) = \langle x_i(t)x_j(0)\rangle$,

$$\mathrm{TE}_{j\to i}(t) = -\frac{1}{2}\ln\left(1 - \frac{\alpha_{ij}(t)}{\beta_{ij}(t)}\right) \tag{67}$$

where

$$\alpha_{ij}(t) = \left(\mathrm{C}_{ii}\mathcal{C}_{ij}(t) - \mathrm{C}_{ij}\mathcal{C}_{ii}(t)\right)^2, \tag{68}$$

$$\beta_{ij}(t) = \left(\mathrm{C}_{ii}\mathrm{C}_{jj} - \mathrm{C}_{ij}^2\right)\left(\mathrm{C}_{ii}^2 - \mathcal{C}_{ii}^2(t)\right), \tag{69}$$

see [13, 141] for the derivation, and we indicate with $\mathrm{C}_{ij} = \mathcal{C}_{ij}(0)$ the correlation matrix at zero lag (i.e. the covariance matrix). The asymmetry $\alpha_{ij}(t) \neq \alpha_{ji}(t)$ and $\beta_{ij}(t) \neq \beta_{ji}(t)$ is a straightforward consequence of the TE asymmetry emerging also in the Gaussian formulation.

It is possible to show that $\mathrm{TE}_{j\to i}(\infty) = 0$, either by definition (65) invoking the independence of events far away in time, or using the correlation decay at large times in equation (67) implying that $\alpha_{ij}(\infty) \to 0$. Analogously, one expects $\mathrm{TE}_{j\to i}(0) = 0$. As a consequence, in many cases, TE is expected to have a skewed bell-shaped curve as a function of the time lag t.

5.2. Response function

The other causal indicator that could be useful to employ in out-of-equilibrium systems is the response function, which belongs to the interventional framework: indeed, the coordinate x_j causally influences the coordinate x_i, if a perturbation of x_j results in a variation of the measured value of x_i. In formulae, we say that $\mathrm{x_j}$ influences $\mathrm{x_i}$, if

$$\mathcal{R}_{ij}(t) = \lim_{\delta x_j(\tau)\to 0} \frac{\overline{\delta x_i(\tau + t)}}{\delta x_j(\tau)} \neq 0 \qquad \text{for some } t > \tau\,, \tag{70}$$

i.e. a small perturbation on $x_j(\tau)$ at time τ results in a non-zero future variation on the average of $x_i(t+\tau)$ over its unperturbed evolution. In equation (70), we again assume statistically stationary dynamics as in equation (66). If δx_j is small enough, it is well known that the quantity (70) can be related to the spontaneous correlations in the unperturbed dynamics by one of the pillars of non-equilibrium statistical mechanics, the fluctuation-response theorem (FRT) [20], also known as fluctuation-dissipation theorem. When the process $\mathbf{x}(t)$ is stationary with invariant PDF $P_s(\mathbf{x})$, the response (70) assumes the clear and general expression equation (27) seen in section 3.

It should be remarked that equation (27) holds for systems with an invariant PDF and in general cases, it expresses the response in terms of complicated multivariate correlation functions. However, in systems governed by stochastic linear dynamics, even with no Gaussian noise, the response turns out to be related only to the two-time correlation function, [24]

$$\mathcal{R}(t) = \mathcal{C}(t)\,\mathrm{C}^{-1}\,. \tag{71}$$

as we already proven in section 3 equation (13).

5.3. A toy model with non-reciprocal interactions

The link between non-reciprocal interactions, causation and lack of equilibrium can be appreciated by considering linear systems, which are fully analytically solvable. As a first example, we consider the minimal non-equilibrium model discussed in [24]: a system of three variables x_t, y_t and z_t, whose values are updated at discrete times according to the rule

$$x_{t+1} = ax_t + \varepsilon y_t + \eta_t^{(x)} \tag{72a}$$

$$y_{t+1} = ax_t + ay_t + \eta_t^{(y)} \tag{72b}$$

$$z_{t+1} = ax_t + az_t + \eta_t^{(z)}\,, \tag{72c}$$

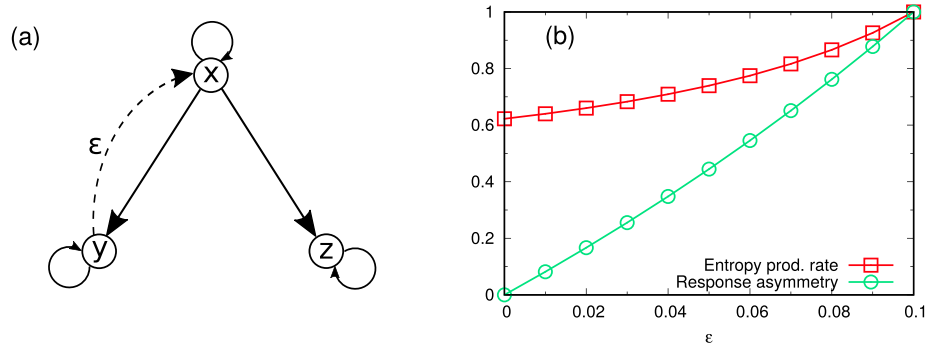

Figure 13. Entropy production rate and response asymmetry in a simple toy model with non-reciprocal interactions. The system is sketched in panel (a), where solid lines refer to a value a = 0.5 in the interaction matrix (see equation (72)) and the link corresponding to the dashed line is taken as a varying parameter ε. Panel (b) shows the entropy production rate (red) and the response asymmetry $\widetilde{R}_{zy} - \widetilde{R}_{yz}$ (green). Both quantities are rescaled by their values at $\varepsilon = 0.1$.

where, η_t's are independent Gaussian variables with zero mean and unitary variance, while a and ε are assigned constants. The model is sketched in figure 13(a). When $\varepsilon = 0$, the variable x is independent of y and z, and drives them in the same way: the system is thus symmetric with respect to the exchange of y and z. As soon as $\varepsilon > 0$, a feedback mechanism indirectly couples z to y (meaning that the former is influenced by the latter). The presence of non-reciprocal interactions drives the system out of equilibrium, and, thanks to linearity, the entropy production rate can be easily computed. Figure 13(b) shows that the entropy production rate is nonzero for every choice of ε.

Although the system is still out of equilibrium at $\epsilon = 0$, when ε is increased, the entropy production rate of the system increases as well, suggesting that the dynamics is becoming more irreversible. The origin of this increment of the time-reversal asymmetry can be understood by looking at the causation indicators introduced in the previous section. By computing the difference between the response function (integrated in time)

$$\widetilde{R}_{zy} = \sum_{t=0}^{\infty} \mathcal{R}_{zy}(t)$$

and

$$\widetilde{R}_{yz} = \sum_{t=0}^{\infty} \mathcal{R}_{yz}(t)\,,$$

one gets a quantitative estimator of the y,z causation asymmetry. This difference is reported in figure 13(b); as expected, it vanishes when $\varepsilon = 0$, meaning that equilibrium is broken by other mechanisms (in this case, the x,y and x,z asymmetries).

This simple example shows that, in the presence of non-reciprocal interactions, response functions (or any other reliable indicators of causation) provide detailed information on the origin of the time-reversal asymmetries that drive the system out of equilibrium. While the entropy production rate is a global quantity, which only signals to what extent the system is out of equilibrium, causation indicators are actually able to unveil the asymmetries that are responsible for the non-equilibrium state [150]. In the following section, we will analyze a case where the scenario is enriched by the presence of temperature gradients.

5.4. Oscillators with non-reciprocal interactions and temperature gradient

In this section, we apply TE and response functions to characterize the effect of spatial symmetry-breaking in an example of linear out-of-equilibrium extended systems [13].

Consider a system of N interacting particles whose individual positions are denoted by $\{x_j\}$, with j ranging between 1 and N. Particles are coupled via nearest-neighbor elastic forces

$$F_j = -k_L\left(x_j - x_{j-1}\right) - k_R\left(x_j - x_{j+1}\right)\,.$$

Periodic boundary conditions $x_0 \equiv x_N$, $x_{N+1} \equiv x_1$ are implemented, and by setting

$$k_L = k_0 - \varepsilon$$
$$k_R = k_0 + \varepsilon\,,$$

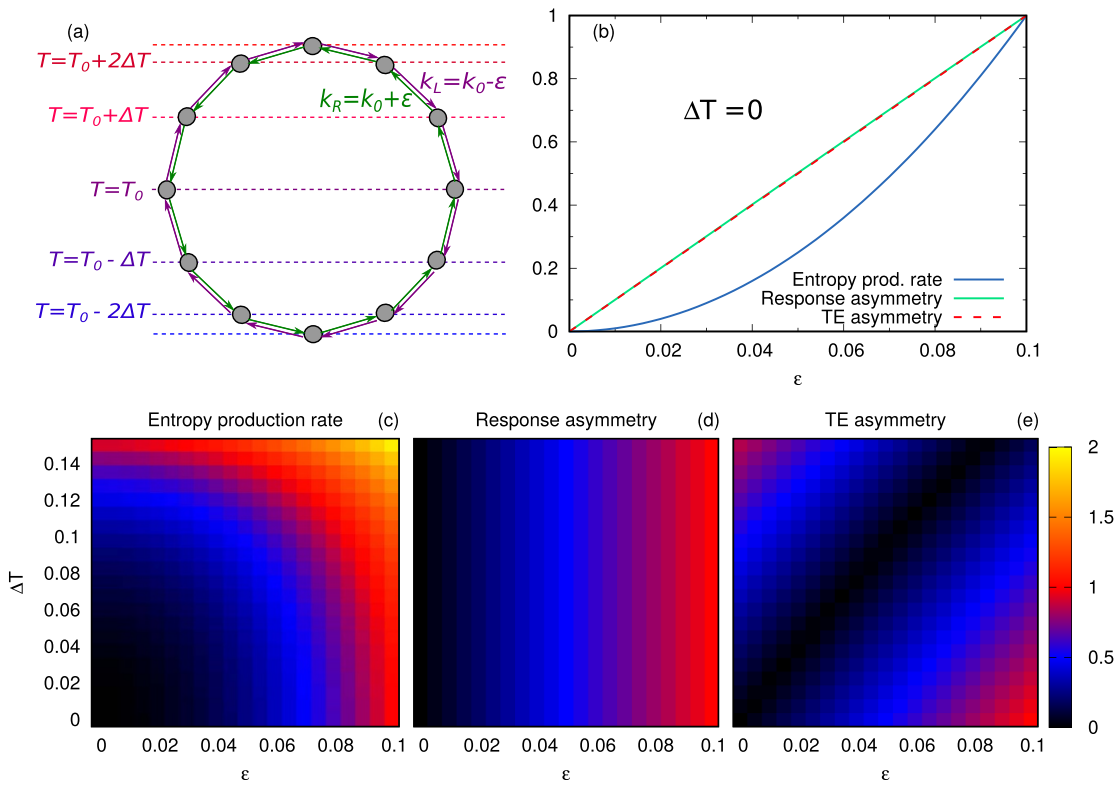

Figure 14. Asymmetry indicators in the ring model. Panel (a): scheme of the interactions between the particles, as well as the temperature gradients. Panel (b): asymmetry indicators and entropy production rate for $\Delta T = 0$, as a function of ε. All quantities are rescaled setting their value at $\varepsilon = 0.1$ equal to unity. Panels (c)–(e): heat maps of the quantities considered in panel (b) as a function of ε and ΔT. Again, all quantities are rescaled with their value for $\varepsilon = 0.1$ and $\Delta T = 0$. Parameters: $T_0 = 1, k_0 = 1, N = 20$.

the symmetry of the interactions is broken as soon as $\varepsilon \neq 0$. Each particle is also subject to a restoring force $-k_0 x_j$, and to the action of an inhomogeneous thermal bath with site-dependent temperature T_j. The stochastic dynamics of x_j can thus be written, in the overdamped limit, as

$$\gamma \dot{x}_j = -3k_0 x_j + k_L x_{j-1} + k_R x_{j+1} + \sqrt{2\gamma k_B T_j}\,\xi_j \tag{73}$$

where ξ_j is zero-mean white Gaussian noise. Hereafter, we adopt dimensionless units corresponding to Boltzmann constant $k_B = 1$ and viscous coefficient $\gamma = 1$.

The system stays in equilibrium if $\varepsilon = 0$ and the bath is homogeneous, $T_j \equiv T_0$. It can be driven out of equilibrium by breaking the detailed balance, in two ways: (a) switching the interactions asymmetry on, $\varepsilon > 0$, so that mechanical currents are induced across the ring; (b) enforcing a thermal gradient

$$T_j = T_0 + \Delta T \left(\left| j - \frac{N}{2} \right| - \frac{N}{4} \right),$$

where ΔT is a suitable constant.

In the absence of mechanical asymmetry, $\varepsilon = 0$, the above choice leads to a heat flux from the hottest sites ($j = 0, j = N$) to the coldest site ($j = N/2$). A schematic representation is shown in figure 14(a). The model has therefore two different sources of spatial asymmetry: the non-reciprocity of the interactions and the temperature gradient.

The dynamics can be written in the form of a linear stochastic process

$$\dot{\mathbf{x}} = -A\mathbf{x} + \boldsymbol{\xi},$$

where A is a $N \times N$ circulant matrix and $\boldsymbol{\xi}$ is a noise with diagonal correlations, i.e. $\nu_{ij} = \langle \xi_i \xi_j \rangle = 2T_i \delta_{ij}$. The properties of circulant matrices ensure that all the eigenvalues of A have a positive real part. As proven in section 3.2 (see also [37]), for such a system the correlation and response functions are respectively

$$\mathcal{C}(t) = \mathrm{e}^{-At} C \quad (\forall t > 0), \qquad \mathcal{R}(t) = \Theta(t)\, \mathrm{e}^{-tA}$$

$\Theta(t)$ being the unitary step-function, and the covariance matrix $C = \mathcal{C}(0)$ of the stationary state verifies $AC + CA^T = \nu$. Moreover, entropy production rate can be written as $\Sigma = \mathrm{Tr}\left(\Delta\nu^{-1}A\right)$ where $\Delta = CA^T - AC$ measures the violation of Onsager's condition.

All the quantities previously introduced for the characterization of out-of-equilibrium systems can be explicitly computed. In figure 14, we compare the behavior of Σ with two observables ΔR and ΔTE that quantify the spatial asymmetry of the response and of the TE. The former is defined as

$$\Delta R = \left| \sum_{j=1}^{N/4-1} \widetilde{R}_{j,N/4} - \sum_{j=N/4+1}^{N/2-1} \widetilde{R}_{j,N/4} \right| \tag{74}$$

where

$$\widetilde{R}_{ij} = \int_0^\infty \mathrm{d}t \mathcal{R}_{ij}(t) \, .$$

This 'integrated response', inspired by the Kubo relations [19], takes into account the cumulative effect of j on i. The imbalance ΔR is therefore vanishing when the effect of the particle $N/4$ on the first $N/4-1$ neighbors on the left and on the right is the same, while it is larger than zero if a spatial asymmetry is present.

Similarly, for the TE rate we introduce the unbalance

$$\Delta\mathrm{TE} = \left| \sum_{j=1}^{N/4-1} \mathrm{TE}_{j,N/4} - \sum_{j=N/4+1}^{N/2-1} \mathrm{TE}_{j,N/4} \right| . \tag{75}$$

Figure 14(b) shows that, for vanishing temperature gradient, ΔR and ΔTE provide the same kind of information, and their value is monotonically related to the entropy production rate. This is consistent with the fact that the (mechanical) asymmetry in the dynamics is the only source of equilibrium violation. In figures 14(c)–(e) a nonzero temperature gradient is also included, and the qualitative difference between response and TE becomes evident: while the former only depends on the interaction forces between the particles, the latter is dramatically affected by the presence of heat flow.

The above example clarifies that the information coming from the analysis of the entropy production has to be complemented by other asymmetry indicators in order to provide an exhaustive description of the local currents leading the system out of equilibrium.

6. Turbulence: a case study

In the previous sections we have mostly focused on simple, mainly stochastic, models; in this section, we end our tour considering an important instance of persistent non-equilibrium phenomenon, namely the turbulent state realized in incompressible flows at high Reynolds number [151].

The evolution of the velocity field, $\boldsymbol{u}(\boldsymbol{x}, t)$, of an incompressible ($\boldsymbol{\nabla} \cdot \boldsymbol{u} = 0$) fluid is ruled by Navier–Stokes equation [152]:

$$D_t \boldsymbol{u} \equiv \partial_t \boldsymbol{u} + \boldsymbol{u} \cdot \boldsymbol{\nabla} \boldsymbol{u} = -\frac{\boldsymbol{\nabla} p}{\rho} + \nu \Delta \boldsymbol{u} + \boldsymbol{f} \, , \tag{76}$$

where D_t denotes the material derivative, $p = p(\boldsymbol{x}, t)$ the pressure, ρ the (constant) mass density, ν the kinematic viscosity and $\boldsymbol{f}$ a stirring force. For $\nu = 0$ and $\boldsymbol{f} = 0$, equation (76) becomes the Euler equation that, in the presence of an ultraviolet cutoff, is known to be an equilibrium system [153]. In viscous fluids ($\nu \neq 0$), the force $\boldsymbol{f}$ injects energy at a scale L at a rate (per unit mass):

$$\varepsilon = \langle \boldsymbol{f} \cdot \boldsymbol{u} \rangle \, , \tag{77}$$

where $\langle [\ldots] \rangle$ denotes an average over space and time. The nonlinear terms of equation (76) preserve the total kinetic energy but redistribute it among the scales. In particular, in three dimensional (3D) turbulence, energy is transferred to smaller and smaller scales till it is dissipated by the viscous forces. Thus, the system eventually reaches a (non-equilibrium) statistically stationary state, where, on average, the injection and dissipation rates balance. Such a process, which is a peculiar feature of 3D turbulent fluids, is dubbed 'direct energy cascade' [154]. A simple handwaving argument (see e.g. [155]) can be used to understand why in 3D turbulence the energy flows from large to small scales. Rewriting equation (76) for the vorticity ($\boldsymbol{\omega} = \boldsymbol{\nabla} \times \boldsymbol{u}$) and ignoring forcing and dissipation, we obtain $\partial_t \boldsymbol{\omega} + \boldsymbol{u} \cdot \boldsymbol{\nabla} \boldsymbol{\omega} = \boldsymbol{\omega} \cdot \boldsymbol{\nabla} \boldsymbol{u}$, where the term in the r.h.s., usually called the vortex stretching term, is clearly responsible for the increase of the square vorticity, i.e. of the

enstrophy. However, the above equation is nothing but the 3D Euler equation, which preserves energy, so for enstrophy to grow energy should be transferred to the small scales, which contribute the most to enstrophy.

In the turbulent state there is a large separation between the scale of energy injection L and that of dissipation [151], which can be estimated by dimensional argument as $\eta = (\nu^3/\varepsilon)^{1/4}$—i.e. the so-called Kolmogorov scale. In the inertial range, $\eta \ll r \ll L$, both energy injection and dissipation are negligible and the statistical properties are believed to be universal and display non-trivial scaling laws [154]. Moreover, the system is characterized by a wide spectrum of timescales from $\tau_L = L/u_{\rm rms}$ (where $u_{\rm rms} = \langle |\boldsymbol{u}|^2 \rangle^{1/2}$) at the largest scale to $\tau_\eta = (\nu/\varepsilon)^{1/2}$ at dissipative scales. Formally, the limit of infinite scale separation, or infinite Reynolds number, $Re = UL/\nu \to \infty$, (U being a typical large-scale velocity) is called 'fully developed turbulence'. Therefore, turbulence is a multi-scale phenomenon involving many spatial scales each with its characteristic time.

By performing some statistical analysis, it is not hard to prove that turbulent systems are out of equilibrium: the nonzero average energy flux across scales, when computed in wavevector space, is roughly the sum of third-order moments of the velocity field, and this nonzero skewness of the velocity PDFs is incompatible with statistical equilibrium.

In the following, we will explore two less straightforward aspects of turbulence. First, as first demonstrated in [25], we will show how asymmetric correlation functions can reveal and somehow quantify the irreversible and thus non-equilibrium character of turbulence by looking at the motion of a single fluid tracer (adopting the so-called Lagrangian view of turbulence), that is by looking at the evolution of a very small, neutrally buoyant particle transported by the flow. Clearly, a single particle trajectory provides only a partial information on the state of the fluid velocity field and, as previously discussed (see, e.g. sections 3.3.1 and 4.2) inferring and quantifying non-equilibrium properties from partial observation is, in general, nontrivial. Second, we will show that asymmetric correlation functions and response functions, thoroughly employed in the previous sections, can be used to reveal the non-equilibrium (equilibrium) character of the physics at scales smaller (larger) than the energy injection scale, as shown in [27] in the context of shell models for turbulence, which constitute a simplified laboratory for turbulent phenomenology that will be detailed below. Before discussing these two aspects, we mention other non-conventional approaches to the study of the nonequilibrium nature of the energy cascade, such as that proposed in [156] where, using ideas from stochastic thermodynamics, an integral fluctuation theorem is verified for experimental data of velocity differences measured at various scales r in the inertial range.

6.1. Lagrangian irreversibility

The dynamics of a fluid tracer, which in a laboratory can be realized by considering a very small particle having the same density of the fluid, is ruled by the following equation

$$\dot{\boldsymbol{X}}(t) = \boldsymbol{V}(t) = \boldsymbol{u}(\boldsymbol{X}(t), t) \ , \tag{78}$$

where $\boldsymbol{X}(t)$ denotes the position of the Lagrangian tracer at time t, and $\boldsymbol{V}(t)$ is the velocity field at the particle position. How to recognize the signature of the non-equilibrium turbulent state by looking at the dynamics of fluid tracers was first discussed in [25, 157] where, using both experimental and numerical Lagrangian trajectories, it was shown that tracers experience slow buildups of kinetic energy followed by sudden discharges, a phenomenon dubbed 'flight-crash' event: a clear sign of time irreversibility at the level of a single tracer particle, and yields breaking of the detailed balance condition since forward and backward transitions are not equiprobable (see section 2.2). This can be revealed by studying the statistics of the tracer kinetic energy per unit mass, $E(t) = \frac{1}{2}|\boldsymbol{V}(t)|^2$.

Figure 15 displays a qualitative demonstration of a flight-crash event. In particular, figure 15(a) displays the 3D evolution of a tracer trajectory with color-coded the rate of energy change, i.e. Lagrangian power $p(t) = {\rm d}E(t)/{\rm d}t = \boldsymbol{A}(t) \cdot \boldsymbol{V}(t)$ ($\boldsymbol{A}(t) = \dot{\boldsymbol{V}}(t)$). While figure 15(b) shows the time evolution of the kinetic energy with a zoom (figure 15(c)) in the region where energy slowly increases and suddenly decreases. The dissimilarity between the rate of increase and decrease of kinetic energy can be measured statistically by the probability of observing an energy change after a time increment τ, $E(t+\tau) - E(t)$. According to the mechanism described above, the PDF of this quantity is expected to be skewed, so that a good measure of irreversibility could be the non-dimensional third-order moment

$$\Phi_E(\tau) = \frac{\langle [E(t+\tau) - E(t)]^3 \rangle}{\langle E(t) \rangle^3} \, . \tag{79}$$

The above quantity, whose numerator, owing to statistical stationarity, can be expressed as the asymmetric correlation function $\langle E(t+\tau)E^2(t)\rangle - \langle E^2(t+\tau)E(t)\rangle$ [16] (see also section 2.2), is negative (figure 16) and its modulus grows at short time separation as τ^3. The short-time behavior is indeed controlled by the third

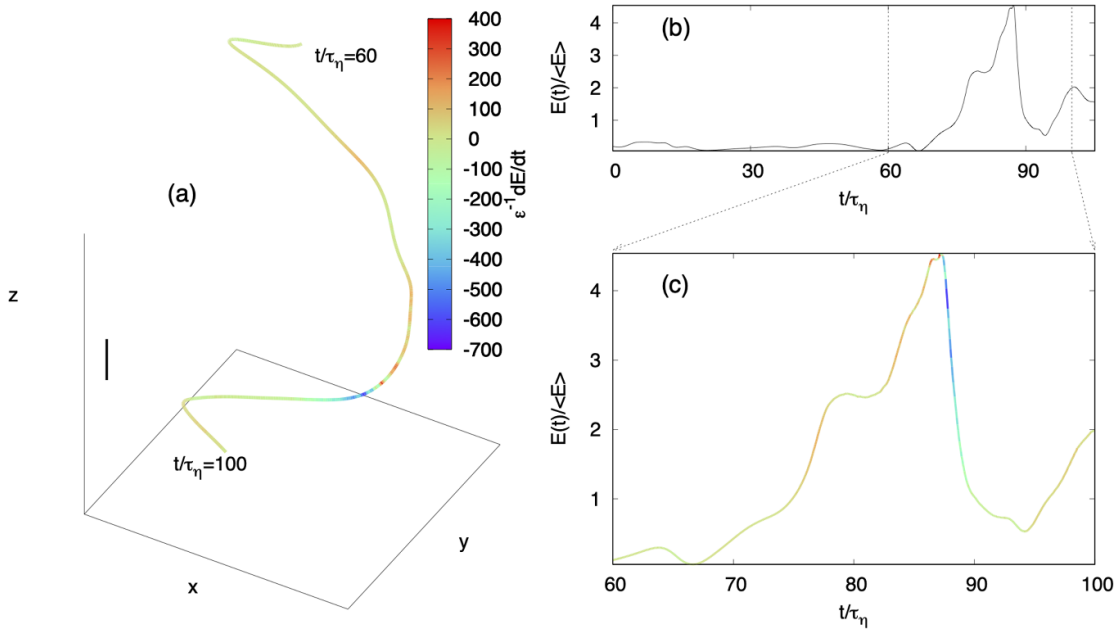

Figure 15. Qualitative explanation of the asymmetry in the statistics of energy increments. (a) Cut of a tracer trajectory in a turbulent flow. Color codes the instantaneous power $p(t) = \mathrm{d}E(t)/\mathrm{d}t = \boldsymbol{A}(t) \cdot \boldsymbol{V}(t)$. (b) Time evolution of the tracer kinetic energy $E(t)$. (c) Enlargement of (b) with the same color coding of (a) to show the so-called 'flight-crash' event where energy grows slowly and decreases quickly. After [25]. The trajectory was taken from the database [158] and refers to tracers evolving in turbulent flow at $Re_\lambda \approx \tau_L/\tau_\eta \approx 400$ obtained by direct numerical simulations with 2048^3 collocation points, as described in [159].

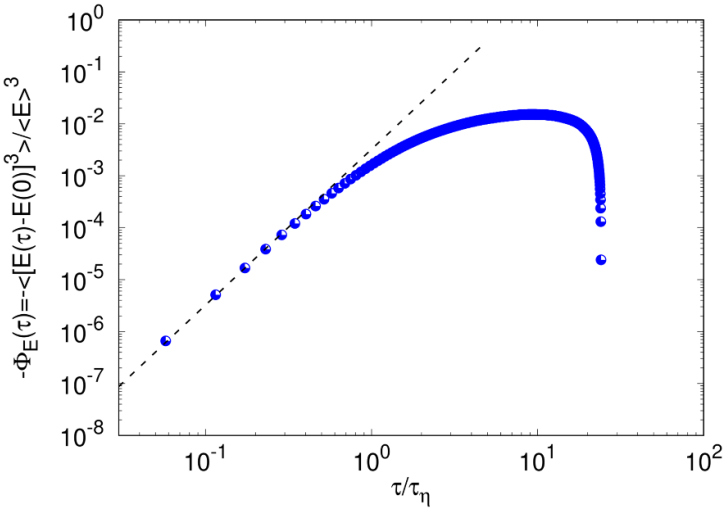

Figure 16. Correlation function of the particle kinetic energy computed as the third moment of the energy increment, as a function of τ, with inverted sign and time axis normalized by the Kolmogorov time τ_η. The small time behavior is cubic in τ, as shown by the dashed line. Data were taken from [158], see also caption of figure 15.

moment of the Lagrangian power, $p(t)$, and the statistics of the latter has been shown to display a non-trivially power law dependence on the Reynolds number [25], which was rationalized in terms of the multifractal model of turbulence [26].

The statistical analysis of flight-crash events can thus be connected with other statistical properties of turbulent flows, and it is quite significant that they allow for detecting non-equilibrium by looking at a very small portion (a single fluid element) of a turbulent flow.

6.2. Coexistence of equilibrium and non-equilibrium in a shell model of turbulence

In 3D turbulence, owing to the direct energy cascade as briefly summarized in the introduction to this section, the energy flow from the scale of injection toward that of dissipation so that the range of scales in between has a clear non-equilibrium character. What happens at scales larger than that of injection is less

clear. Numerical and experimental studies [160, 161] support the view [154] according to which the statistics of these large scales are compatible with statistical equilibrium, as for the Euler equation with ultraviolet cutoff [153]. This is evidenced, for instance, by energy equipartition taking place between these modes. Yet recent works [162, 163] showed that an equilibrium description is not completely correct because long-range interactions exist between small and large scales. Such feature is responsible, e.g. for a dependence of the spectrum at wavenumber smaller than the forced one from the specific forcing employed [163].

In principle, an answer to this riddle could be given by analyzing suitable time correlation functions. However, this is not an easy task in direct numerical simulations of equation (76) for several reasons including the fact that the phenomenon of sweeping (i.e. the advection of small-scale eddies by larger-scale eddies) can complicate the behavior of time correlations [164]. For this reason, in [27], this problem was approached in the framework of shell models in which, while retaining the main features of the turbulent energy cascade, sweeping is absent by construction.

The key idea of shell models [165–167] is to consider a collection of N interacting complex variables u_n, $n = 1, \ldots, N$, associated with wavenumbers $k_n = k_0 2^{n-1}$ describing a sequence of spherical shells in k-space with exponentially-growing radii. The shell variables u_n roughly represent velocity fluctuations at length scales $\sim 1/k_n$. Mimicking the Fourier representation of the Navier–Stokes equation, each shell variable evolves with an equation of the form

$$\dot{u}_n = ik_n Q[u,u] - \nu k_n^2 u_n + f_n\,, \tag{80}$$

where the last two terms represent dissipation and forcing, while quadratic term $Q(u,u)$ models the nonlinear (advection) term of equation (76). In principle, $Q(u,u)$ should couple each mode to all the others in a way to preserve the conservation laws of the Euler equation. In shell models, owing to the idea of locality [155] (i.e. that the most relevant interaction involves close-by wavenumbers), only nearest and next-to-nearest neighbors interactions are retained (we shall comment this assumption at the end of the section). For Sabra shell model [168], the quadratic term reads

$$Q[u,u] = 2u_{n+2}u^*_{n+1} - \tfrac{1}{2}u_{n+1}u^*_{n-1} + \tfrac{1}{4}u_{n-1}u_{n-2}\,, \tag{81}$$

where $*$ denotes complex conjugation, and boundary conditions $u_k = 0$ for $k < 1$ and $k > N$. The coefficients are chosen such that, as for the Navier–Stokes equation, in the inviscid unforced case ($\nu = f_n = 0$), two global conserved quantities exist, the total energy $E = \sum_{n=1}^{N} e_n$ and total helicity $H = \sum_{n=1}^{N} (-1)^n k_n e_n$, where:

$$e_n = |u_n|^2/2 \tag{82}$$

is the energy content of shell n. Shell models have a multiscale character, each shell variable having its own typical timescale. This is needed to reproduce the large hierarchy of time- and length-scales present in real turbulent flows.

As many studies have made clear, shell models share many features with turbulent flows, such as a well defined direct energy cascade with an energy flux ε, in the shells in between forcing and dissipation, which on average equal the energy injection and dissipation rates. The flux out of shell M, $\Pi_M^{(E)}$, due to the nonlinear term can be computed as

$$\Pi_M^{(E)} = -\sum_{n=1}^{M} \frac{\mathrm{d}e_n}{\mathrm{d}t} = k_M \mathrm{Im}\left[2u_M^* u_{M+1}^* u_{M+2} + u_{M-1}^* u_M^* u_{M+1}/2\right]. \tag{83}$$

Figure 17 shows the average energy per shell $\langle e_n \rangle$, which in shell models is also the energy spectrum. As clear from the figure, there is a clear difference between shells larger or smaller (i.e. scales below or above) than the two forced shells (indicated by filled symbols): larger ones are in the range of direct energy cascade, and show the expected scaling behavior of the energy spectrum (main panel) and a constant positive energy flux (inset). Conversely, shells smaller than the forced ones display energy equipartition and zero energy flux. Asymmetric time correlation functions [16] have been then studied to further inquire about the statistical character at scales above and below the forcing scale. In particular, in [27] it was studied

$$\Psi_{e_n}(\tau) = \frac{\langle e_n^2(t)\, e_n(t+\tau)\rangle - \langle e_n(t)\, e_n^2(t+\tau)\rangle}{\langle e_n^3(t)\rangle}\,, \tag{84}$$

in order to quantify time irreversible fluctuations shell by shell. Its behavior for shells larger or smaller than forcing is shown in figure 18. The correlation functions in the cascade range (main panel), i.e. at scales smaller than the forced ones, display a clear non-zero signal a nontrivial dependence on τ, which is linked to

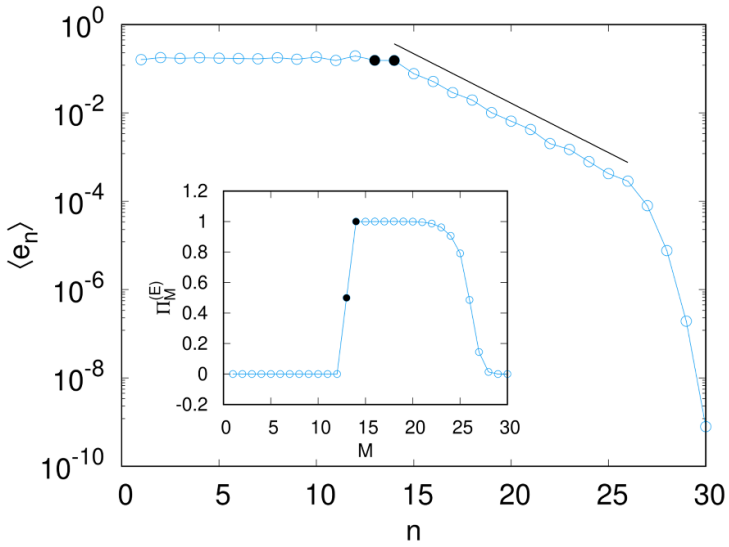

Figure 17. Numerical simulation of Sabra shell model with $N = 30$ shells and forcing on shells $n_f = \{13, 14\}$ (filled circles). Main: energy spectrum, showing equipartition for $n < n_f$ and anomalous scaling $\langle e_n \rangle \sim k_n^{-\zeta(2)} \sim 2^{-n\zeta(2)}$ for $n > n_f$. $\zeta(2) = 0.74(4)$ is the second-order anomalous exponent, and the black solid line indicates this scaling law. Inset: average energy flux out of shell M, which is zero for $n < n_f$ and equal to $\varepsilon = 1$ for $n > n_f$. Adapted (figure) with permission from [27], Copyright (2024) by the American Physical Society.

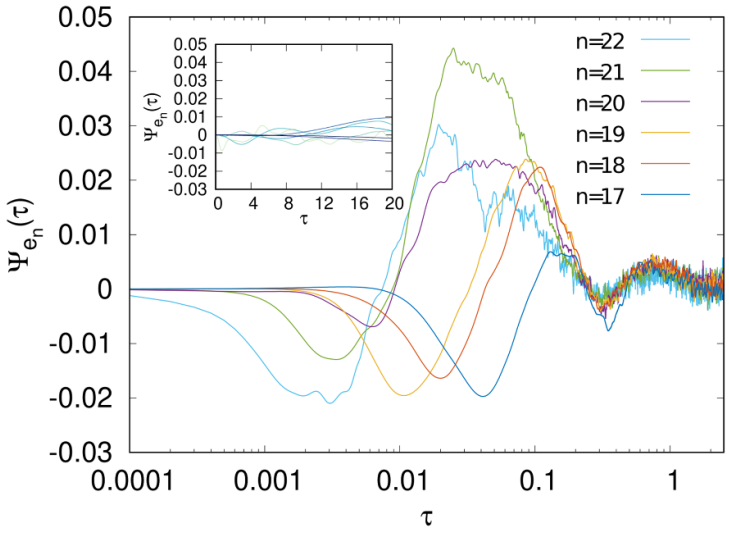

Figure 18. Asymmetric time correlation functions (84) for shells with index larger (main panel) and smaller (inset) than forced shells, which represent smaller and larger scales, respectively. The functions in the inset range from $n = 5$ (darker) to $n = 11$ (lighter). Adapted (figure) with permission from [27], Copyright (2024) by the American Physical Society.

energy gains and losses experienced by these shells [27]. Conversely, at scales larger than the forced ones the correlations are compatible with zero as expected for a reversible dynamics, i.e. at equilibrium.

Further insights into the different physics at scales larger/smaller than the forcing scale can be obtained by studying how a perturbation on the energy of a given shell influences the energy content of nearby shells. This can be realized by inspecting the following 'energy response functions':

$$R_{m,n}(t) = \frac{\overline{\delta e_n}(t)}{\delta e_m} , \tag{85}$$

in which the initial impulsive perturbation on shell m is of the order of typical energy fluctuations measured on that shell. Figure 19 displays a comparison between response functions when perturbation and responses are in the cascade range (panel (a)) or in the equipartition range (panel (b)). The former functions are rescaled as, $\delta e_m R_{m,n}(t)/\langle e_n \rangle = \overline{\delta e_n}(t)/\langle e_n \rangle$, thereby measuring the average energy deviation relative to the corresponding steady-state value. Dissimilarities between panels (a) and (b) are recognizable: while the

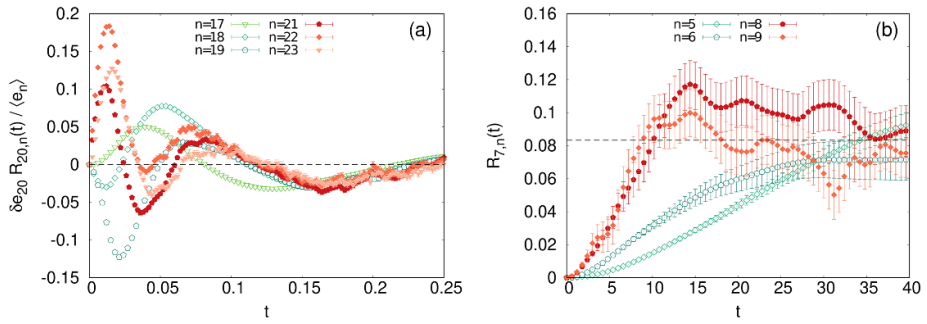

Figure 19. Energy response functions (85) measured at shells larger (filled symbols, shades of red) or smaller (empty symbols, shades of green) than the perturbed shell. (a) Rescaled response functions for shells in the cascading range: the perturbation acts at shell $m = 20$ and the response is shown for three shells smaller (greenish curves) and larger (reddish curves) within the inertial range; (b) response functions for shells in the equipartition range: the perturbation acts at shell $m = 7$ and the response is shown for two shells smaller (greenish curves) and larger (reddish curves) within the equipartition range. Adapted (figure) with permission from [27], Copyright (2024) by the American Physical Society.

functions in the cascade range show initially both positive and negative values, then followed by a decay to zero, those in the equipartition range are all positive and reach a common positive asymptotic value. In a few words, the former behavior is connected to the presence of an underlying energy flux directed toward small scales, while the latter is easily explainable with equilibrium statistical mechanics, assuming the small scales to form a conservative (sub)system. For the cascade range, it is also interesting to note the differences between the responses at shell larger and smaller than the perturbed shell, while the former initially gain in energy the latter lose energy, an asymmetry which is absent in the equipartition range. Such an asymmetry is reminiscent of those that have been discussed in section 5. More details can be found in [27].

These results reveal that the shell model with intermediate-scale forcing shows an interesting coexistence of equilibrium and non-equilibrium properties, at scales respectively larger and smaller than forcing. We conclude with a word of caution in extending these findings to real turbulent flows. As discussed earlier one of the assumptions used to build the shell model is that in the quadratic term of equation (81) only local-in-scale interactions are retained. As discussed in [162, 163] the main obstacle in having statistical equilibrium at scales larger than the forcing one is the presence of non-local interactions. It would thus be very desirable to devise a numerical study to inspect properly defined correlation and/or response functions in direct numerical simulations of the Navier–Stokes equation to test the equilibrium/non-equilibrium character of these scales.

7. Final remarks and conclusions

In this review, we discussed several tools and methods for the characterization of different facets of the statistical features in non-equilibrium systems and some readers might feel that the matter was excessively scattered. Such a feeling is somehow correct, however, it is not entirely our responsibility. Rephrasing Lev Tolstoy famous incipit, we can say that *all the equilibrium systems share quite similar features, each non-equilibrium system has its own peculiarity*.

In a nutshell, all the properties of an equilibrium system are embodied in the dependence of its partition function on temperature, pressure, applied fields, and other state variables. Conversely and unfortunately, in non-equilibrium systems, there is nothing similar to the simple and elegant recipes one can use in the equilibrium case. It is natural to wonder about the reasons behind such a significant difference.

Let us remind the grounds of the (apparent) simplicity of the equilibrium statistical mechanics[13]: once the proper invariant distribution, i.e. the microcanonical one, has been chosen, one has a way to builda consistent mathematical theory. On the contrary, in non-equilibrium system it is not easy at all, apart in few special cases, to determine the invariant distribution.

By considering the features of a chaotic dissipative system, e.g. the Navier–Stokes equation, we can understand the great difficulties in building a theory for the statistical theory of NE systems. Unlike the Hamiltonian cases, the asymptotic dynamics of a dissipative chaotic system will take place on a strange attractor whose invariant measure cannot be smooth, i.e. it is not continuous with respect to the Lebesgue measure, and usually, it is described by a multifractal measure [28]. This unpleasant technical problem can

[13] Actually there is not general consensus on the conceptual aspects of the statistical mechanics, but this is not relevant for our discussion [169].

be prevented by introducing a small noise, such that the problem of the singularity of the invariant measure is removed. Such a procedure is not only a mathematical trick, because it is quite natural to assume that any system is inherently noisy, e.g. due to the influence of the external environment [170].

Once the mathematical difficulties about the non-singular character of the invariant measure are removed, one has to find the invariant distribution of a corresponding Fokker–Planck equation of the system. This is surely a well-defined problem, but rather difficult even in low-dimensional systems. For instance, up to now, nobody has been able to find the invariant probability distribution of the Lorenz model with noisy terms. Therefore, we have that even for noisy chaotic dissipative systems there is not a well-defined (operative) protocol to determine the invariant probability. This is the first clear difference with Hamiltonian systems.

In addition, the stationary distribution provides answers to some questions only, i.e. mean values; while to understand the dynamical features, such as correlation functions and responses, a more detailed ability is needed to master the system under investigation.

Beyond the obvious technical difficulties of dealing with nonequilibrium, one has to treat a plethora of different problems that are absent in equilibrium cases. In particular, in out-of-equilibrium high-dimensional systems, the interplay among different degrees of freedom or in general among their parts generates a wealth of features that cannot be described in a simple framework.

The need of studying and measuring dynamical quantities implies a knowledge of the system along all of its characteristic time scales: such time scales can grow in number and reduce in separation, when the dimensionality of the system increases, making the analysis of irreversibility difficult or even impossible. Building upon this general problem, in this Review we have shown with several examples and approaches, the elusive nature of entropy production, which is usually considered a central quantity in characterizing irreversibility. Entropy production is a global quantity which requires knowledge of all important currents in a system, and can be severely underestimated if some part of the system is not accessible, for instance for lack of space or time resolution. On the contrary, we have shown how a 'skillful' use of correlation and response functions in certain cases can be more informative and characterize non-equilibrium in the lack of a precise knowledge of the system. There are of course possible pitfalls, particularly in the case of linear systems where the coarse-graining may completely remove any signature of irreversibility, but there are also several interesting recent results which suggest how inference of the so-called 'distance from non-equilibrium' in a system can be improved.

Data availability statement

All data that support the findings of this study are included within the article (and any supplementary files).

Acknowledgments

We thanks our collaborators on the issues here discussed: A Baldassarri, L Caprini, L Cerino, A Gnoli, U Marini Bettolo Marconi, L Peliti, A Plati, C Sarra and A Sarracino. In addition, we are grateful to L Caprini and U Marini Bettolo Marconi for their careful reading of the manuscript and useful remarks. MB and MV were supported by ERC Advanced Grant RG.BIO (Contract No. 785932). MV was also supported by MIUR FARE 2020 (Project 'INFO.BIO' No. R18JNYYMEY). AP, AV, FC and DL acknowledge the financial support from the MIUR PRIN 2017 (Project 'CO-NEST' No. 201798CZLJ). FC, AP, MV and AV acknowledge funding from the Italian Ministero dell'Università e della Ricerca under the programme PRIN 2022 ("re-ranking of the final lists"), number 2022KWTEB7, cup B53C24006470006.

Appendix

A.1. Entropy production rate for Markov processes

The definition of entropy production rate Σ for a continuous process is

$$\Sigma = \lim_{\mathcal{T}\to\infty} \left\langle \frac{1}{\mathcal{T}} \ln \frac{\mathrm{Prob}\left(\mathbf{X}^{(\mathcal{T})}_{\rightarrow}\right)}{\mathrm{Prob}\left(\mathbf{X}^{(\mathcal{T})}_{\leftarrow}\right)} \right\rangle = \lim_{\mathcal{T}\to\infty} \Sigma^{(\mathcal{T})} \tag{86}$$

where $\mathbf{X}^{(\mathcal{T})}_{\rightarrow}$ and $\mathbf{X}^{(\mathcal{T})}_{\leftarrow}$ denote the direct and inverse path respectively, and the average $\langle\cdot\rangle$ is taken with respect to the probability $\mathrm{Prob}(\mathbf{X}^{(\mathcal{T})}_{\rightarrow})$ of the direct path. In the case of Markov processes it is possible to provide an expression for Σ in terms of the transition probability $\mathcal{W}_t(\mathbf{x}|\mathbf{y})$ of going from state $\mathbf{y}$ to $\mathbf{x}$ in a time t,

normalized as

$$\int \mathrm{d}\mathbf{x}\, \mathcal{W}_t(\mathbf{x}|\mathbf{y}) = 1\,,$$

and of the stationary measure

$$\pi(\mathbf{x}) = \lim_{t\to\infty} \mathcal{W}_t(\mathbf{x}|\mathbf{y})\,.$$

In order to see this, we first divide the interval $[0,\mathcal{T})$ into n sub-intervals of length $\Delta t = \mathcal{T}/n$, and we approximate the probability of the direct $\mathbf{X}_{\rightarrow}^{(\mathcal{T})}$ and the inverse $\mathbf{X}_{\leftarrow}^{(\mathcal{T})}$ continuous-time trajectories with the probabilities of the discrete-time paths

$$\begin{aligned}\mathrm{Prob}\left(\mathbf{X}_{\rightarrow}^{(\mathcal{T})}\right) &\simeq P(\mathbf{x}(0)=\mathbf{x}_0, \mathbf{x}(\Delta t)=\mathbf{x}_1, \ldots, \mathbf{x}(\mathcal{T})=\mathbf{x}_n)\\ &= \pi(\mathbf{x}_0)\prod_{i=1}^{n}\mathcal{W}_{\Delta t}(\mathbf{x}_i|\mathbf{x}_{i-1})\end{aligned}$$

and

$$\begin{aligned}\mathrm{Prob}\left(\mathbf{X}_{\leftarrow}^{(\mathcal{T})}\right) &\simeq P(\mathbf{x}(0)=\mathbf{x}_n, \mathbf{x}(\Delta t)=\mathbf{x}_{n-1}, \ldots, \mathbf{x}(\mathcal{T})=\mathbf{x}_0)\\ &= \pi(\mathbf{x}_n)\prod_{i=1}^{n}\mathcal{W}_{\Delta t}(\mathbf{x}_{i-1}|\mathbf{x}_i)\,.\end{aligned}$$

By replacing the above expressions into equation (86), we can compute a discrete-time approximation of $\Sigma^{(\mathcal{T})}$, which will in general depend on Δt. The exact value will be recovered at the end of the calculation by taking the limit $\Delta t \to 0$, keeping $\mathcal{T}$ fixed. We get

$$\begin{aligned}\Sigma_{\Delta t}^{(\mathcal{T})} &= \frac{1}{n\Delta t}\int \mathrm{d}\mathbf{x}_0\ldots\mathrm{d}\mathbf{x}_n \pi(\mathbf{x}_0)\prod_{i=1}^{n}\mathcal{W}_{\Delta t}(\mathbf{x}_i|\mathbf{x}_{i-1})\left\{\ln\frac{\pi(\mathbf{x}_0)}{\pi(\mathbf{x}_n)} + \sum_{i=1}^{n}\ln\frac{\mathcal{W}_{\Delta t}(\mathbf{x}_i|\mathbf{x}_{i-1})}{\mathcal{W}_{\Delta t}(\mathbf{x}_{i-1}|\mathbf{x}_i)}\right\} =\\ &= \frac{1}{\Delta t}\int \mathrm{d}\mathbf{x}\pi(\mathbf{x})\int \mathrm{d}\mathbf{y}\mathcal{W}_{\Delta t}(\mathbf{y}|\mathbf{x})\ln\frac{\mathcal{W}_{\Delta t}(\mathbf{y}|\mathbf{x})}{\mathcal{W}_{\Delta t}(\mathbf{x}|\mathbf{y})} =\\ &= \frac{1}{\Delta t}\int \mathrm{d}\mathbf{x}\mathrm{d}\mathbf{y} P_{\Delta t}(\mathbf{x},\mathbf{y})\ln\frac{P_{\Delta t}(\mathbf{x},\mathbf{y})}{P_{\Delta t}(\mathbf{y},\mathbf{x})} = \Sigma_{\Delta t}\end{aligned} \tag{87}$$

where $P_{\Delta t}(\mathbf{x},\mathbf{y}) = \pi(\mathbf{x})\mathcal{W}_{\Delta t}(\mathbf{y}|\mathbf{x})$ is the joint probability of having $\mathbf{x}$ at time 0 and $\mathbf{y}$ at time t. In the computation above, we exploited the identity

$$\int \mathrm{d}\mathbf{x}\mathrm{d}\mathbf{y}\,\pi(\mathbf{x})\,\mathcal{W}_{\Delta t}(\mathbf{y}|\mathbf{x})\,(\ln\pi(\mathbf{y}) - \ln\pi(\mathbf{x})) = 0$$

and the chain rule $\pi(\mathbf{x}) = \int \mathrm{d}\mathbf{y}\,\pi(\mathbf{y})\mathcal{W}_{\Delta t}(\mathbf{x}|\mathbf{y})$. Note that, as expected, in the case of Markov processes $\Sigma_{\Delta t}^{(\mathcal{T})}$ does not actually depend on $\mathcal{T}$. This means that the $\mathcal{T}\to\infty$ limit appearing in the definition (86) is trivial. The value of Σ for the continuous-time case is then recovered in the limit $\Delta t \to 0$.

A.2. Entropy production rate for Gaussian linear processes

Let us consider the D-dimensional linear stochastic dynamics driven by a Gaussian noise, i.e.

$$\dot{\mathbf{x}} + \mathrm{A}\mathbf{x} = \boldsymbol{\xi} \qquad \boldsymbol{\xi} \sim \mathcal{G}_{\mathrm{D}}(\boldsymbol{\xi}) = \frac{\mathrm{e}^{-\frac{1}{2}\boldsymbol{\xi}^{T}\mathrm{D}^{-1}\boldsymbol{\xi}}}{\sqrt{|2\pi\,\mathrm{D}|}}$$

for which a direct computation allow us to write the evolution $\mathbf{x}\to\mathbf{y}$ in a time t as

$$\mathbf{y} = \mathrm{e}^{-t\mathrm{A}}\mathbf{x} + \boldsymbol{\eta}\,,$$

where $\boldsymbol{\eta}$ is a Gaussian noise $\boldsymbol{\eta}\sim\mathcal{G}_{\mathrm{M}_t}(\boldsymbol{\eta})$ with covariance matrix

$$\mathrm{M}_t = \int_0^t \mathrm{d}s\,\mathrm{e}^{-s\mathrm{A}}\mathrm{D}\mathrm{e}^{-s\mathrm{A}^{T}}\,.$$

In this way, we have an explicit expression for the transition rate

$$\mathcal{W}_t(\mathbf{y}|\mathbf{x}) = \int \mathrm{d}\boldsymbol{\eta}\, \mathcal{G}_{\mathrm{M}_t}(\boldsymbol{\eta})\, \delta\left(\mathbf{y} - \mathrm{e}^{-t\mathrm{A}}\mathbf{x} - \boldsymbol{\eta}\right) = \mathcal{G}_{\mathrm{M}_t}\left(\mathbf{y} - \mathrm{e}^{-t\mathrm{A}}\mathbf{x}\right) \tag{88}$$

and then, since $\lim_{t\to\infty} \mathrm{M}_t = \mathrm{C}$, we have an explicit expression even for the stationary measure

$$\pi(\mathbf{y}) = \lim_{t\to\infty} \mathcal{W}_t(\mathbf{y}|\mathbf{x}) = \mathcal{G}_{\mathrm{C}}(\mathbf{y}) = \frac{\mathrm{e}^{-\frac{1}{2}\mathbf{y}^T\mathrm{C}^{-1}\mathbf{y}}}{\sqrt{|2\pi\,\mathrm{C}|}}\,.$$

We can compute $\Sigma_{\Delta t}$ from equation (87) by averaging with the joint probability

$$\mathcal{P}_{\Delta t}(\mathbf{x},\mathbf{y}) = \pi(\mathbf{x})\,\mathcal{W}_{\Delta t}(\mathbf{y}|\mathbf{x}) = \mathcal{G}_{\mathrm{C}}(\mathbf{x})\,\mathcal{G}_{\mathrm{M}_{\Delta t}}\left(\mathbf{y} - \mathrm{e}^{-\Delta t\mathrm{A}}\mathbf{x}\right) \tag{89}$$

the logarithm of the ratio $\mathcal{P}_{\Delta t}(\mathbf{x},\mathbf{y})/\mathcal{P}_{\Delta t}(\mathbf{y},\mathbf{x})$ as prescribed in equation (87), i.e.

$$\begin{aligned}
\Sigma_{\Delta t} &= \frac{1}{2\Delta t}\left\langle \left(\mathbf{x} - \mathrm{e}^{-\Delta t\mathrm{A}}\mathbf{y}\right)^T \mathrm{M}_{\Delta t}^{-1}\left(\mathbf{x} - \mathrm{e}^{-\Delta t\mathrm{A}}\mathbf{y}\right) + \mathbf{y}^T\mathrm{C}^{-1}\mathbf{y}\right\rangle + \\
&- \frac{1}{2\Delta t}\left\langle \left(\mathbf{y} - \mathrm{e}^{-\Delta t\mathrm{A}}\mathbf{x}\right)^T \mathrm{M}_{\Delta t}^{-1}\left(\mathbf{y} - \mathrm{e}^{-\Delta t\mathrm{A}}\mathbf{x}\right) + \mathbf{x}^T\mathrm{C}^{-1}\mathbf{x}\right\rangle = \\
&= \frac{1}{\Delta t}\left\langle \mathbf{x}^T\left(\mathrm{e}^{-\Delta t\mathrm{A}^T}\mathrm{M}_{\Delta t}^{-1} - \mathrm{M}_{\Delta t}^{-1}\mathrm{e}^{-\Delta t\mathrm{A}}\right)\mathbf{y}\right\rangle = \\
&= \frac{1}{\Delta t}\left\langle \mathbf{x}^T\left(\mathrm{e}^{-\Delta t\mathrm{A}^T}\mathrm{M}_{\Delta t}^{-1} - \mathrm{M}_{\Delta t}^{-1}\mathrm{e}^{-\Delta t\mathrm{A}}\right)\mathrm{e}^{-\Delta t\mathrm{A}}\mathbf{x}\right\rangle = \\
&= \frac{1}{\Delta t}\mathrm{Tr}\left\{\left(\mathrm{e}^{-\Delta t\mathrm{A}^T}\mathrm{M}_{\Delta t}^{-1} - \mathrm{M}_{\Delta t}^{-1}\mathrm{e}^{-\Delta t\mathrm{A}}\right)\mathrm{e}^{-\Delta t\mathrm{A}}\mathrm{C}\right\}.
\end{aligned}$$

In doing the above steps, we took advantage of the fact that the marginal distributions $\int \mathrm{d}\mathbf{y}\,\mathcal{P}_{\Delta t}(\mathbf{x},\mathbf{y})$ and $\int \mathrm{d}\mathbf{x}\,\mathcal{P}_{\Delta t}(\mathbf{x},\mathbf{y})$ are identical, and they coincide with the stationary measure: this implies that several averages involving only one variable among $\mathbf{x}$ and $\mathbf{y}$ cancel each other out, since they appear twice, with reversed signs. The last two steps are the consequence of

$$\int \mathrm{d}\mathbf{y}\,\mathcal{W}_{\Delta t}(\mathbf{y}|\mathbf{x})\,\mathbf{y} = \mathrm{e}^{-\Delta t\mathrm{A}}\mathbf{x}$$

and

$$\left\langle \mathbf{x}^T\mathrm{B}\mathbf{x}\right\rangle = \mathrm{Tr}\left(\mathrm{BC}\right) = \mathrm{Tr}\left(\mathrm{CB}\right) \quad \forall \mathrm{B}\,.$$

At the leading order of Δt, since $\mathrm{M}_{\Delta t} \simeq \Delta t\mathrm{D}$ and $\mathrm{e}^{-\Delta t\mathrm{A}} \simeq 1 - \Delta t\mathrm{A}$, we have

$$\Sigma_{\Delta t} = \frac{1}{\Delta t}\left\{\mathrm{Tr}\left(\mathrm{D}^{-1}\mathrm{AC}\right) - \mathrm{Tr}\left(\mathrm{A}^T\mathrm{D}^{-1}\mathrm{C}\right)\right\} + \mathrm{Tr}\left\{\left(\mathrm{A}^T\mathrm{D}^{-1} - \mathrm{D}^{-1}\mathrm{A}\right)\mathrm{AC}\right\} + \mathcal{O}(\Delta t)$$

It can be seen that the term of order $1/\Delta t$ vanishes because of the cyclic property of the trace and the symmetry of D and C:

$$\mathrm{Tr}\left(\mathrm{D}^{-1}\mathrm{AC}\right) = \mathrm{Tr}\left(\mathrm{CD}^{-1}\mathrm{A}\right) = \mathrm{Tr}\left(\mathrm{A}^T\mathrm{D}^{-1}\mathrm{C}\right).$$

Recalling the equality $\mathrm{AC} + \mathrm{CA}^T = \mathrm{D}$ valid for Orstein-Uhlenbeck processes [37], we finally get, taking the limit $\Delta t \to 0$,

$$\Sigma = \mathrm{Tr}\left\{\left(\mathrm{CA}^T - \mathrm{AC}\right)\mathrm{D}^{-1}\mathrm{A}\right) = \mathrm{Tr}\left\{\left(\mathrm{A}^T\mathrm{D}^{-1} - \mathrm{D}^{-1}\mathrm{A}\right)\mathrm{AC}\right\}.$$

A.3. Simulation algorithm for linear stochastic processes

Linear stochastic processes, such as $\dot{\mathbf{x}} + \mathrm{A}\mathbf{x} = \xi + \zeta$ in which Poissonian random jumps ζ are added to a typical Gaussian noise ξ, can be exactly simulated, with an error due exclusively to the numerical precision of the calculator and the goodness of the random number generator. The idea is based on the fact that, in the absence of jumps, the propagator $\mathcal{W}_t(\mathbf{x}'|\mathbf{x})$ from $\mathbf{x}$ to $\mathbf{x}'$ in a time t is well known, it is Gaussian with mean $\mathrm{e}^{-t\mathrm{A}}\mathbf{x}$ and covariance matrix $\mathrm{M}_t = \int_0^t \mathrm{d}s\mathrm{e}^{-s\mathrm{A}}\mathrm{D}\mathrm{e}^{-s\mathrm{A}^T}$. This means that, regardless of the value of t and in absence of jumps, we can obtain the value of $\mathbf{x}'$ simply by adding to the value $\mathrm{e}^{-t\mathrm{A}}\mathbf{x}$ a random vector $\mathbf{z}$ extracted from a normal distribution $\mathcal{G}_{\mathrm{M}_t}(\mathbf{z})$. The presence of jumps it is only a small complication to this rule. In fact, once the sampling frequency $f = 1/\delta$ with which we want temporally discretize the trajectories of the system has been chosen, we just have to know in advance the time of the next jump and appropriately

break the evolution into two pieces, before and after the jump, in the time interval at which the jump occurs. Now we describe the algorithm in the general case in which the jumps affect only some components and the Poissonian rates and the distribution of the intensity with which these processes occur may be different between one component and another. All other cases, for example that of an equal rate for all components or a distribution of dependent jumps, should be simpler. Let δ the sampling time, A the drift matrix, D the covariance matrix of Gaussian noise, $\mathcal{J}$ the set of component afflicted by jumps and $\{\lambda_i, P_i(u)\}_{i\in\mathcal{J}}$ the set of rates and intensity distribution of such jumps. First of all, we note that, for any value of t, we are able to numerically compute $\mathcal{R}(t) = \mathrm{e}^{-t\mathrm{A}}$ and $\mathrm{M}_t = \int_0^t \mathrm{d}s\, \mathrm{e}^{-s\mathrm{A}}\mathrm{D}\mathrm{e}^{-s\mathrm{A}^T}$ through appropriate matrix diagonalizations and analytical simplification. Then we assume that we have the appropriate random number generators for all distribution we consider: the multi-normal one whatever the covariance matrix M_t is, the Poissonian one $\lambda\mathrm{e}^{-\lambda t}$ and the set of $\{P_i(u)\}_{i\in\mathcal{J}}$ for jumps intensity. With such assumptions the flow of the algorithm can be organized into following routines.

INIT	Set the initial state $\mathbf{x}$, extract with probability $\lambda_i \mathrm{e}^{-\lambda_i t_i}$ the times of the next jumps for all the components in $\mathcal{J}$, store such times in a set $\mathcal{T} = \{t_i\}_{i\in\mathcal{J}}$, call UPDATE, then set $t = \delta$ and call SELECT;
UPDATE	Find the index k of the smallest time $\tau = t_k$ in the set $\mathcal{T}$, delete t_k from such set and shift all other remains times $t_i \to t_i - \tau$;
SELECT	if $\tau > \delta$ call GAUSS, print $\mathbf{x}$ and set $t = \delta$, otherwise call JUMP;
GAUSS	Iterate with recursion rule $\mathcal{R}(t)\mathbf{x} + \mathbf{z}_t \to \mathbf{x}$ with $\mathbf{z}_t \sim \mathcal{G}_{\mathrm{M}_t}(\mathbf{z}_t)$, set $\tau = \tau - t$ and call SELECT;
JUMP	iterate with $\mathcal{R}(\tau)\mathbf{x} + \mathbf{z}_\tau \to \mathbf{x}$, then set $x_k = x_k + u$ where u is extract from the distribution $P_k(u)$, set $t = t - \tau$ then extract a new time $t_k \sim \lambda_k \mathrm{e}^{-\lambda_k t}$ for the index k, add this time to set $\mathcal{T}$, call UPDATE then call SELECT.

ORCID iDs

Dario Lucente https://orcid.org/0000-0002-9070-2326
Marco Baldovin https://orcid.org/0000-0003-3559-4032
Fabio Cecconi https://orcid.org/0000-0001-8351-248X
Massimo Cencini https://orcid.org/0000-0001-7073-5000
Niccolò Cocciaglia https://orcid.org/0009-0001-7201-2444
Andrea Puglisi https://orcid.org/0000-0002-7229-9457
Massimiliano Viale https://orcid.org/0000-0003-4808-4103

References

[1] de Groot S and Mazur P 1984 *Non-Equilibrium Thermodynamics* (*Dover Books on Physics*) (Dover Publications)
[2] Kubo R, Toda M and Hashitsume N 1991 *Statistical Physics II: Nonequilibrium Statistical Mechanics* (Springer)
[3] Livi R and Politi P 2017 *Nonequilibrium Statistical Physics: A Modern Perspective* (Cambridge University Press)
[4] Maes C and Netočný K 2003 Time-reversal and entropy *J. Stat. Phys.* **110** 269–310
[5] Esposito M, Lindenberg K and Van den Broeck C 2010 Entropy production as correlation between system and reservoir *New J. Phys.* **12** 013013
[6] Bialek W, Cavagna A, Giardina I, Mora T, Silvestri E, Viale M and Walczak A M 2012 Statistical mechanics for natural flocks of birds *Proc. Natl Acad. Sci.* **109** 4786–91
[7] Cercignani C 2006 *Ludwig Boltzmann: The Man Who Trusted Atoms* (Oxford University Press)
[8] Kreuzer H J 1981 *Nonequilibrium Thermodynamics and Its Statistical Foundations* (Oxford University Press)
[9] Ruelle D 1996 Positivity of entropy production in nonequilibrium statistical mechanics *J. Stat. Phys.* **85** 1–23
[10] Sekimoto K 2010 *Stochastic Energetics* (Springer)
[11] Seifert U 2012 Stochastic thermodynamics, fluctuation theorems and molecular machines *Rep. Prog. Phys.* **75** 126001
[12] Peliti L and Pigolotti S 2021 *Stochastic Thermodynamics: An Introduction* (Princeton University Press)
[13] Sarra C, Baldovin M and Vulpiani A 2021 Response and flux of information in extended nonequilibrium dynamics *Phys. Rev.* E **104** 024116
[14] Crisanti A, Puglisi A and Villamaina D 2012 Nonequilibrium and information: the role of cross correlations *Phys. Rev.* E **85** 061127
[15] Lucente D, Viale M, Gnoli A, Puglisi A and Vulpiani A 2023 Revealing the nonequilibrium nature of a granular intruder: the crucial role of non-Gaussian behavior *Phys. Rev. Lett.* **131** 078201
[16] Pomeau Y 1982 Symétrie des fluctuations dans le renversement du temps *J. Phys.* **43** 859–67
[17] Josserand C, Le Berre M, Lehner T and Pomeau Y 2017 Turbulence: does energy cascade exist? *J. Stat. Phys.* **167** 596–625
[18] Ruelle D 1998 General linear response formula in statistical mechanics and the fluctuation-dissipation theorem far from equilibrium *Phys. Lett.* A **245** 220–4
[19] Kubo R 1966 The fluctuation-dissipation theorem *Rep. Prog. Phys.* **29** 255
[20] Marconi U M B, Puglisi A, Rondoni L and Vulpiani A 2008 Fluctuation–dissipation: response theory in statistical physics *Phys. Rep.* **461** 111–95
[21] Barato A C and Seifert U 2015 Thermodynamic uncertainty relation for biomolecular processes *Phys. Rev. Lett.* **114** 158101
[22] Seifert U 2018 Stochastic thermodynamics: from principles to the cost of precision *Physica* A **504** 176–91

[23] Aurell E and Del Ferraro G 2016 Causal analysis, correlation-response and dynamic cavity *J. Phys.: Conf. Ser.* **699** 012002
[24] Baldovin M, Cecconi F and Vulpiani A 2020 Understanding causation via correlations and linear response theory *Phys. Rev. Res.* **2** 043436
[25] Xu H, Pumir A, Falkovich G, Bodenschatz E, Shats M, Xia H, Francois N and Boffetta G 2014 Flight–crash events in turbulence *Proc. Natl Acad. Sci.* **111** 7558–63
[26] Cencini M, Biferale L, Boffetta G and De Pietro M 2017 Time irreversibility and multifractality of power along single particle trajectories in turbulence *Phys. Rev. Fluids* **2** 104604
[27] Cocciaglia N, Cencini M and Vulpiani A 2024 Nonequilibrium statistical mechanics of the turbulent energy cascade: irreversibility and response functions *Phys. Rev.* E **109** 014113
[28] Cencini M, Cecconi F and Vulpiani A 2009 *Chaos: From Simple Models to Complex Systems* (World Scientific)
[29] Ohm G S 1827 *Die Galvanische Kette: Mathematisch* (TH Riemann)
[30] Cerino L, Cecconi F, Cencini M and Vulpiani A 2016 The role of the number of degrees of freedom and chaos in macroscopic irreversibility *Physica* A **442** 486–97
[31] Goldstein S 2012 *Typicality and Notions of Probability in Physics* (Springer) pp 59–71
[32] Arnold V I and Avez A 1968 *Ergodic Problems in Classical Mechanics* (Benjamin)
[33] Baldovin M, Marino R and Vulpiani A 2023 Ergodic observables in non-ergodic systems: the example of the harmonic chain *Physica* A **630** 129273
[34] Baldovin M, Caprini L and Vulpiani A 2019 Irreversibility and typicality: a simple analytical result for the Ehrenfest model *Physica* A **524** 422–9
[35] Lanford O E 1975 *Time Evolution of Large Classical Systems* (Springer)
[36] Cencini M, Cecconi F, Falcioni M and Vulpiani A 2008 Role of chaos for the validity of statistical mechanics laws: diffusion and conduction *The Fermi-Pasta-Ulam Problem: A Status Report* (Springer) pp 123–49
[37] Gardiner C 1990 *Handbook of Stochastic Methods for Physics, Chemistry and the Natural Sciences* (Springer)
[38] Bilotto P, Caprini L and Vulpiani A 2021 Excess and loss of entropy production for different levels of coarse graining *Phys. Rev.* E **104** 024140
[39] Kubo R 1957 Statistical-mechanical theory of irreversible processes. I. General theory and simple applications to magnetic and conduction problems *J. Phys. Soc. Japan* **12** 570–86
[40] Caprini L, Marconi U M B, Puglisi A and Vulpiani A 2018 Comment on entropy production and fluctuation theorems for active matter? *Phys. Rev. Lett.* **121** 139801
[41] Dabelow L, Bo S and Eichhorn R 2019 Irreversibility in active matter systems: fluctuation theorem and mutual information *Phys. Rev.* X **9** 021009
[42] Lebowitz J L and Spohn H 1999 A Gallavotti–Cohen-type symmetry in the large deviation functional for stochastic dynamics *J. Stat. Phys.* **95** 333–65
[43] Cover T M and Thomas J A 2006 *Elements of Information Theory* (*Wiley Series in Telecommunications and Signal Processing*) 2nd edn (Wiley-Interscience)
[44] Gomez-Marin A, Parrondo J M R and Van den Broeck C 2008 Lower bounds on dissipation upon coarse graining *Phys. Rev.* E **78** 011107
[45] Lucente D, Baldassarri A, Puglisi A, Vulpiani A and Viale M 2022 Inference of time irreversibility from incomplete information: linear systems and its pitfalls *Phys. Rev. Res.* **4** 043103
[46] Kawaguchi K and Nakayama Y 2013 Fluctuation theorem for hidden entropy production *Phys. Rev.* E **88** 022147
[47] Martínez I A, Bisker G, Horowitz J M and Parrondo J M R 2019 Inferring broken detailed balance in the absence of observable currents *Nat. Commun.* **10** 3542
[48] Bisker G, Martínez I A, Horowitz J M and Parrondo J M R 2024 Reply to: Comment on "Inferring broken detailed balance in the absence of observable currents" *Nat. Commun.* **15** 8679
[49] Hartich D and Godec A 2024 Comment on "Inferring broken detailed balance in the absence of observable currents" *Nat. Commun.* **15** 8678
[50] van der Meer J, Degünther J and Seifert U 2023 Time-resolved statistics of snippets as general framework for model-free entropy estimators *Phys. Rev. Lett.* **130** 257101
[51] Ciliberto S, Imparato A, Naert A and Tanase M 2013 Heat flux and entropy produced by thermal fluctuations *Phys. Rev. Lett.* **110** 180601
[52] Scalliet C, Gnoli A, Puglisi A and Vulpiani A 2015 Cages and anomalous diffusion in vibrated dense granular media *Phys. Rev. Lett.* **114** 198001
[53] Maggi C, Marconi U M B, Gnan N and Di Leonardo R 2015 Multidimensional stationary probability distribution for interacting active particles *Sci. Rep.* **5** 10742
[54] Caprini L, Marconi U M B, Puglisi A and Vulpiani A 2019 The entropy production of Ornstein–Uhlenbeck active particles: a path integral method for correlations *J. Stat. Mech.* 053203
[55] Gilson M, Tagliazucchi E and Cofré R 2023 Entropy production of multivariate Ornstein–Uhlenbeck processes correlates with consciousness levels in the human brain *Phys. Rev.* E **107** 024121
[56] Sekizawa D, Ito S and Oizumi M 2024 Decomposing thermodynamic dissipation of linear Langevin systems via oscillatory modes and its application to neural dynamics *Phys. Rev.* X **14** 041003
[57] Sarracino A and Vulpiani A 2019 On the fluctuation-dissipation relation in non-equilibrium and non-Hamiltonian systems *Chaos* **29** 083132
[58] Speck T and Seifert U 2006 Restoring a fluctuation-dissipation theorem in a nonequilibrium steady state *Europhys. Lett.* **74** 391–6
[59] Prost J, Joanny J-F and Parrondo J M R 2009 Generalized fluctuation-dissipation theorem for steady-state systems *Phys. Rev. Lett.* **103** 090601
[60] Caprini L 2021 Generalized fluctuation–dissipation relations holding in non-equilibrium dynamics *J. Stat. Mech.* 063202
[61] Caprini L, Puglisi A and Sarracino A 2021 Fluctuation–dissipation relations in active matter systems *Symmetry* **13** 81
[62] Baldovin M, Caprini L and Vulpiani A 2021 Handy fluctuation-dissipation relation to approach generic noisy systems and chaotic dynamics *Phys. Rev.* E **104** L032101
[63] Baiesi M, Maes C and Wynants B 2009 Fluctuations and response of nonequilibrium states *Phys. Rev. Lett.* **103** 010602
[64] Cugliandolo L F 2011 The effective temperature *J. Phys. A: Math. Theor.* **44** 483001
[65] Puglisi A, Sarracino A and Vulpiani A 2017 Temperature in and out of equilibrium: a review of concepts, tools and attempts *Phys. Rep.* **709** 1–60

[66] Villamaina D, Baldassarri A, Puglisi A and Vulpiani A 2009 The fluctuation-dissipation relation: how does one compare correlation functions and responses? *J. Stat. Mech.* P07024
[67] Mori H 1965 Transport, collective motion and Brownian motion *Prog. Theor. Phys.* **33** 423–55
[68] Mori H 1965 A continued-fraction representation of the time-correlation functions *Prog. Theor. Phys.* **34** 399–416
[69] Harada T and Sasa S-I 2005 Equality connecting energy dissipation with a violation of the fluctuation-response relation *Phys. Rev. Lett.* **95** 130602
[70] Harada T and Sasa S-I 2006 Energy dissipation and violation of the fluctuation-response relation in nonequilibrium Langevin systems *Phys. Rev.* E **73** 026131
[71] Filliger R and Reimann P 2007 Brownian gyrator: a minimal heat engine on the nanoscale *Phys. Rev. Lett.* **99** 230602
[72] Ciliberto S, Imparato A, Naert A and Tanase M 2013 Statistical properties of the energy exchanged between two heat baths coupled by thermal fluctuations *J. Stat. Mech.* P12014
[73] Argun A, Soni J, Dabelow L, Bo S, Pesce G, Eichhorn R and Volpe G 2017 Experimental realization of a minimal microscopic heat engine *Phys. Rev.* E **96** 052106
[74] Lucente D, Puglisi A, Viale M and Vulpiani A 2023 Statistical features of systems driven by non-Gaussian processes: theory & practice *J. Stat. Mech.* 113202
[75] Sato K-i 1999 *Lévy Processes and Infinitely Divisible Distributions* (Cambridge University Press)
[76] Kyprianou A E 2014 *Fluctuations of Lévy Processes With Applications: Introductory Lectures* (Springer)
[77] Schilling R L and Davar K 2017 *From Lévy-Type Processes to Parabolic Spdes* (Springer)
[78] Kanazawa K, Sagawa T and Hayakawa H 2012 Stochastic energetics for non-Gaussian processes *Phys. Rev. Lett.* **108** 210601
[79] Kanazawa K, Sano T G, Sagawa T and Hayakawa H 2015 Minimal model of stochastic athermal systems: origin of non-Gaussian noise *Phys. Rev. Lett.* **114** 090601
[80] Kanazawa K, Sano T G, Sagawa T and Hayakawa H 2015 Asymptotic derivation of Langevin-like equation with non-Gaussian noise and its analytical solution *J. Stat. Phys.* **160** 1294–335
[81] Kanazawa K 2017 *Statistical Mechanics for Athermal Fluctuation: Non-Gaussian Noise in Physics* (Springer)
[82] Zakine R, Solon A, Gingrich T and Van Wijland F 2017 Stochastic stirling engine operating in contact with active baths *Entropy* **19** 193
[83] Fodor E, Hayakawa H, Tailleur J and van Wijland F 2018 Non-Gaussian noise without memory in active matter *Phys. Rev.* E **98** 062610
[84] Białas K and Spiechowicz J 2023 Mechanism for giant enhancement of transport induced by active fluctuations *Phys. Rev.* E **107** 064120
[85] Goldobin D S, di Volo M and Torcini A 2024 Discrete synaptic events induce global oscillations in balanced neural networks *Phys. Rev. Lett.* **133** 238401
[86] Eliazar I and Klafter J 2003 Lévy-driven Langevin systems: targeted stochasticity *J. Stat. Phys.* **111** 739–68
[87] Kuśmierz Ł, Dybiec B and Gudowska-Nowak E 2018 Thermodynamics of superdiffusion generated by Lévy–Wiener fluctuating forces *Entropy* **20** 658
[88] Abel M, Biferale L, Cencini M, Falcioni M, Vergni D and Vulpiani A 2000 Exit-time approach to ε-entropy *Phys. Rev. Lett.* **84** 6002
[89] Gaspard P and Wang X-J 1993 Noise, chaos and (ε, τ)-entropy per unit time *Phys. Rep.* **235** 291–343
[90] Boffetta G, Cencini M, Falcioni M and Vulpiani A 2002 Predictability: a way to characterize complexity *Phys. Rep.* **356** 367–474
[91] Łuczka J, Czernik T and Hänggi P 1997 Symmetric white noise can induce directed current in ratchets *Phys. Rev.* E **56** 3968
[92] Białas K, Łuczka J, Hänggi P and Spiechowicz J 2020 Colossal Brownian yet non-Gaussian diffusion induced by nonequilibrium noise *Phys. Rev.* E **102** 042121
[93] Białas K, Łuczka J and Spiechowicz J 2022 Periodic potential can enormously boost free particle transport induced by active fluctuations (arXiv:2209.01465)
[94] Spiechowicz J, Łuczka J and Hänggi P 2013 Absolute negative mobility induced by white Poissonian noise *J. Stat. Mech.* P02044
[95] Spiechowicz J, Hänggi P and Łuczka J 2014 Brownian motors in the microscale domain: enhancement of efficiency by noise *Phys. Rev.* E **90** 032104
[96] Cocconi L, Garcia-Millan R, Zhen Z, Buturca B and Pruessner G 2020 Entropy production in exactly solvable systems *Entropy* **22** 1252
[97] Seifert U 2019 From stochastic thermodynamics to thermodynamic inference *Annu. Rev. Condens. Matter Phys.* **10** 171–92
[98] Puglisi A, Pigolotti S, Rondoni L and Vulpiani A 2010 Entropy production and coarse graining in Markov processes *J. Stat. Mech.* P05015
[99] Schnakenberg J 1976 Network theory of microscopic and macroscopic behavior of master equation systems *Rev. Mod. Phys.* **48** 571–85
[100] Horowitz J M and Gingrich T R 2019 Thermodynamic uncertainty relations constrain non-equilibrium fluctuations *Nat. Phys.* **16** 15–20
[101] Gingrich T R, Horowitz J M, Perunov N and England J L 2016 Dissipation bounds all steady-state current fluctuations *Phys. Rev. Lett.* **116** 120601
[102] Gingrich T R, Rotskoff G M and Horowitz J M 2017 Inferring dissipation from current fluctuations *J. Phys. A: Math. Theor.* **50** 184004
[103] Dechant A and Sasa S-I 2018 Current fluctuations and transport efficiency for general Langevin systems *J. Stat. Mech.* 063209
[104] Koyuk T and Seifert U 2020 Thermodynamic uncertainty relation for time-dependent driving *Phys. Rev. Lett.* **125** 260604
[105] Dechant A and Sasa S-I 2020 Fluctuation–response inequality out of equilibrium *Proc. Natl Acad. Sci.* **117** 6430–6
[106] Liu K, Gong Z and Ueda M 2020 Thermodynamic uncertainty relation for arbitrary initial states *Phys. Rev. Lett.* **125** 140602
[107] Pietzonka P 2022 Classical pendulum clocks break the thermodynamic uncertainty relation *Phys. Rev. Lett.* **128** 130606
[108] Hasegawa Y and Van Vu T 2019 Uncertainty relations in stochastic processes: an information inequality approach *Phys. Rev.* E **99** 062126
[109] Lee J S, Park J-M and Park H 2021 Universal form of thermodynamic uncertainty relation for Langevin dynamics *Phys. Rev.* E **104** L052102
[110] Plati A, Puglisi A and Sarracino A 2023 Thermodynamic bounds for diffusion in nonequilibrium systems with multiple timescales *Phys. Rev.* E **107** 044132
[111] Plati A, Puglisi A and Sarracino A 2024 Thermodynamic uncertainty relations in the presence of non-linear friction and memory *J. Phys. A: Math. Theor.* **57** 155001
[112] Dieball C and Godec A 2023 Direct route to thermodynamic uncertainty relations and their saturation *Phys. Rev. Lett.* **130** 087101

[113] Li J, Horowitz J M, Gingrich T R and Fakhri N 2019 Quantifying dissipation using fluctuating currents *Nat. Commun.* **10** 1–9
[114] Van Vu T, Vo V T and Hasegawa Y 2020 Entropy production estimation with optimal current *Phys. Rev.* E **101** 042138
[115] Manikandan S K, Gupta D and Krishnamurthy S 2020 Inferring entropy production from short experiments *Phys. Rev. Lett.* **124** 120603
[116] Otsubo S, Ito S, Dechant A and Sagawa T 2020 Estimating entropy production by machine learning of short-time fluctuating currents *Phys. Rev.* E **101** 062106
[117] Dechant A and Sasa S-I 2021 Continuous time reversal and equality in the thermodynamic uncertainty relation *Physical Review Research* **3** L042012
[118] Dechant A and Sasa S-I 2021 Improving thermodynamic bounds using correlations *Phys. Rev.* X **11** 041061
[119] Di Terlizzi I, Gironella M, Herraez-Aguilar D, Betz T, Monroy F, Baiesi M and Ritort F 2024 Variance sum rule for entropy production *Science* **383** 971–6
[120] Koyuk T and Seifert U 2022 Thermodynamic uncertainty relation in interacting many-body systems *Phys. Rev. Lett.* **129** 210603
[121] Gilpin W, Bull M S and Prakash M 2020 The multiscale physics of cilia and flagella *Nat. Rev. Phys.* **2** 74–88
[122] Goldstein R E, Polin M and Tuval I 2011 Emergence of synchronized beating during the regrowth of eukaryotic flagella *Phys. Rev. Lett.* **107** 148103
[123] Hwang W and Hyeon C 2018 Energetic costs, precision and transport efficiency of molecular motors *J. Phys. Chem. Lett.* **9** 513–20
[124] Maggi C, Saglimbeni F, Sosa V C, Di Leonardo R, Nath B and Puglisi A 2023 Thermodynamic limits of sperm swimming precision *PRX Life* **1** 013003
[125] Costantini G and Puglisi A 2024 Thermodynamic precision of a chain of motors: the difference between phase and noise correlation *J. Stat. Mech.* 024003
[126] Dechant A 2023 Thermodynamic constraints on the power spectral density in and out of equilibrium (arXiv:2306.00417)
[127] Roldán E and Parrondo J M R 2012 Entropy production and Kullback-Leibler divergence between stationary trajectories of discrete systems *Phys. Rev.* E **85** 031129
[128] Lynn C W, Holmes C M, Bialek W and Schwab D J 2022 Decomposing the local arrow of time in interacting systems *Phys. Rev. Lett.* **129** 118101
[129] Lynn C W, Holmes C M, Bialek W and Schwab D J 2022 Emergence of local irreversibility in complex interacting systems *Phys. Rev.* E **106** 034102
[130] Roldán E, Barral J, Martin P, Parrondo J M R and Jülicher F 2021 Quantifying entropy production in active fluctuations of the hair-cell bundle from time irreversibility and uncertainty relations *New J. Phys.* **23** 083013
[131] Skinner D J and Dunkel J 2021 Estimating entropy production from waiting time distributions *Phys. Rev. Lett.* **127** 198101
[132] Skinner D J and Dunkel J 2021 Improved bounds on entropy production in living systems *Proc. Natl Acad. Sci.* **118** e2024300118
[133] Ehrich J 2021 Tightest bound on hidden entropy production from partially observed dynamics *J. Stat. Mech.* 083214
[134] Harunari P E, Dutta A, Polettini M and Roldán E 2022 What to learn from a few visible transitions' statistics? *Phys. Rev.* X **12** 041026
[135] van der Meer J, Ertel B and Seifert U 2022 Thermodynamic inference in partially accessible Markov networks: a unifying perspective from transition-based waiting time distributions *Phys. Rev.* X **12** 031025
[136] Loos S A M and Klapp S H L 2020 Irreversibility, heat and information flows induced by non-reciprocal interactions *New J. Phys.* **22** 123051
[137] Loos S A M, Arabha S, Rajabpour A, Hassanali A and Roldán E 2023 Nonreciprocal forces enable cold-to-hot heat transfer between nanoparticles *Sci. Rep.* **13** 4517
[138] Schreiber T 2000 Measuring information transfer *Phys. Rev. Lett.* **85** 461
[139] Barnett L, Barrett A B and Seth A K 2009 Granger causality and transfer entropy are equivalent for Gaussian variables *Phys. Rev. Lett.* **103** 238701
[140] Chandler D and Percus J K 1988 *Introduction to Modern Statistical Mechanics* (American Institute of Physics)
[141] Cecconi F, Costantini G, Guardiani C, Baldovin M and Vulpiani A 2023 Correlation, response and entropy approaches to allosteric behaviors: a critical comparison on the ubiquitin case *Phys. Biol.* **20** 056002
[142] Coventry A M 2006 *Hume's Theory of Causation* (A&C Black)
[143] Lahiri S, Nghe P, Tans S J, Rosinberg M L and Lacoste D 2017 Information-theoretic analysis of the directional influence between cellular processes *PLoS One* **12** e0187431
[144] Granger C W 1969 Investigating causal relations by econometric models and crossspectral methods *Econometrica* **37** 424–38
[145] Pearl J 2009 *Causality* (Cambridge University Press)
[146] Baldovin M, Cecconi F, Provenzale A and Vulpiani A 2022 Extracting causation from millennial-scale climate fluctuations in the last 800 kyr *Sci. Rep.* **12** 15320
[147] Falasca F, Perezhogin P and Zanna L 2024 Data-driven dimensionality reduction and causal inference for spatiotemporal climate fields *Phys. Rev.* E **109** 044202
[148] Giorgini L T, Deck K, Bischoff T and Souza A 2024 Response theory via generative score modeling *Phys. Rev. Lett.* **133** 267302
[149] Paluš M, Komárek V, Hrnčíř Z and Štěrbová K 2001 Synchronization as adjustment of information rates: detection from bivariate time series *Phys. Rev.* E **63** 046211
[150] Hempel T and Loos S A 2024 A simple reconstruction method to infer nonreciprocal interactions and local driving in complex systems (arXiv:2403.09243)
[151] Falkovich G and Sreenivasan K R 2006 Lessons from hydrodynamic turbulence *Phys. Today* **59** 43–49
[152] Landau L D and Lifshitz E M 1959 *Fluid Mechanics* (Pergamon)
[153] Kraichnan R H 1973 Helical turbulence and absolute equilibrium *J. Fluid Mech.* **59** 745–52
[154] Frisch U 1995 *Turbulence: The Legacy of A. N. Kolmogorov* (Cambridge University Press)
[155] Rose H and Sulem P 1978 Fully developed turbulence and statistical mechanics *J. Phys.* **39** 441–84
[156] Nickelsen D and Engel A 2013 Probing small-scale intermittency with a fluctuation theorem *Phys. Rev. Lett.* **110** 214501
[157] Pumir A, Xu H, Boffetta G, Falkovich G and Bodenschatz E 2014 Redistribution of kinetic energy in turbulent flows *Phys. Rev.* X **4** 041006
[158] Lanotte A, Calzavarini E, Toschi F, Bec J, Biferale L and Cencini M 2011 Heavy particles in turbulent flows RM-2007-GRAD-2048.ST0 (available at: https://data.4tu.nl/articles/dataset/Heavy_particles_in_turbulent_flows_RM-2007-GRAD-2048_St0/12709904/1)
[159] Bec J, Biferale L, Cencini M, Lanotte A S and Toschi F 2010 Intermittency in the velocity distribution of heavy particles in turbulence *J. Fluid Mech.* **646** 527–36

[160] Alexakis A and Brachet M-E 2019 On the thermal equilibrium state of large-scale flows *J. Fluid Mech.* **872** 594–625
[161] Gorce J-B and Falcon E 2022 Statistical equilibrium of large scales in three-dimensional hydrodynamic turbulence *Phys. Rev. Lett.* **129** 054501
[162] Hosking D N and Schekochihin A A 2023 Emergence of long-range correlations and thermal spectra in forced turbulence *J. Fluid Mech.* **973** A13
[163] Ding M, Xie J-H and Wang J 2024 Departure from the statistical equilibrium of large scales in forced three-dimensional homogeneous isotropic turbulence *J. Fluid Mech.* **984** A71
[164] Poulain C, Mazellier N, Chevillard L, Gagne Y and Baudet C 2006 Dynamics of spatial Fourier modes in turbulence: sweeping effect, long-time correlations and temporal intermittency *Eur. Phys. J.* B **53** 219–24
[165] Bohr T, Jensen M H, Paladin G and Vulpiani A 1998 *Dynamical Systems Approach to Turbulence* (Cambridge University Press)
[166] Biferale L 2003 Shell models of energy cascade in turbulence *Annu. Rev. Fluid Mech.* **35** 441–68
[167] Ditlevsen P D 2010 *Turbulence and Shell Models* (Cambridge University Press)
[168] L'vov V S, Podivilov E, Pomyalov A, Procaccia I and Vandembroucq D 1998 Improved shell model of turbulence *Phys. Rev.* E **58** 1811–22
[169] Chibbaro S, Rondoni L and Vulpiani A 2014 *Reductionism, Emergence and Levels of Reality: The Importance of Being Borderline* (Springer)
[170] Eckmann J-P and Ruelle D 1985 Ergodic theory of chaos and strange attractors *The Theory of Chaotic Attractors* (Springer) pp 273–312